

16. QUATERNARY CaCO₃ INPUT AND PRESERVATION WITHIN ANTARCTIC INTERMEDIATE WATER: MINERALOGIC AND ISOTOPIC RESULTS FROM HOLES 818B AND 817A, TOWNSVILLE TROUGH (NORTHEASTERN AUSTRALIA MARGIN)

Geoffrey A. Haddad,² André W. Droxler,² Dick Kroon,³ and Danny W. Müller⁴

ABSTRACT

The Quaternary history of metastable CaCO₃ input and preservation within Antarctic Intermediate Water (AAIW) was examined by studying sediments from ODP Holes 818B (745 mbsl) and 817A (1015 mbsl) drilled in the Townsville Trough on the southern slope of the Queensland Plateau. These sites lie within the core of modern AAIW, and near the aragonite saturation depth (~1000 m). Thus, they are well positioned to monitor chemical changes that may have occurred within this water mass during the past 1.6 m.y. The percent of fine aragonite content, percent of fine magnesian calcite content, and percent of whole pteropods (>355 µm) were used to separate the fine aragonite input signal from the CaCO₃ preservation signal. Stable δ¹⁸O and δ¹³C isotopic ratios were determined for the planktonic foraminifer *Globigerinoides sacculifer* and, in Hole 818B, for the benthic foraminifer *Cibicidoides* spp. to establish the oxygen isotope stratigraphy and to study the relationship between intermediate and shallow water δ¹³C of ΣCO₂ and the relationship between benthic foraminiferal δ¹³C and CaCO₃ preservation within intermediate waters of the Townsville Trough. Data were converted from depth to age using oxygen isotope stratigraphy, nanostratigraphy, and foraminiferal biostratigraphy. Several long hiatuses and the absence of magnetostratigraphy did not permit time series analysis.

The principal results of the CaCO₃ preservation study include the following (1) a general increase in CaCO₃ preservation between 0.9 and 1.6 Ma; (2) a CaCO₃ dissolution maximum near 0.9 Ma, primarily expressed in the Hole 818B fine aragonite record; (3) an abrupt and permanent increase of fine aragonite content between 0.86 and 0.875 Ma in both Holes 818B and 817A probably reflecting a dramatic increase of fine carbonate sediment production on the Queensland Plateau; (4) an improvement in CaCO₃ preservation near 0.87 Ma, which accompanied the increase of sediment input, indicated by the first appearance of whole pteropods in the deeper Hole 817A and a "spike" in the percent whole pteropods in Hole 818B; (5) a period of strong CaCO₃ dissolution during the mid-Brunhes Chron from 0.36 to 0.41 Ma; and (6) a complex CaCO₃ preservation pattern between 0.36 Ma and the present characterized by a general increase in CaCO₃ preservation through time with good preservation during interglacial stages and poor preservation during glacial stages.

The long-term aragonite preservation histories for Holes 818B and 817A appear to be similar in general shape, although different in detail, to CaCO₃ preservation records from the deep Indian and central equatorial Pacific oceans as well as from intermediate water sites in the Bahamas and the Maldives. All of these areas have experienced CaCO₃ dissolution at about 0.9 Ma and during the mid-Brunhes Chron. However, the late Quaternary (0 to 0.36 Ma) glacial to interglacial preservation pattern in Holes 818B and 817A is out of phase with CaCO₃ preservation records for sediments deposited in Pacific deep and bottom waters. The sharp increase in bank production and export from the Queensland Plateau and the coincident improvement of CaCO₃ preservation between 0.86 and 0.875 Ma may have been synchronous with the initiation of the Great Barrier Reef and roughly coincides with an increase in carbonate accumulation on the Bahama banks, in the western North Atlantic Ocean, and on Mururoa atoll, in the central South Pacific Ocean. The development of these reef systems during the middle Quaternary may be related to the transition in the frequency and amplitude of global sea level change from 41 k.y. low amplitude cycles prior to 0.9 Ma to 100 k.y. high amplitude cycles after 0.73 Ma.

Carbon isotopic analyses show that benthic foraminiferal δ¹³C values (*Cibicidoides* spp.) have been heavier than planktonic foraminiferal δ¹³C values (*G. sacculifer*) throughout most of the last 0.54 m.y., which may indicate that ¹³C-enriched intermediate water (AAIW) occupied the Townsville Trough during much of the late Quaternary. Furthermore, both planktonic and benthic foraminiferal δ¹³C values are often observed to be heaviest during interglacial to glacial transitions, and lightest during glacial to interglacial transitions. We suggest that this pattern is the result of changes in the preformed δ¹³C of ΣCO₂ of AAIW and may reflect changes in nutrient utilization by primary producers in Antarctic surface waters, changes in the δ¹³C of upwelled Circumpolar Deep Water, or changes in the extent and/or temperature of equilibration between surface water and atmospheric CO₂ within the Antarctic Polar Frontal Zone (the source area for AAIW). Finally, the poor correlation between percent of whole pteropods (aragonite preservation) and δ¹³C of *Cibicidoides* spp. may be the result of a decoupling of δ¹³C from CO₂ due to the numerous and complex variables that combine to produce the preformed δ¹³C of AAIW.

INTRODUCTION

The relationship between late Quaternary deep-sea carbonate sediments and climate change has been the subject of numerous studies in the past forty years since Arrhenius (1952) first suggested that cyclical variations in late Quaternary calcium carbonate (CaCO₃)

content may reflect climatically induced variations in surface water productivity. Although productivity is certainly a major factor governing the accumulation of CaCO₃ on the seafloor (Emerson and Bender, 1981; Arrhenius, 1988; Archer, 1990, 1991), it has become increasingly evident that water-column chemistry is often the dominant control on seafloor CaCO₃ accumulation via variations of CaCO₃ preservation (e.g., Berger, 1973; Farrell and Prell, 1989; 1991). CaCO₃ dissolution is known to increase with water depth due to the effect of hydrostatic pressure on the solubility of carbonate minerals (Hawley and Pytkowicz, 1969). In addition to the hydrostatic effect, high CO₂ concentrations in the water column also promote CaCO₃ dissolution. For instance, high pCO₂ is associated with the oxygen minimum zone that is present at middle and low latitudes in much of the world oceans at depths between 500 and 1000 m. In

¹ McKenzie, J.A., Davies, P.J., Palmer-Julson, A., et al., 1994. *Proc. ODP, Sci. Results*, 133: College Station, TX (Ocean Drilling Program).

² Department of Geology and Geophysics, Rice University, P.O. Box 1892, Houston, TX 77256, U.S.A.

³ Department of Geology and Geophysics, University of Edinburgh, West Mains Road, Edinburgh EH9 3JW, Scotland.

⁴ Geologisches Institut, ETH Zentrum, CH-8092 Zürich, Switzerland.

intermediate and deep water masses, $p\text{CO}_2$ increases with watermass age due to the accumulation of CO_2 through the oxidation of organic matter. Because the world oceans contain approximately 60 times the amount of carbon present in the atmosphere (mainly as bicarbonate [HCO_3^-] and carbonate [CO_3^{2-}]) and they are thought to control atmospheric carbon over time spans of 10^2 to 10^5 years (Broecker et al., 1980; Berger, 1985; Sundquist, 1985), an understanding of CaCO_3 precipitation and dissolution in seawater is extremely important if we are to decipher the possible relationship between atmospheric CO_2 fluctuations and global climate change.

Deep-water Paleocirculation: Seawater $p\text{CO}_2$ and CaCO_3 in Deep-sea Sediments

The preservation of CaCO_3 (primarily calcite) in modern deep-sea sediments is directly linked to ocean circulation. Today, relatively warm, saline, O_2 -rich, and CO_2 -poor North Atlantic Deep Water (NADW) forms by evaporative cooling in the high-latitude North Atlantic Ocean and flows southward to Antarctica, where it upwells and mixes with water of the Antarctic Circumpolar Current (Worthington, 1970; Dietrich et al., 1980). In the Antarctic region, Circumpolar Deep Water mixes with very cold and dense shelf water and sinks to the ocean floor to form Antarctic Bottom Water (AABW), while cold, low salinity surface water sinks within the Antarctic Polar Frontal Zone, in the vicinity of the Antarctic Polar Front (APF), to form Antarctic Intermediate Water (AAIW) (Glasby, 1990). The core of AAIW sinks to about 1000 mbsl and then ascends slightly as it flows northward where it can be traced to at least 10°S in the Pacific Ocean (Craig et al., 1981). Besides AABW, AAIW is the most important water mass spreading northward from the Southern Ocean (Glasby, 1990). The deep water in the Pacific Ocean (Pacific Common Water), which occupies water depths below AAIW and above AABW, is primarily a mixture of AABW, AAIW, and NADW (Dietrich et al., 1980). Pacific Common Water becomes increasingly nutrient and CO_2 -rich northward through the accumulated effects of organic matter oxidation. Modern deep-ocean circulation has been simply described as a thermohaline conveyor belt that begins in the high-latitude North Atlantic Ocean with the formation of NADW and ends with the upwelling of cold, nutrient-rich, O_2 -poor deep water in the North Pacific Ocean (Broecker et al., 1988). The pattern and strength of the deep-water circulation of the world ocean has varied through time as inferred from the variable distribution and preservation of CaCO_3 in deep-sea sediment cores (see Volat et al., 1980; Crowley, 1985; Farrell and Prell, 1989; and Berger, 1992 for a review) and from the study of paleoceanographic nutrient tracers such as $\delta^{13}\text{C}$ (see Curry et al., 1988, for a summary) and Cd/Ca (see Boyle, 1988a, for a summary) measured in fossil foraminifers.

Quaternary CaCO_3 preservation patterns of deep-sea sediments have been determined based on various dissolution indices. Among these, the most commonly used indices include CaCO_3 content, foraminifer (calcite) fragmentation, and foraminifer assemblages (Berger, 1968; Bé et al., 1975; Thunell, 1976; Peterson and Prell, 1985a). Until the early 1980s, it was widely accepted that the CaCO_3 preservation histories of the Atlantic and Indo-Pacific oceans were generally out of phase. In the Atlantic Ocean, preservation was determined to be poor during past glacial stages and good during interglacial stages (Gardner, 1975; Damuth, 1975; Volat et al., 1980; Balsam, 1983; Crowley, 1983; Diester-Haas, 1985). In contrast, the Indo-Pacific ocean was characterized by good CaCO_3 preservation during glacial stages and poor preservation during interglacial stages (Oba, 1969; Hays et al., 1969; Berger, 1973; Thompson and Saito, 1974; Pisiás et al., 1975; Adelseck, 1977; Volat et al., 1980). To explain the out-of-phase CaCO_3 preservation patterns, Luz and Shackleton (1975) and Crowley (1985) proposed a basin to basin fractionation of carbonate between the Atlantic and Indo-Pacific oceans linked to variability of NADW production.

The Quaternary CaCO_3 preservation pattern is apparently more complex than earlier suggested. Berger (1977) described a pteropod (aragonite) preservation "spike" in sediment cores from the Atlantic

Ocean that occurred during the transition from the last glacial maximum (LGM) to the Holocene. This CaCO_3 preservation spike was also identified in deeper water by an increase in foraminifer preservation centered on the transition from the LGM to the Holocene (Berger, 1977). By comparing CaCO_3 dissolution records spanning the last 0.4 m.y. from the eastern North Atlantic and the Pacific oceans, Crowley (1985) determined that the preservation history of the two basins has been out-of-phase at times, due to changes in deep-water production rates, and in-phase at times, due to changes in the partitioning between oceanic, terrestrial, and atmospheric carbon reservoirs. Similar findings have been presented for the deep Pacific Ocean (e.g., Farrell and Prell 1989, 1991) and for the Indian Ocean (Peterson and Prell, 1985; Williams et al., 1985). The globally in-phase episodes of CaCO_3 preservation/dissolution may be directly tied to rapid (on the order of 10^2 to 10^3 yr) changes in atmospheric CO_2 concentration related to sea-level induced changes in the shelf to basin fractionation of carbon (Broecker, 1982), to changes in the terrestrial biomass (Shackleton, 1977), to variations in surface-water productivity (Siegenthaler and Wenk, 1984; Sarmiento and Toggweiler, 1985; Toggweiler and Sarmiento, 1985; Keir, 1988; Martin, 1990), or to a restructuring of the deep and intermediate ocean circulation (Boyle and Keigwin, 1987). Long-term CaCO_3 preservation trends have also been identified in the deep-sea record. For instance, time intervals of unusually low CaCO_3 content, possibly due to intense dissolution of deep-sea carbonates, have been observed during the mid-Brunhes Chron between 0.2 and 0.6 Ma (Adelseck, 1977; Peterson and Prell, 1985b; Crowley, 1985; Farrell and Prell, 1989) and also near 0.9 Ma (Hays et al., 1969; Saito et al., 1975; Moore et al., 1982; Vincent, 1985; Farrell and Prell, 1991).

Intermediate-water Paleoceanography

Chemical Tracers

While the pattern of deep-sea carbonate preservation is beginning to emerge for the Quaternary, very little is known of the carbonate preservation history of intermediate water masses (roughly defined as waters between 500 and 2000 m). Due to the stability of calcite at intermediate water depths, very little calcite dissolution occurs within intermediate waters and, therefore, well-established calcite dissolution indices are generally not useful for studying intermediate-water CaCO_3 preservation. To reconstruct past intermediate water chemistry and circulation, most paleoceanographers have relied instead on chemical tracers of seawater nutrients measured on the tests of foraminifers. The most utilized tracers include $\delta^{13}\text{C}$, which becomes lighter (more negative) as nutrients increase, and the Cd/Ca ratio of foraminiferal calcite (Boyle, 1988a), which becomes greater as seawater $[\text{PO}_4^{3-}]$ increases (see Mix et al., 1991 for an excellent review of nutrient tracers in intermediate water). The link between nutrient concentrations and CaCO_3 preservation is through the following simplified reactions:



Boyle (1986a, 1986b, 1988b) suggested that a doubling of the overturn rate of intermediate waters during the LGM may have strengthened the biological pump by increasing upwelling of nutrients to surface waters and stimulating higher glacial surface-water productivity. The nutrients originating from intermediate water would have been transferred to deep waters via an increase in the rain of organic particulates. This mechanism, by which nutrients were transferred from intermediate to deep waters due to better ventilation of glacial intermediate waters, has been called the "Boyle Effect" (Mix et al., 1991). The "Boyle Effect" predicts that during the LGM, the deep ocean, as a whole, would have been Cd and nutrient enriched, ^{13}C -depleted, and more corrosive than today, whereas intermediate waters (<2000 m

water depth) would have been Cd and nutrient depleted, ¹³C-enriched, and less corrosive than today (Boyle, 1986a, 1986b, 1988b). One important consequence of the "Boyle Effect" is that higher surface-water productivity would have drawn down atmospheric pCO₂ and may have been at least partially responsible for the 80 p.p.m.v. lower glacial atmospheric CO₂ concentration measured in ice cores (Barnola et al., 1987). The "Boyle Effect" provides a good explanation for the heavy values of planktonic foraminiferal δ¹³C during the LGM, observed in numerous sediment cores from low and mid-latitudes (e.g., Curry and Crowley, 1987; Oppo and Fairbanks, 1989), and can also explain the glacial/interglacial intermediate and deep water foraminiferal δ¹³C and Cd/Ca records from the Atlantic Ocean and Caribbean Sea (Boyle and Keigwin, 1987; Cofer-Shabica, 1987; Oppo and Fairbanks, 1987; Zahn et al., 1987; Curry et al., 1988; Duplessy et al., 1988). Data from the Pacific Ocean, although less convincing, also support the Boyle nutrient transfer hypothesis (Mix et al., 1991). However, because of the small difference observed in the Pacific intermediate-to-deep δ¹³C gradient between glacial and interglacial stages, and the difference between the frequency of δ¹³C fluctuations and the CO₂ concentration measured in Antarctic ice cores, Mix et al. (1991) argued that the "Boyle Effect" could not have been the only mechanism responsible for the glacial to interglacial change in atmospheric pCO₂. Boyle's nutrient transfer hypothesis predicts that nutrient and Cd depleted, ¹³C-enriched intermediate water would have preserved CaCO₃ at intermediate water depths (<2000 m) during the LGM (and possibly during previous glacial stages) while nutrient and Cd enriched, ¹³C-depleted deep water would have been more corrosive to CaCO₃ (Le and Shackleton, 1992).

Metastable CaCO₃ Preservation

In addition to chemical tracers measured on foraminifers, aragonite should also be a good monitor of intermediate-water chemistry and circulation. Aragonite is a metastable polymorph of CaCO₃ that undergoes dissolution at much shallower water depths than calcite and is, therefore, sensitive to CaCO₃ saturation fluctuations above the calcite lysocline. Marine aragonite has two principal sources. First, aragonite is formed in the pelagic realm by pteropods and heteropods (from here on pteropods and heteropods will be grouped as "pteropods"). These holoplanktonic gastropods secrete an aragonitic shell within the upper 500 m of the ocean (Bé and Gilmer, 1977). Although pteropod ooze covers only 0.6% by area of the deep seafloor (Berger, 1978), pteropod aragonite may constitute as much as 50% of the total CaCO₃ flux out of the euphotic zone (Betzer et al., 1984). Until fairly recently, the importance of pteropod aragonite in the oceanic carbonate system has been greatly underestimated, primarily because of the relatively small amount of pteropod aragonite recovered in deep-sea sediments and in long-term deployment of sediment traps (Betzer et al., 1984). Secondly, in addition to pteropod aragonite, aragonite is the principal carbonate mineral organically produced and inorganically precipitated on carbonate platforms and reefs today. Aragonite mud, primarily produced by calcareous green algae or inorganically precipitated, is swept off shallow-water carbonate platforms and settles into the deep surroundings of carbonate banks (Supko, 1963; Kier and Pilkey, 1971; Neumann and Land, 1975; Boardman, 1978; Droxler et al., 1983; Droxler, 1984; Boardman and Neumann, 1984; Slowey, 1985; Shinn et al., 1989). Magnesian calcite (Mg calcite), produced by red algae and foraminifers, is also exported with aragonite into deep water. Mg calcite, characterized by an excess of >12 mol % Mg, is even more soluble than aragonite (Walter and Morse, 1984).

The seafloor accumulation of periplatform sediment is not only a function of input, which is primarily controlled by sea level (Supko, 1963; Kier and Pilkey, 1971; Boardman and Neumann, 1984), but is also a function of seafloor preservation (Droxler et al., 1983; Droxler, 1984; Haddad, 1986; Droxler et al., 1988; Droxler et al., 1990; Glaser and Droxler, in press). Droxler et al. (1988, 1991) demonstrated, in the Bahamas and the Caribbean Sea, that the aragonite and Mg calcite

content in surficial sediments is directly related to the saturation state of the water column with respect to these minerals. Droxler et al. (1983) suggested that aragonite cycles, present in late Quaternary sediments near the Bahama Banks, were the result of climatically-induced fluctuations of aragonite preservation and thus were analogous to CaCO₃ cycles identified in cores from the deep North Atlantic Ocean. However, because aragonite input is in-phase with the interpreted preservation history in the Bahamas (high input with good preservation, low input with poor preservation), it is difficult to separate the input and preservation signals. Based on the work of Chen (1964, 1968), Berner et al. (1976), Berner (1977), Berger (1978), Berner and Honjo (1981), Byrne et al. (1984), and Betzer et al. (1984), Haddad (1986) showed that pteropod preservation can be used to help separate the relative importance of aragonite input vs. aragonite preservation in periplatform sediments. This study showed that, during the past 0.5 m.y., pteropods were more fragmented and often more dissolved (as determined by Scanning Electron Microscopy) during glacial intervals than during interglacial intervals at water depths as shallow as 665 m within the Northwest Providence Channel, Bahamas. Further work on periplatform records from the Maldives has shown that pteropod fragmentation is a much more sensitive monitor of aragonite preservation, near the aragonite saturation depth, than is fine aragonite content (Droxler et al., 1990; Cullen and Droxler, 1990). However, at periplatform water depths considerably below the aragonite saturation depth, where pteropods are rare or absent, the input signal of metastable carbonate can be strongly overprinted by dissolution (Droxler et al., 1990).

Study Objectives

This study of Quaternary periplatform sediments in the Queensland Plateau region of the southwest Pacific Ocean is part of our effort to determine the global extent of long-term aragonite preservation patterns within intermediate water depths. Previous studies of long records from the Bahamas and the Maldives have shown striking similarities in aragonite content and particularly in pteropod fragmentation, with pronounced dissolution maxima at 0.35 to 0.4 Ma and near 0.9 Ma (Droxler et al., 1988; Droxler et al., 1990; Haddad et al., 1990). Both of these intervals are characterized by unusually high CaCO₃ dissolution in deep-sea records (Hays et al., 1969; Vincent, 1985; Crowley, 1985; Farrell and Prell, 1989, 1991). Intermediate-water CaCO₃ preservation is important in the context of emerging theories tying global CO₂ change to ocean circulation and the exchange of carbon between surface, intermediate, deep, and bottom water reservoirs. Holes 818B and 817A, drilled during ODP Leg 133, were recovered from intermediate water depths and contain Quaternary records of periplatform and nannofossil ooze. We have generated detailed records of percent of fine aragonite and Mg calcite content, percent whole pteropods, and foraminiferal δ¹⁸O and δ¹³C to address the following questions:

1. What is the Quaternary history of shallow carbonate production on the Queensland Plateau as recorded by aragonite and Mg calcite input into the adjacent Townsville Trough?
2. What is the age relationship, if any, between Quaternary carbonate production on the Queensland Plateau, the Great Barrier Reef, and on other platforms of the world?
3. What is the Quaternary carbonate preservation history within intermediate waters of the Townsville Trough?
4. How does Quaternary metastable carbonate preservation in the Townsville Trough compare to other intermediate and deep-water CaCO₃ preservation records from the Pacific, Indian, and Atlantic oceans?
5. What has been the relationship between surface and intermediate water δ¹³C within the Townsville Trough and how might these δ¹³C data relate to changes in AAIW formation and surface-water productivity during the Quaternary?

MODERN HYDROGRAPHY AND PHYSIOGRAPHY

Holes 818B and 817A were drilled on the southern slope of the Queensland Plateau on the northern margin of the Townsville Trough (Fig. 1). Hole 818B was drilled at a water depth of 745 mbsl on an inclined terrace of the middle slope (18°3.8'S; 150°2.5'E). Hole 817A was drilled at 1016 mbsl on the lower slope ~30 km to the southwest of Site 818B (19°9.5'S; 149°45.5'E). These sites lie within the AAIW mass, which sinks within the Antarctic Polar Frontal Zone, in the vicinity of the APF (Glasby, 1990), and flows northward at depths between 500 and 1500 m into the South Atlantic, the Indian, and the South Pacific oceans (Dietrich et al., 1980). This water mass flows into the Townsville Trough from the southeast at a depth of 650 to 1100 m (AAIW core depth 700–1000 m) (Wyrki, 1960). AAIW can be recognized in the Coral Sea by a range of water temperatures from 4° to 6°C, low salinity from 34.2‰ to 34.5‰ and a relatively high O₂ concentration of 4.2 mL/L (Pickard et al., 1977).

The dominant surface currents along the south margin of the Townsville Trough are from the north-northwest. During the winter months, the South Equatorial Current flows from east to west over the Queensland Plateau, then turns south through the Townsville Trough and joins the East Australian Current (Pickard et al., 1977). Surface circulation during the summer months is influenced by the Northwest Monsoon Current (Pickard et al., 1977). Tropical cyclones also affect this area, with an average of two each year in the western Coral Sea (Pickard et al., 1977). These cyclones enter the study area from the northeast and likely influence sediment dispersal. Modern surface-water temperatures in this region range from 26° to 29°C during the austral summer and from 21° to 26°C during the austral winter (Pickard et al., 1977).

The nearest source of shallow-water carbonate to Holes 817A and 818B is Tregrosse Reef, located 30 km to the northeast of Hole 818B and 60 km northeast of Hole 817A. Tregrosse Reef is a 5100-km² atoll-type carbonate platform characterized by a 40- to 60-m-deep lagoon rimmed by a barrier reef (Davies, McKenzie, Palmer-Julson, et al., 1991). Other neighboring reefs on the Queensland Plateau include Flinders Reef and Holmes Reef located to the northwest, and Coringa Bank located to the north of Holes 818B and 817A. The Great Barrier Reef is located approximately 120 km to the southwest of Hole 817A on the southwest margin of the Townsville Trough. Fine carbonate sediments produced on the Queensland Plateau, and possibly a minor component from the Great Barrier Reef, are swept into deep water and accumulate today on the slope of the Queensland Plateau and within the Townsville Trough (Davies, McKenzie, Palmer-Julson, et al., 1991).

METHODS AND STRATIGRAPHY

Sample Processing and Sediment Description

The Quaternary section of Hole 817A was sampled every 20 cm down to Section 133-817A-7H-5, 108–110 cm (60.28 mbsf), and then one sample per section was taken down to 133-817A-8H-1, 65–67 cm (63.35 mbsf). Hole 818B was sampled every 20 cm down to Sample 133-818B-3H-CC, 5–7 cm (27.28 mbsf), and then three samples per section were taken (approximately 1 sample/50 cm) down to Sample 133-818B-9H-7, 115–117 cm (84.55 mbsf). Care was taken during sampling to avoid disturbed zones at the top and bottom of each core section.

Pleistocene sediments sampled in Holes 818B and 817A can be generally classified as micrite ooze, but shipboard descriptions range from nannofossil micrite ooze to foraminifer micrite ooze with bioclasts, pteropod shells, and nannofossils (Davies, McKenzie, Palmer-Julson, et al., 1991). All samples contain benthic and planktonic foraminifers. Fine aragonite (exported from adjacent banks and reefs) content reaches 30% or more for most of the Quaternary section (0–84.55 mbsf) of Hole 818B and in the upper 41.75 m of Hole 817A.

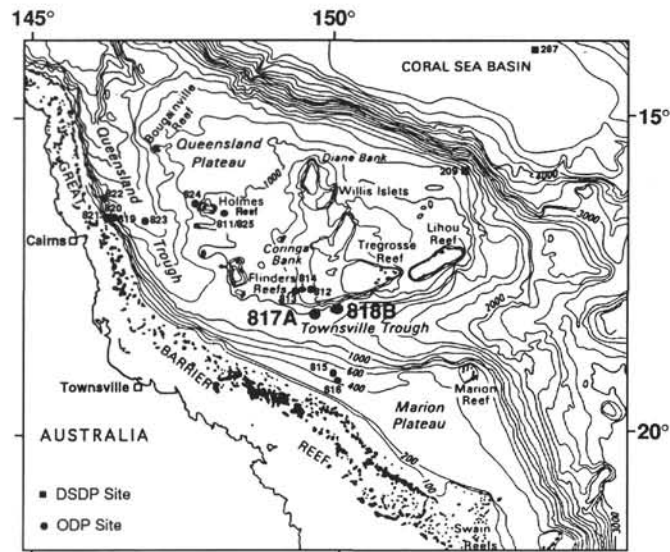


Figure 1. Location map for Holes 818B and 817A.

Thus, these sediments can be further classified as periplatform ooze after Schlager and James (1978).

Each 10-cm³ sample was oven-dried at 60°C and weighed. Dried samples were soaked in pH 8 buffered distilled water and then wet-sieved through a 63-μm mesh screen. The coarse fraction (>63 μm) was dried, weighed, and dry-sieved to separate (1) the 300 to 355-μm size fraction for stable isotopic analysis of planktonic foraminifers, and (2) the >355-μm fraction for pteropod fragmentation study. The fine fraction (<63 μm) was allowed to settle in beakers until the water cleared. Water then was decanted and the fine fraction was oven-dried at 60°C and weighed. The percent fine fraction was determined by the ratio: % Fine = fine fraction weight / (fine fraction weight + coarse fraction weight) × 100. All % Fine values are listed in Appendixes A and B.

Carbonate Content and Mineralogy of the Fine Fraction

CaCO₃ content of the fine fraction (<63 μm) was determined by carbonate bomb (Müller and Gastner, 1971). A known amount of sample was placed in a sealed chamber, attached to a pressure gauge, and reacted with 50% concentrated HCl. The pressure generated by CO₂ gas evolved during the dissolution reaction was measured and compared to the pressure released from reacting a known amount of 100% CaCO₃ standard. Percent of CaCO₃ was then calculated by the simple ratio:

$$\% \text{CaCO}_3 = (P \text{ sample} / Wt \text{ sample}) / (P \text{ standard} / Wt \text{ standard}) \times 100,$$

where P = pressure, and Wt = weight. Precision for the method was ±2% as determined from analyzing sample replicates. The composition of the insoluble residue was not determined. Values of percent of carbonate in the fine fraction are listed in Appendixes A and B.

Relative proportions of fine fraction (<63 μm) aragonite, calcite, and Mg calcite were determined by X-ray-diffraction analyses. Samples were powdered by lightly grinding them in an agate mortar and were packed, with the use of a spatula, into aluminum sample holders, according to the procedure of Milliman (1974). Each sample was analyzed using a Phillips-Norelco Model 12045 diffractometer driven by Dapple Systems Controller Thetaplug software. X-rays were generated using a Cu-Kα source set at 35 kV and 30 mA. A scan of 25.5° to 27.5° was used to determine the primary aragonite peak, and a second scan from 28.5° to 32° was used to identify calcite, Mg calcite,

and dolomite peaks. Areas under the primary aragonite peak and the deconvolved magnesian calcite and calcite peaks were integrated above the background radiation counts. Reproducibility of the deconvolution method was better than 5%. Aragonite content was determined by comparing the ratio of aragonite to calcite (calcite and Mg calcite) for each sample to a standard curve. Mg calcite content, and dolomite if present, was calculated assuming a linear relationship between Mg calcite, dolomite, and calcite. The precision of this technique is better than 5% (Droxler, 1984). Mineralogic data are presented in Appendixes A and B as % Fine Aragonite = % Aragonite in the fine fraction \times % CaCO₃ the fine fraction; % Fine Calcite = % Calcite in the fine fraction \times % CaCO₃ in the fine fraction; % Fine Mg Calcite = % Mg calcite in the fine fraction \times % CaCO₃ in the fine fraction.

Percentage of Whole Pteropods

The percentage of whole pteropods was determined for the >355 μm size fraction. Samples were split to 500 to 1000 grains, and all whole pteropods, pteropod fragments, and "other grains" were counted. Pteropods were considered to be fragmented if more than half of the shell was broken. No correction was made for physical breakage resulting from sample processing. "Other grains" mostly consisted of planktonic and benthic foraminifers, with minor amounts of bioclasts and cemented grains. Pteropod data are presented as Percent whole pteropods = (# whole pteropods)/(# whole + # fragmented pteropods) \times 100. If no pteropods were present in a sample, a percent whole pteropods value of 0% was assigned. It is important to note that the absence of pteropods can be the result of dissolution or nondeposition. We were unable to determine which of these factors was more important. All data are listed in Appendixes A and B.

Evaluation of Dissolution Indices

Holes 818B and 817A were drilled in water depths near the present aragonite lysocline of 1000 m, as projected from GEOSECS Station 269 in the western South Pacific Ocean (Broecker et al., 1982) (Fig. 2). Thus, downcore variation of the fine aragonite content in these holes should primarily record an input signal overprinted by dissolution during time intervals when the aragonite lysocline was shallower than today. The same scenario should hold for the downcore variation of Mg calcite. However, the Mg calcite record is hard to interpret as a partial dissolution/preservation record because, in addition to bank-derived Mg calcite sediments, Mg calcite cements, with decreasing Mg concentrations with increasing water depth, commonly form at water depths shallower than 1200 m near carbonate platforms (Schlager and James, 1978). Furthermore, Mg calcite is highly diagenetically reactive (Schlanger and Douglas, 1974) and is rarely present at great depth below the seafloor in periplatform sediments.

Aragonite and Mg calcite may also dissolve within sediments deposited above the aragonite and Mg calcite lysoclines. In a study of calcite dissolution on the Ninetyeast Ridge, Peterson and Prell (1985a) documented up to 60% fragmentation of foraminifers and 20% to 30% loss of CaCO₃ above the calcite lysocline. In this case, dissolution was attributed to corrosive pore waters which resulted from oxidation of organic matter in the sediments. Emerson et al. (1985) used models that estimated the particulate organic carbon flux to the sediment-water interface and determined that a major fraction of this carbon flux degrades within the sediments. Supralysocline organic carbon degradation within the sediments can not be ruled out as a factor in promoting dissolution in Holes 818B and 817A. However, $\delta^{13}\text{C}$ values of *G. sacculifer* (generally less than 1.5‰ PDB) indicate that surface-water productivity was relatively low in this region of the Townsville Trough during the Quaternary and, therefore, organic carbon flux to the seafloor may have been low as well. In addition, high oxygen levels within AAIW should have strongly enhanced oxidation of organic matter settling through the water column and on the seafloor prior to its burial.

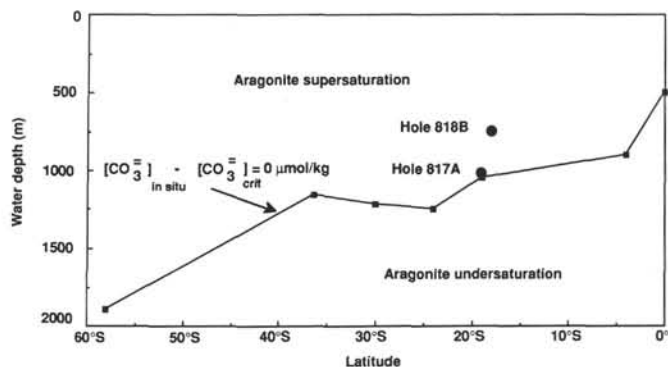


Figure 2. Aragonite saturation depth versus latitude for the western South Pacific Ocean compiled from GEOSECS data (Broecker et al., 1982). The saturation depth is defined after Broecker and Takahashi (1978) as the depth in which $[\text{CO}_3^{2-}]_{\text{in situ}} - [\text{CO}_3^{2-}]_{\text{crit}} = 0$. $[\text{CO}_3^{2-}]_{\text{in situ}}$ is the measured $[\text{CO}_3^{2-}]$ at in-situ temperature and pressure and $[\text{CO}_3^{2-}]_{\text{crit}} = 93 \times e^{0.14(Z-4)} \mu\text{mol/kg}$ where Z is water depth in km.

In spite of their limitations, the percent of fine aragonite and fine Mg calcite content were considered as dissolution indices due to their sensitivity to changes in the carbonate saturation state of intermediate waters (Droxler et al., 1988; Droxler et al., 1991). However, because preservation can be synchronous with high sea level and high input of metastable carbonates, and dissolution can be synchronous with low sea level and low input of metastable carbonates, it is not feasible to separate the input from dissolution signals by determining the percent flux of fine aragonite and Mg calcite content alone. Pteropods, on the other hand, potentially provide the means to separate the input and dissolution signals because they are a planktonic source of aragonite and their occurrence and fragmentation are not directly related to bank-top processes or sea level change.

The percent of whole pteropods (a measure of pteropod fragmentation) was used as a dissolution index, analogous to indexes of calcite dissolution in deep-sea sediments based upon foraminiferal fragmentation (Berger, 1968; Bé et al., 1975; Thunell, 1976; Peterson and Prell, 1985a). Studies of modern seafloor sediments have shown that pteropod fragments increase below the aragonite lysocline because partial dissolution of the thin pteropod shells makes them more susceptible to breakage (Chen, 1968; Almogi-Labin et al., 1986). Percent of whole pteropods was used rather than simply the abundance of pteropods because changes in pteropod abundance may largely be related to pteropod productivity and bear little relationship to preservation (Gardulski et al., 1986). We were not able to completely avoid the complication of variable pteropod productivity, however, because we calculated a percent of whole pteropods value of 0% if the sample contained no pteropods. Clearly a sample that is void of pteropods may simply be the result of no pteropod productivity and have no relationship to aragonite dissolution.

Variable dissolution susceptibility between different pteropod species is a function of shell surface area (Acker, 1988) and can be a limiting factor in the use of percent whole pteropods as a dissolution index. A percent whole pteropod record that does not take the pteropod assemblage into account may be skewed at times towards dissolution or preservation depending on whether dissolution susceptible or resistant forms dominate. Finally, pteropod fragmentation can also occur in the absence of dissolution. Pilska (1989) collected pteropod fragments in long-duration sediment traps deployed above the aragonite saturation depth in the Northwest Providence Channel, Bahamas. Pteropod fragmentation may result from predation by fish and whales (Bé and Gilmer, 1977) and the fragility of pteropod shells makes them prone to breakage on the seafloor under the influence of strong bottom currents and bioturbation. Some breakage is unavoidable during sample processing.

Stable Isotope Analyses

The planktonic foraminifer *Globigerinoides sacculifer* was used for stable oxygen and carbon isotopic analyses. From 20 to 30 individuals of *G. sacculifer* were hand-picked from a narrow size fraction between 300 and 355 μm in order to reduce ontogenetic effects on the measured isotopic composition (see Oppo and Fairbanks, 1989). Samples were ultrasonically cleaned in distilled water to remove any fine material clinging to the tests. Cleaned foraminifer tests were reacted with orthophosphoric acid at 90°C and the evolved CO_2 gas was analyzed using a VG Isogas Precision Isotope Ratio Mass Spectrometer (PRISM) (D. Kroon, University of Edinburgh, Stable Isotope Laboratory). Foraminifer samples were run with a stable marble reference (SMI) and measured values were converted to the PDB standard. Precision for $\delta^{18}\text{O}$ analyses was $\pm 0.085\text{‰}$ (the standard deviation for 100 analyses of SMI, performed over several months). Precision for $\delta^{13}\text{C}$ analyses was $\pm 0.04\text{‰}$. All $\delta^{18}\text{O}$ and $\delta^{13}\text{C}$ values for *G. sacculifer* in Hole 818B and $\delta^{18}\text{O}$ values for *G. sacculifer* in Hole 817A are tabulated in Appendixes A and B, respectively. Reported isotope data cover the entire Quaternary for Hole 818B and the last 1.0 m.y. for Hole 817A.

The foraminifer *Cibicidoides* spp. was used to determine benthic stable oxygen and carbon isotopic ratios for the top 17.95 m of Hole 818B. About 5 to 10 specimens of *Cibicidoides* spp. from the 300 to 355 μm size fraction of each sample were sonicated with hydrogen peroxide and distilled water and then roasted in vacuo at 400°C for one hour. Samples were then reacted in a common acid bath of orthophosphoric acid at 82°C on a VG Isogas Autocarbonate preparation system. Isotopic ratios of purified CO_2 gas were measured on-line with a triple collector VG Isogas Precision Isotope Ratio Mass

Spectrometer (PRISM) (D. Müller, ETH-Zürich, Stable Isotope Laboratory). Isotopic ratios are expressed in standard notation relative to PDB. Analytical precision was $\pm 0.13\text{‰}$ for $\delta^{18}\text{O}$ and $\pm 0.06\text{‰}$ for $\delta^{13}\text{C}$. All stable isotope data are tabulated in Appendixes A and B.

Biostratigraphy

Nannostratigraphy datums are based on shipboard and shore-based research of S. Gartner. Pleistocene nannofossil biohorizons used for this study include *Emiliana huxleyi* FAD (0.275 Ma), *Pseudoemiliana lacunosa* LAD (0.465 Ma), small *Gephyrocapsa* Acme top (0.93 Ma), *Gephyrocapsa* Acme base (1.1 Ma), and *Calcidiscus tropicus* LAD (1.48 Ma). For a discussion of nannostratigraphy methods, the reader is referred to Gartner (this volume). The only foraminifer datum used from the Pleistocene was the *Globigerinoides ruber* (pink) LAD at the boundary between stages 6 and 5e (Thompson et al., 1979). The disappearance of *G. ruber* (pink) is thought to have been synchronous throughout the Indian and Pacific oceans. The *Globigerinoides fistulosus* LAD (1.6 Ma) was used to define the boundary between the Pliocene and Pleistocene.

Age Models for Holes 818B and 817A

The Quaternary age models for Holes 818B and 817A are based on oxygen isotope stratigraphy, nannostratigraphy, and foraminiferal biostratigraphy. Magnetostratigraphic studies proved unsuccessful in Sites 818 and 817. Table 1 shows the various datum levels used to convert depth to age and Figures 3A and 3B are graphs of age vs. depth for the Quaternary sections of Holes 818B and 817A.

Table 1. Oxygen isotope and biostratigraphic control for depth to age conversion.

Age (Ma)	Datum level ^a	Depth (mbsf)	
		Hole 818B	Hole 817A
0.012	Stage 1/2 boundary	1.25	1.04
0.024	Stage 2/3 boundary	2.35	1.56
0.059	Stage 3/4 boundary	3.25	4.95
0.071	Stage 4/5 boundary	4.05	5.95
~ 0.125	HO <i>Globigerinoides ruber</i> (pink) ¹	8.36	15.25
(0.125/0.220)	Hiatus 818B	(8.36/8.40)	
0.128	Stage 5/6 boundary	-	16.25
0.186	Stage 6/7 boundary	-	19.45
0.245	Stage 7/8 boundary	9.05	23.75
0.275	LO <i>Emiliana huxleyi</i> ²	9.53	25.07
0.303	Stage 8/9 boundary	10.54	26.75
(0.323/0.352)	Hiatus 818B	(11.04/11.10)	
(0.32/0.748)	Hiatus 817A	(27.60/27.75)	
0.362	Stage 10/11 boundary	11.44	-
0.423	Stage 11/12 boundary	13.52	-
0.465	HO <i>Pseudoemiliana lacunosa</i> ³	14.03	-
0.478	Stage 12/13 boundary	16.14	-
0.524	Stage 13/14 boundary	17.44	-
0.565	Stage 14/15 boundary	19.15	-
0.620	Stage 15/16 boundary	25.65	-
0.659	Stage 16/17 boundary	26.65	-
0.760	Stage 20/21 boundary	-	29.10
0.780	Stage 21/22 boundary	-	31.45
0.807	Stage 22/23 boundary	-	34.53
0.830	Stage 23/24 boundary	-	36.03
0.850	Stage 24/25 boundary	-	36.75
0.870	Stage 25/26 boundary	-	40.50
0.880	Stage 26/27 boundary	-	42.25
0.920	Stage 27/28 boundary	-	43.40
0.93	Stage 28/29 boundary	-	44.50
0.93	HO small <i>Gephyrocapsa</i> Acme top ⁴	53.51	45.56
1.1	LO small <i>Gephyrocapsa</i> Acme top ⁵	-	51.56
1.48	HO <i>Calcidiscus tropicus</i> ⁶	80.51	63.09
(1.49/1.60)	Hiatus 817A		(63.35/63.45)
(1.56/2.29)	Hiatus 818B	(84.25/84.58)	
1.60	HO <i>Globigerinoides fistulosus</i>	-	63.45
1.88	HO <i>Discoaster brouweri</i>	-	72.56
(1.88/2.58)	Hiatus 817A		(72.56/72.60)

Note: 1-6 = biostratigraphic datums keyed to arrows in Figures 3-5.

^aAges for isotope stages 1 through 17 are from SPECMAP (Imbrie et al., 1984). Stages 20 through 29 are from Ruddiman et al. (1989).

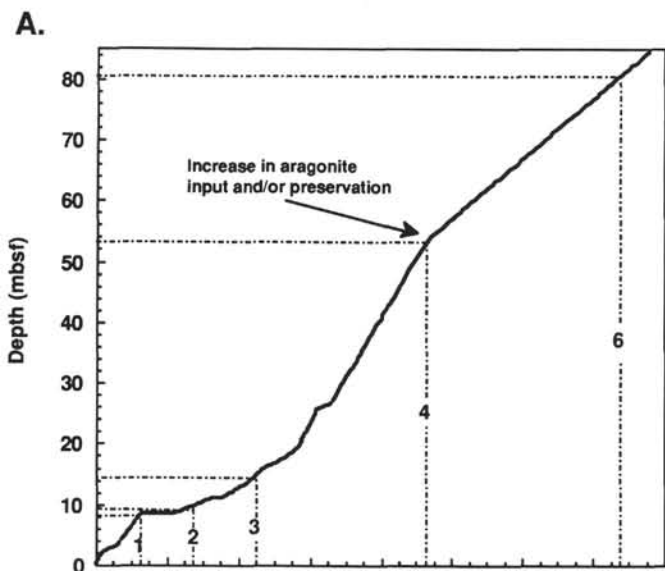


Figure 3. Age vs. depth curves. **A.** Top 84.5 m of Hole 818B. **B.** Top 63 m of Hole 817A. Numbers on dashed lines indicate the biostratigraphic control and are keyed to Table 1.

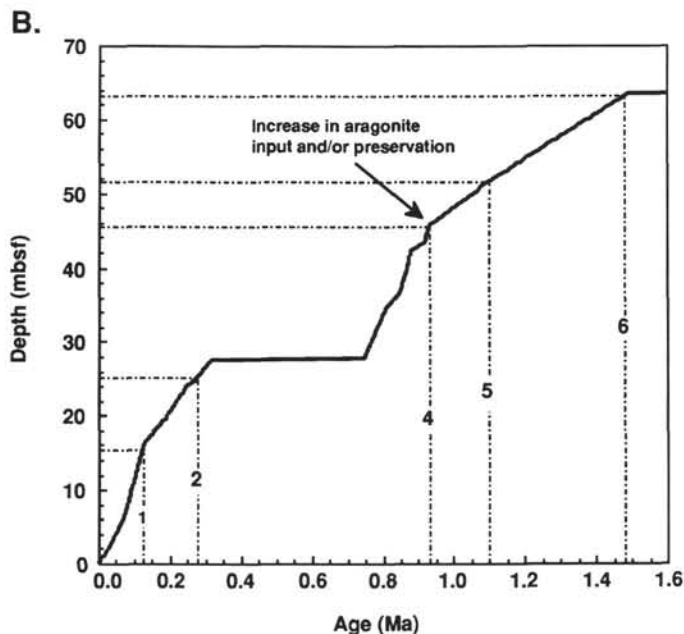


Figure 3 (continued).

Hole 818B

Constrained by the *Emiliania huxleyi* FAD and the *Pseudoemiliania lacunosa* LAD, we were able to identify $\delta^{18}\text{O}$ stages 1 through 17 with only two short duration hiatuses. By using the SPECMAP stacked $\delta^{18}\text{O}$ record and chronology (Imbrie et al., 1984) for the identification and age assignment of isotope stages and boundaries, we placed the first hiatus at a depth of 8.36 m (0.125–0.220 Ma) and the second hiatus at 10.84 m (0.315–0.320 Ma). We also used the *Globigerinoides ruber* (pink) LAD to define the datum corresponding to the boundary between stages 6 and 5/6 (5e) at 8.36 mbsf. This marker gave us confidence that a hiatus existed between stages 5 and 7 and not higher in the core. Below the stage 16/17 boundary, we were unable to identify stage boundaries with much confidence, although

our $\delta^{18}\text{O}$ record exists to 3.0 Ma (see also Droxler et al., this volume). Therefore, below 26.65 mbsf (0.659 Ma) we have used only nannostratigraphy to define the datum levels. A major hiatus was identified at 84.25 mbsf that separates the earliest Pleistocene (1.56 Ma) from late Pliocene (2.29 Ma) sediments. Core depths were converted to age by assuming that sedimentation rates were constant between the various datum levels.

Hole 817A

With the aid of nannostratigraphy, we have identified $\delta^{18}\text{O}$ stages 1 through 8 and 21 through 26. The ages for isotope stages 1 through 8 were determined by correlation to SPECMAP (Imbrie et al., 1984). The *Globigerinoides ruber* (pink) LAD (stage 5e) at 15.25 mbsf gave confidence to our assignment of the stage 5/6 boundary. Because of the close stratigraphic spacing of *E. huxleyi* FAD at 26.75 m (0.275 Ma), *P. lacunosa* LAD at 28.07 m (≥ 0.465 Ma), and the small *Gephyrocapsa* Acme top LAD at 45.56 m (0.93 Ma), we identified a major hiatus at 27.75 m (0.32–748 Ma). The ages for isotope stages 21 through 29 were determined by correlation to the orbitally tuned and stacked $\delta^{18}\text{O}$ record from Site 607 in the North Atlantic Ocean (Ruddiman et al., 1989). Below a core depth of 44.25 m, we relied solely on nannostratigraphy and foraminiferal biostratigraphy datums to construct our age model. Based on the assumption that sedimentation rates were constant between datums, we identified a possible hiatus at 63.35 mbsf (1.49–1.60 Ma).

RESULTS

Data Presentation

All data are plotted vs. both depth (Figs. 4 and 5) and time. However, in the "Results" section (this chapter) we have chosen to describe the data relative only to time, based on our age model developed in the preceding section and shown in Figures 3A and 3B. The Quaternary record of (1) percentage of fine aragonite content, (2) percentage of fine Mg calcite content, and (3) percentage of whole pteropods ($>355 \mu\text{m}$), presented below, is subdivided into three intervals from 0 to 0.5 Ma, 0.5 to 1.0 Ma, and 1.0 to 1.6 Ma to allow the records to be read more easily. All data for Holes 818B and 817A are listed in Appendixes A and B.

Percentage of Fine Aragonite

Hole 818B

Figure 6 shows the Quaternary variations in Hole 818B of percent of fine aragonite content and the planktonic $\delta^{18}\text{O}$ record based on *Globigerinoides sacculifer*. For the interval from 1.0 to 1.6 Ma, the percent of fine aragonite content fluctuated between 35% and 60% with an overall 10% increase in the aragonite content from an average of 42% at 1.5 Ma to an average of 52% at 1.0 Ma (Fig. 6C). Fine aragonite content generally co-varies with the $\delta^{18}\text{O}$ record; low aragonite values correspond to heavy $\delta^{18}\text{O}$ values and high aragonite values correspond to light $\delta^{18}\text{O}$ values. Exceptions to this general relationship include intervals from 1.275 to 1.375 Ma and 1.075 to 1.1 Ma during which low percent of fine aragonite content corresponds to light $\delta^{18}\text{O}$ values and high percent of fine aragonite content values corresponds to heavy $\delta^{18}\text{O}$ values.

A short duration minimum of aragonite content (40%) centered at 0.87 Ma is followed by an abrupt and permanent increase in the percent of fine aragonite content occurring near 0.86 Ma (Fig. 6B). The average percent of fine aragonite content increased at that time from 52% for the interval from 0.87 to 1.0 Ma, to values that averaged 60% for the interval from 0 to 0.86 Ma. As observed for the early Pleistocene, $\delta^{18}\text{O}$ and aragonite generally covary; most aragonite minima correspond to heavy $\delta^{18}\text{O}$ values and most aragonite maxima correspond to light $\delta^{18}\text{O}$ values. The relationship between the aragonite and $\delta^{18}\text{O}$ records for the interval from 0 to 0.5 Ma is, however, not as clear as in the early

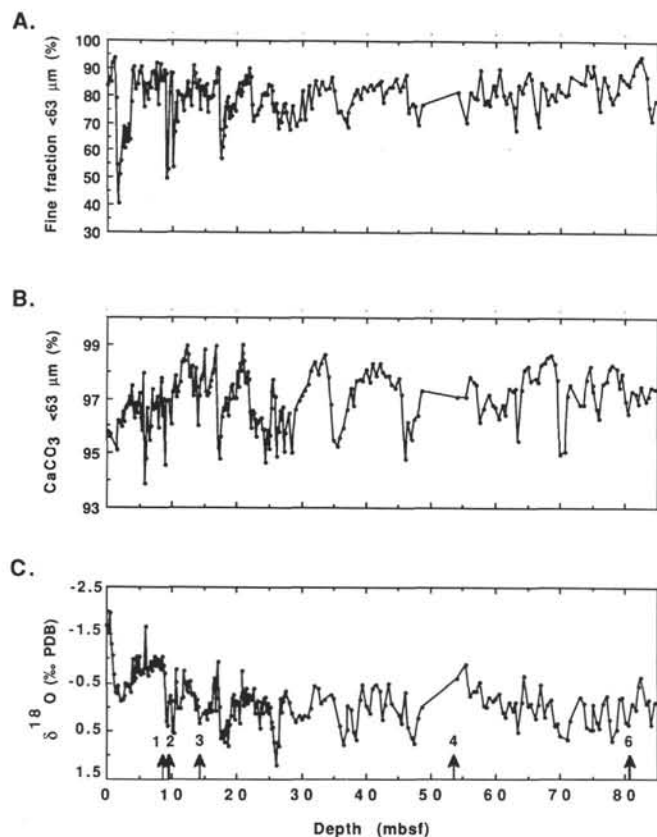


Figure 4. Depth variations for the top 84.5 m of Hole 818B. **A.** Percentage of fine fraction (<63 μm). **B.** Percentage of CaCO₃ (<63 μm) content. **C.** δ¹⁸O (‰ PDB) for *Globigerinoides sacculifer*. **D.** Percentage of aragonite in the fine fraction. **E.** Percentage of Mg calcite in the fine fraction. **F.** Percentage of whole pteropods (>355 μm). Numbers with arrows in Figures 4C and 4F refer to biostratigraphic markers listed in Table 1.

and middle Pleistocene (Fig 6A). Although there is very little variation in the percent of fine aragonite content between 0 and 0.5 Ma, it is worth noting that the interval from 0.35 to 0.475 Ma is marked by relatively high aragonite content during glacial stage 12 (heavy δ¹⁸O values), and low aragonite content during interglacial stage 11 (Fig. 6A). This is the reverse of the relationship commonly observed between δ¹⁸O and fine aragonite earlier in the record.

Hole 817A

Figure 7 displays the Quaternary record of percent of fine aragonite content and the δ¹⁸O values measured for *G. sacculifer* in Hole 817A. δ¹⁸O analyses were not performed on samples older than 0.975 Ma. No aragonite occurs in Hole 817A within Pliocene or older sediments (Droxler et al., this volume; Davies, McKenzie, Palmer-Julson, et al., 1991). From 1.0 to 1.6 Ma, the percent of fine aragonite content fluctuates between 0% and 20% and displays a general increase from the first appearance of aragonite at 1.6 Ma (Fig. 7C). The early Pleistocene aragonite fluctuations appear to be cyclical. Eleven aragonite cycles can be identified between 0.9 and 1.35 Ma (Figs. 7B and 7C) resulting in an average duration of 41 k.y. per cycle. A step 45% in the percent of fine aragonite record occurs at 0.875 Ma, when aragonite values abruptly increase from 5% at 0.9 Ma to 50% at 0.875 Ma (Fig. 7B). This conspicuous step in the aragonite content is nearly synchronous with the 8% step observed in Hole 818B (Fig. 6B). The percent of fine aragonite content generally remains higher in the interval following the distinct step than before and averages approximately 40% between 0.75 and 0.875 Ma. Nearly 0.5 m.y. is

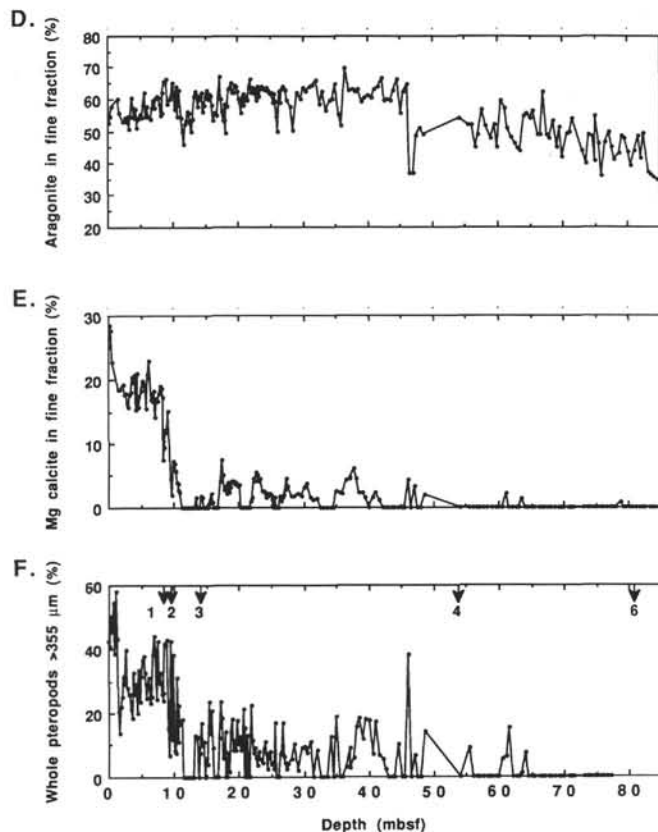


Figure 4 (continued).

missing in the Hole 817A record during the middle and late Pleistocene corresponding to the period between 0.32 and 0.75 Ma. No clear correlation between the δ¹⁸O record and the percent of fine aragonite content is evident prior to the hiatus. After the hiatus, the percent of fine aragonite content fluctuates between 30% and 50%, averaging 40% as during the interval before the hiatus (Fig. 7A). The aragonite and δ¹⁸O records clearly covary during the interval from 0 to 0.32 Ma; high aragonite content corresponds to light δ¹⁸O values (interglacial stages) and low aragonite content corresponds to heavy δ¹⁸O values (glacial stages).

Percentage of Fine Mg Calcite

Hole 818B

The Quaternary records of percent of fine Mg calcite content and the δ¹⁸O measured for *G. sacculifer* for Hole 818B are compared in Figure 8. Mg calcite only sporadically occurs during the interval from 1.0 to 1.6 Ma (Fig. 8C) with trace values of 2% or less at 1.44 (first occurrence of Mg calcite in Hole 818B), 1.3, and 1.08 Ma. During the interval from 0.5 to 1.0 Ma (Fig. 8B), Mg calcite intermittently occurs with average values of 5%. Mg calcite is barely detectable in stage 12 (0.425–0.475 Ma) with values not exceeding 2% (Fig. 8A). Mg calcite is totally absent from 0.35 to 0.42 Ma during stage 11 and early stage 10. After the hiatus from 0.32 to 0.352 Ma, and before the hiatus from 0.125 to 0.220 Ma (late stage 9 through early stage 7), Mg calcite values vary from 2% to 15%. After the hiatus from 0.125 to 0.220 Ma, Mg calcite content averaged 17% and fluctuated very little before increasing to 28% during stage 1.

Hole 817A

The Quaternary records of percent of fine Mg calcite content and δ¹⁸O measured for *G. sacculifer* in Hole 817A, are shown in Figure

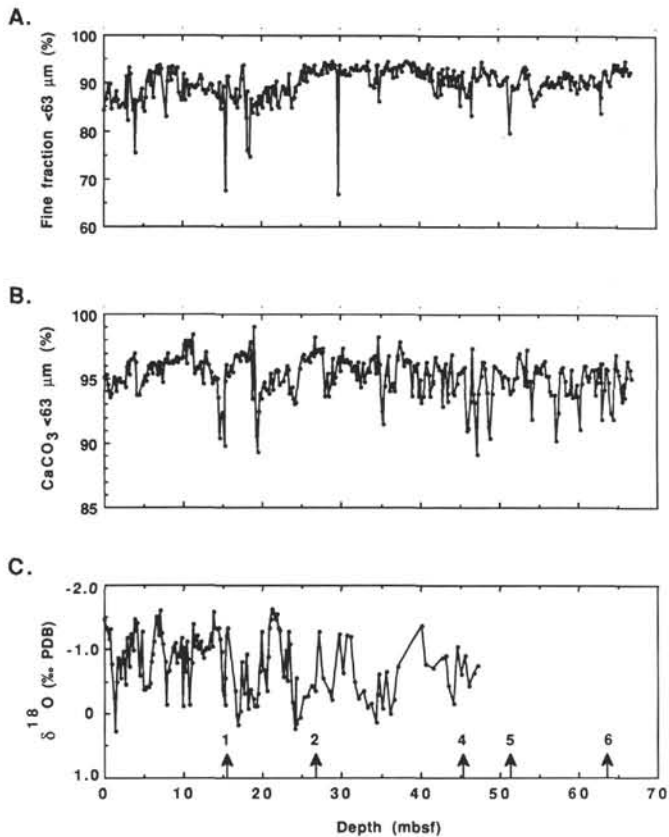


Figure 5. Depth variations for the top 63 m of Hole 817A. **A.** Percentage of fine fraction (<63 μm). **B.** Percentage of CaCO_3 (<63 μm) content. **C.** $\delta^{18}\text{O}$ (‰ PDB) for *Globigerinoides sacculifer*. **D.** Percentage of aragonite in the fine fraction. **E.** Percentage of Mg calcite in fine fraction. **F.** Percentage of whole pteropods (>355 μm). Numbers with arrows in Figures 5C and 5F refer to biostratigraphic markers listed in Table 1.

9. Fine Mg calcite is first detected at 0.29 Ma during stage 8, therefore, Mg calcite appeared much later than in Hole 818B where it was first detected at 1.44 Ma. From stage 8 to early stage 5, fine Mg calcite values varied between 0% and 8%. From early stage 5 to stage 1, Mg calcite values averaged about 10% and ranged between 0% near 0.1 Ma and 19% at 0.085 Ma. Mg calcite covaried with $\delta^{18}\text{O}$ from stages 1 to 5 with high percent Mg calcite content corresponding to light $\delta^{18}\text{O}$ values and low percent Mg calcite content corresponding to heavy $\delta^{18}\text{O}$ values.

Percentage of Whole Pteropods

Hole 818B

The Quaternary records of percent of whole pteropods (>355 μm) and the $\delta^{18}\text{O}$ measured for *G. sacculifer* in Hole 818B are shown in Figure 10. Whole pteropods first occurred in Hole 818B at 1.14 Ma and they intermittently appeared from 1.075 to 1.09 Ma (Fig. 10C), at 0.97 Ma, 0.88 Ma, and at 0.87 Ma (Fig. 10B). The percent whole pteropods for these occurrences is always less than 20%. A spike of 38% whole pteropods occurred at 0.86 Ma and separates an early period during which whole pteropods are generally absent (0.87–1.6 Ma), from a later period during which whole pteropods are generally present (0–0.87 Ma). This pteropod spike also corresponds with the sudden increase in the percent of fine aragonite content in Hole 818B mentioned above (see Fig. 6B). The percent of whole pteropods fluctuates between 0% and 22% for the interval between 0.5 and 0.86 Ma and appears to covary with the $\delta^{18}\text{O}$ values; high values of whole

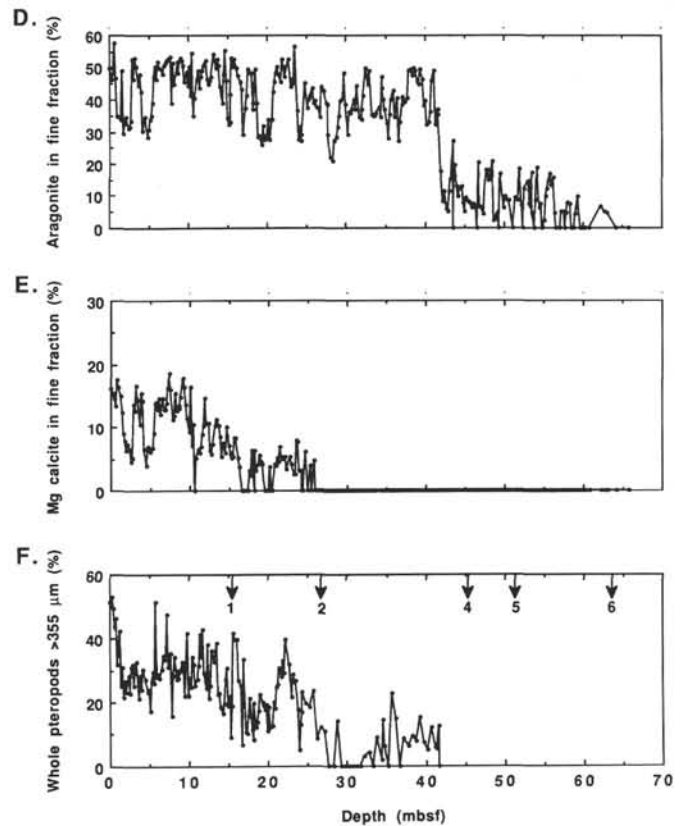


Figure 5 (continued).

pteropods correspond to light $\delta^{18}\text{O}$ values, whereas low whole pteropod values correspond to heavy $\delta^{18}\text{O}$ values.

During the interval from 0.36 to 0.41 Ma (during stage 11), whole pteropods are absent from 0.36 to 0.41 Ma (during stage 11) and from 0.475 to 0.5 Ma (late during stage 13), whereas whole pteropods are present during stage 12 and early stage 11. The interval from 0.35 to 0.5 Ma is, therefore, anomalous in that high percent whole pteropods corresponds to heavy $\delta^{18}\text{O}$ values (glacial stages) and low percent whole pteropods corresponds to light $\delta^{18}\text{O}$ values (interglacial stages). This covariation is the opposite of the pattern observed before 0.5 Ma and after 0.32 Ma. After the hiatus, which extended from 0.32 to 0.35 Ma, percent of whole pteropods varied between 7% and 58%. The highest percent of whole pteropods occurred at the glacial to interglacial transition between stages 8 and 7 and between stages 2 and 1. During the last 0.32 m.y., high values of percent whole pteropods correspond to light $\delta^{18}\text{O}$ values and low whole pteropod values correspond to heavy $\delta^{18}\text{O}$ values.

Hole 817A

The Quaternary records of percent whole pteropods (>355 μm) and $\delta^{18}\text{O}$ measured for *G. sacculifer* for Hole 817A are shown in Figure 11. Whole pteropods first occur in Hole 817A at 0.877 Ma (Fig. 11B), synchronous with the sharp 40% increase in the percent of fine aragonite content in this hole (see Fig. 7B). Between 0.748 and 0.877 Ma (between the first appearance of whole pteropods and the early Brunhes hiatus), the percent of whole pteropods fluctuated between 0% and 20%. After the hiatus, during the last 0.32 m.y., the percent of whole pteropods ranged between 5% and 53% and increased on average through the interval (Fig. 11A). Percent of whole pteropods and planktonic foraminiferal $\delta^{18}\text{O}$ records clearly covary during the last 0.32 m.y.; high percent of whole pteropods correspond

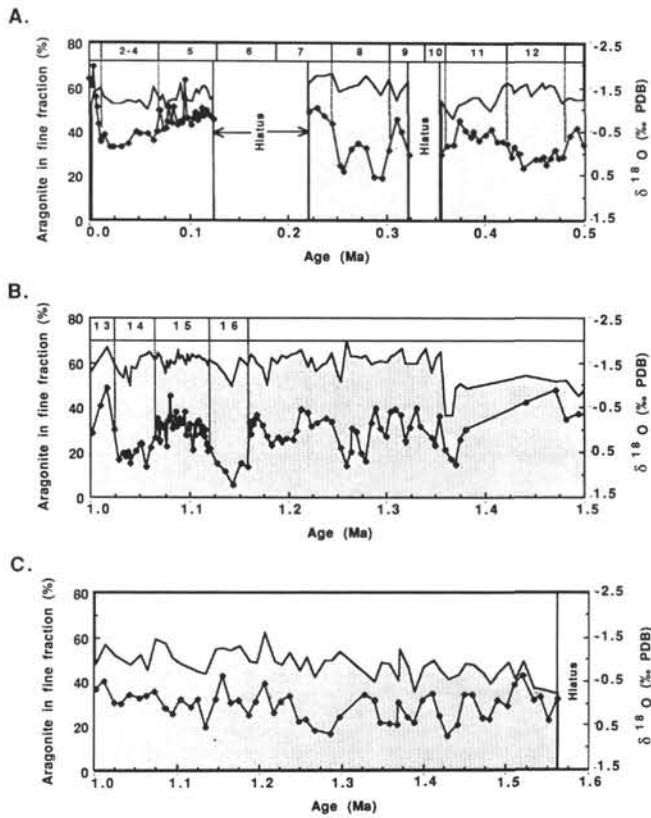


Figure 6. Age variations in Hole 818B of percent of fine aragonite content (shaded pattern) compared to the $\delta^{18}\text{O}$ record (solid line with solid dots) determined from *Globigerinoides sacculifer* for three intervals. **A.** 0 to 0.5 Ma. **B.** 0.5 to 1.0 Ma. **C.** 1.0 to 1.6 Ma. Numbers at the top of the graphs refer to oxygen isotope stages.

to light $\delta^{18}\text{O}$ values, whereas low percent of whole pteropods correspond to heavy $\delta^{18}\text{O}$ values. Stage 3 is an exception to this relationship in which a low percentage of whole pteropods corresponds with anomalously light $\delta^{18}\text{O}$ values.

Stable Isotope Analyses

Stable oxygen and carbon isotopic ratios were measured in Hole 818B on the planktonic foraminifer *Globigerinoides sacculifer* and the benthic foraminifer *Cibicidoides* spp. Only *G. sacculifer* was analyzed for oxygen and carbon isotopic ratios in Hole 817A. All isotope data are listed in Appendixes A and B. The primary objective for determining foraminiferal $\delta^{18}\text{O}$ for these holes was to develop a $\delta^{18}\text{O}$ stratigraphy, constrained by biostratigraphy, in order to produce a higher resolution chronostratigraphy for Holes 818B and 817A. Foraminiferal $\delta^{13}\text{C}$ was measured to study glacial and interglacial AAIW formation, Coral Sea surface water productivity, and to investigate the exchange of carbon between surface and intermediate water during the late Pleistocene.

Oxygen Isotope Analyses

Hole 818B

Oxygen isotope stage boundaries in Hole 818B were determined for stages 1 through 16 using the variations of $\delta^{18}\text{O}$ values for *G. sacculifer* and *Cibicidoides* spp., coupled with biostratigraphic datums (see Table 1). The $\delta^{18}\text{O}$ record for *G. sacculifer* in Hole 818B

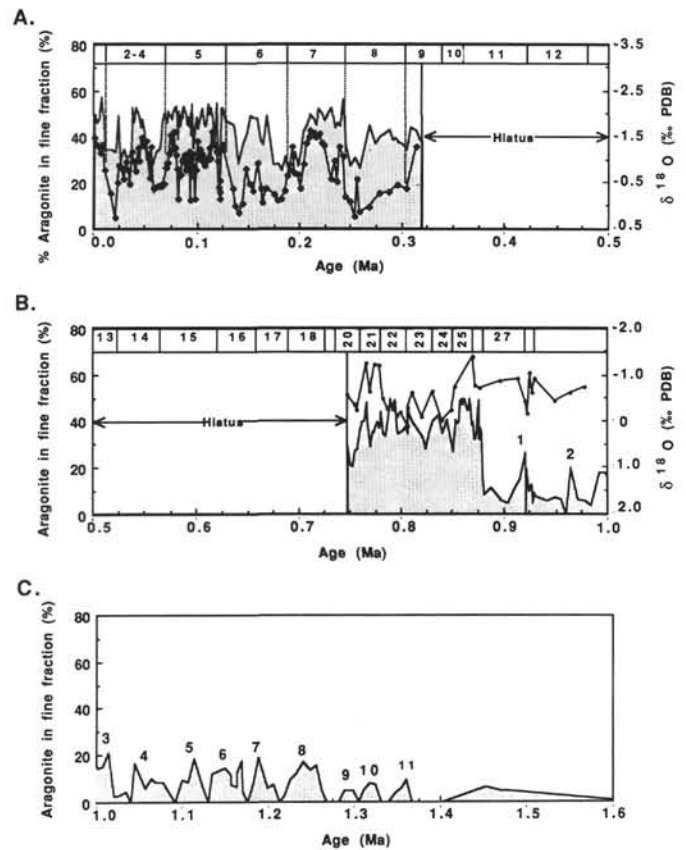


Figure 7. Age variations in Hole 817A of percent of fine aragonite content (shaded pattern) compared to the $\delta^{18}\text{O}$ record (solid line with solid dots) determined from *Globigerinoides sacculifer* for three intervals. **A.** 0 to 0.5 Ma. **B.** 0.5 to 1.0 Ma. **C.** 1.0 to 1.6 Ma. (Only the percentage of fine aragonite content is available for the last interval.) Numbers at the top of the graphs refer to oxygen isotope stages. The numbers above the aragonite peaks count the 11 aragonite cycles between 0.9 and 1.35 Ma that occur at the same periodicity as the 41 k.y. Milankovitch obliquity cycles observed in $\delta^{18}\text{O}$ records for the same time interval.

shows a general trend of decreasing isotopic ratios from stage 16 to the present (Fig. 12A). Each glacial stage, with the exception of stage 8, becomes progressively lighter from stage 16 to stage 4, and each interglacial stage, with the exception of stage 9, becomes lighter from stage 15 to stage 1. Glacial to interglacial $\delta^{18}\text{O}$ amplitudes from stage 1 through 16 range from 1.1‰ for the stage 12/11 transition, to 1.82‰ for the stage 2/1 transition. Amplitudes between light and heavy $\delta^{18}\text{O}$ intervals prior to stage 16 were generally 1‰ or less.

The trend observed in the *G. sacculifer* $\delta^{18}\text{O}$ record from stage 16 to the present is not evident in the *Cibicidoides* spp. record (Fig. 12B). In addition, although the correlation between the records is generally good, an overlay of the *G. sacculifer* and *Cibicidoides* spp. $\delta^{18}\text{O}$ records reveals several mismatches. Stage 12, identified from the *G. sacculifer* $\delta^{18}\text{O}$ record and the HO of *Pseudoemiliana lacunosa*, is anomalously light in $\delta^{18}\text{O}$ for *Cibicidoides* spp. and $\delta^{18}\text{O}$ values for *Cibicidoides* spp. during the early part of stage 13, also identified from the *G. sacculifer* $\delta^{18}\text{O}$ record, are anomalously heavy. The average difference between the $\delta^{18}\text{O}$ values for *G. sacculifer* and *Cibicidoides* spp. was 2.5‰ from late stage 14 to the most recent hiatus extending from 0.125 to 0.220 Ma. After this hiatus there is a shift during the last 0.12 m.y. to a difference of 3.0‰ to 3.5‰ between the planktonic and benthic records. It is unclear whether this separation between the planktonic and benthic isotopic ratios is real or the result of analytical error.

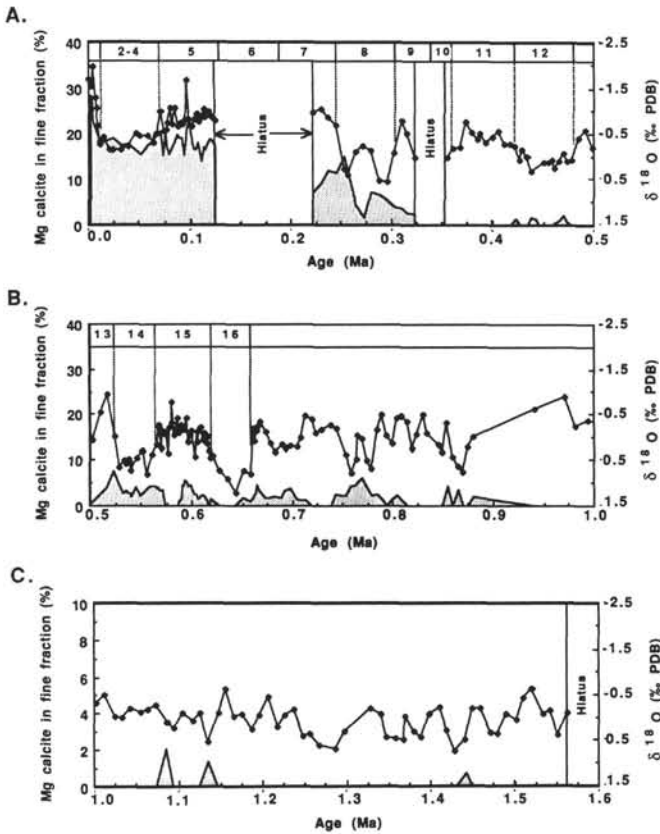


Figure 8. Age variations in Hole 818B of percent of fine Mg calcite content (shaded pattern) compared to the $\delta^{18}\text{O}$ record (solid line with solid dots) determined from *Globigerinoides sacculifer* for three intervals. **A.** 0 to 0.5 Ma. **B.** 0.5 to 1.0 Ma. **C.** 1.0 to 1.6 Ma. Numbers at the top of the graphs refer to oxygen isotope stages.

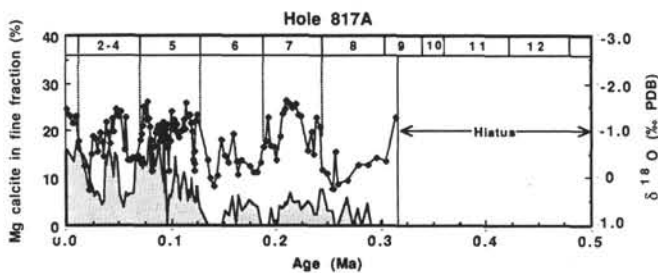


Figure 9. Age variations in Hole 817A of percent of fine Mg calcite content (shaded pattern) compared to the $\delta^{18}\text{O}$ record (solid line with solid dots) determined from *Globigerinoides sacculifer* for the interval between 0 and 0.5 Ma. Numbers at the top of the graph refer to oxygen isotope stages.

Hole 817A

Hole 817A oxygen isotope stage boundaries for stages 1 through 9 and 20 through 29 were determined using the $\delta^{18}\text{O}$ measured for *G. sacculifer* and were constrained by biostratigraphy. These two intervals are separated by a 0.428 m.y.-long hiatus that extended from 0.32 to 0.748 Ma. The $\delta^{18}\text{O}$ record in Hole 817A does not display any general trend through time comparable to the decreasing isotopic ratios observed in Hole 818B during the last 0.55 m.y. (Fig. 12C). After the hiatus, glacial to interglacial $\delta^{18}\text{O}$ amplitudes range from 1.73‰ for the stage 2/1 transition to 1.86‰ for the stage 8/7 transition. Notable irregularities in the Hole 817A $\delta^{18}\text{O}$ record include the lack of identifiable substages during stage 5 and anomalously light $\delta^{18}\text{O}$ values during stage 3. For the period before the hiatus, stages 20

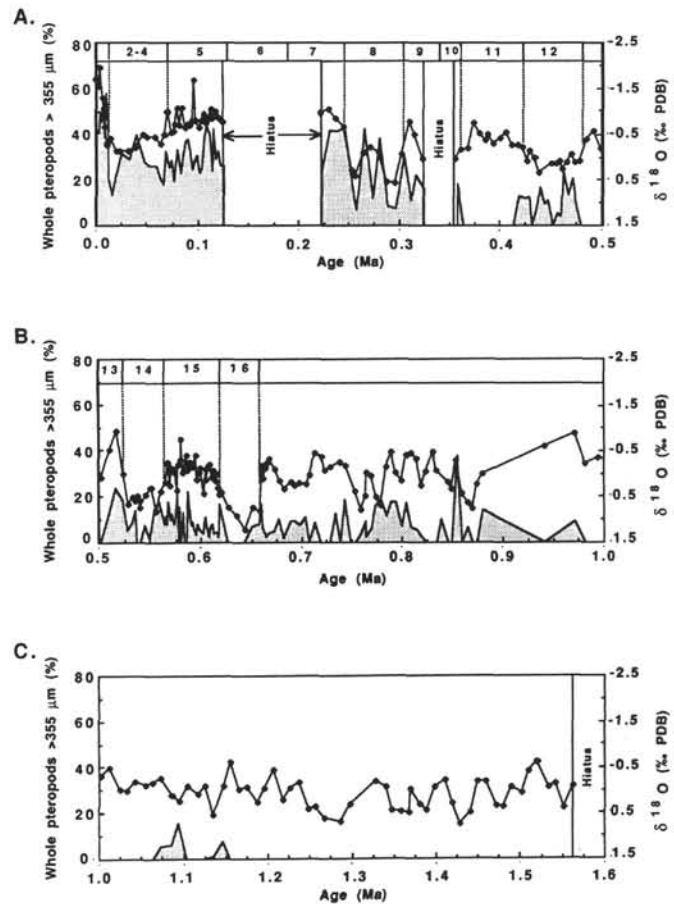


Figure 10. Age variations in Hole 818B of percent whole pteropods (>355 μm) (shaded pattern) compared to the $\delta^{18}\text{O}$ record (solid line with solid dots) determined from *Globigerinoides sacculifer* for three periods. **A.** 0 to 0.5 Ma. **B.** 0.5 to 1.0 Ma. **C.** 1.0 to 1.6 Ma. Percentage of whole pteropods = (# whole pteropods)/(# whole pteropods + # fragmented pteropods). Low percentage of whole pteropods values implies poor preservation. Numbers at the top of the graphs refer to oxygen isotope stages.

through 29 were identified by visual correlation to the Ruddiman et al. (1989) $\delta^{18}\text{O}$ record, however, these Hole 817A stage assignments remain tentative. No samples older than 0.98 Ma were analyzed for $\delta^{18}\text{O}$ in Hole 817A.

Carbon Isotope Analyses

The Quaternary carbon and oxygen isotopic ratios measured for *Globigerinoides sacculifer* in Hole 818B are plotted together in Figure 13. From 1.22 to 1.6 Ma, $\delta^{13}\text{C}$ values fluctuated between 1.25‰ and 1.96‰ with a periodicity of approximately 35 k.y. (Fig. 13C). $\delta^{13}\text{C}$ values for this time interval averaged 1.53‰. There is a shift toward lighter $\delta^{13}\text{C}$ values at about 1.2 Ma and $\delta^{13}\text{C}$ dropped to 0.74‰ by 1.14 Ma. For the interval from 1.0 to 1.6 Ma, heavy $\delta^{13}\text{C}$ values generally correspond to heavy $\delta^{18}\text{O}$ values and light $\delta^{13}\text{C}$ values correspond to light $\delta^{18}\text{O}$ values. From 0.5 to 1.0 Ma, $\delta^{13}\text{C}$ values average 1.0‰ and range from -0.137‰ at 0.517 Ma to 1.404‰ at 0.994 Ma (Fig. 13B). From 0.75 to 0.875 Ma, $\delta^{13}\text{C}$ was consistently heavy when $\delta^{18}\text{O}$ was heavy and $\delta^{13}\text{C}$ was light when $\delta^{18}\text{O}$ was light, as observed in the older part of the record. From 0.525 to 0.75 Ma, $\delta^{13}\text{C}$ and $\delta^{18}\text{O}$ do not clearly display any covariance. After 0.525 Ma, a new pattern emerged in which $\delta^{13}\text{C}$ values generally are light during the transition from glacial to interglacial stages and/or during the early part of interglacial stages and $\delta^{13}\text{C}$ values generally are heavy during

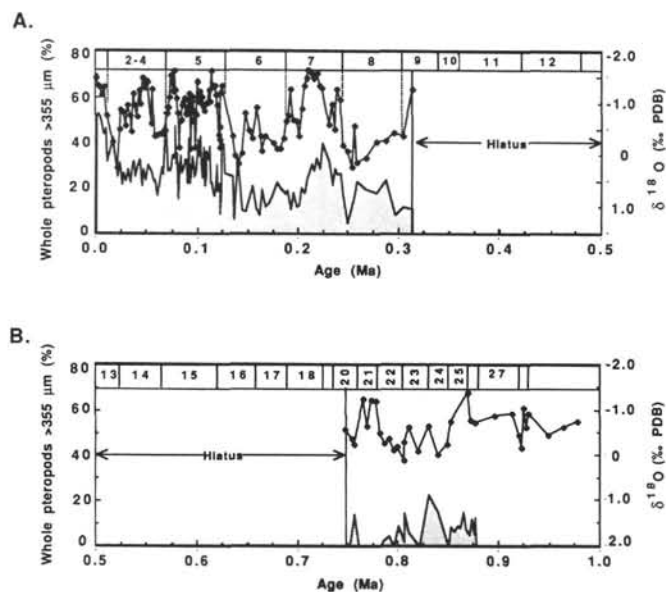


Figure 11. Age variations in Hole 818B of percentage of whole pteropods (>355 μm) (shaded pattern) compared to the $\delta^{18}\text{O}$ record (solid line with solid dots) determined from *Globigerinoides sacculifer* for two periods. **A.** 0 to 0.5 Ma. **B.** 0.5 to 1.0 Ma. No whole pteropods occur in Hole 817A before 0.875 Ma. Percentage of whole pteropods = (# whole pteropods)/(# whole pteropods + # fragmented pteropods). Low percentages of whole pteropods imply poor preservation. Numbers at the top of the graphs refer to oxygen isotope stages.

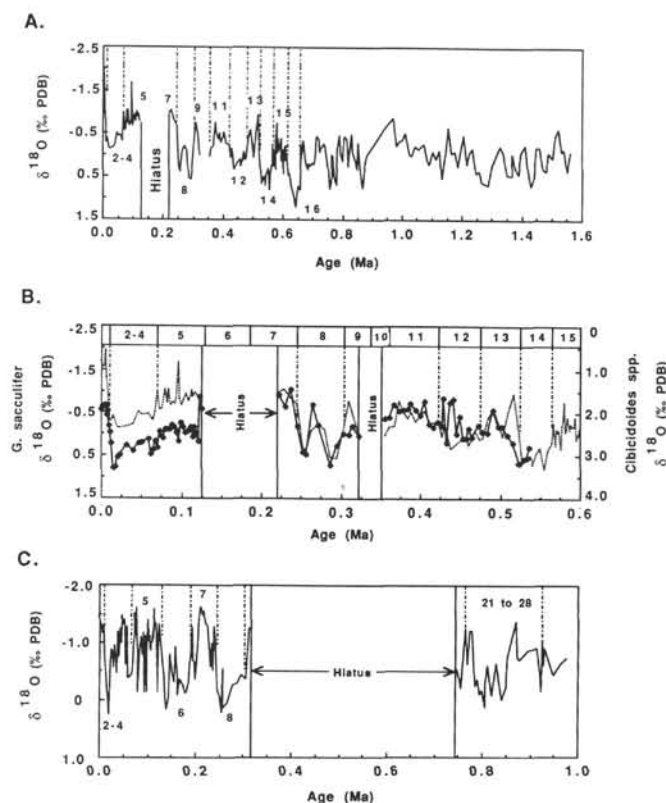


Figure 12. **A.** Quaternary $\delta^{18}\text{O}$ (‰ PDB) record for *Globigerinoides sacculifer* in Hole 818B. **B.** Comparison of $\delta^{18}\text{O}$ records for *G. sacculifer* (dashed line) and *Cibicides* spp. (solid line with solid dots) for the past 0.54 m.y. **C.** $\delta^{18}\text{O}$ record for *Globigerinoides sacculifer* for the past 1 m.y. in Hole 817A.

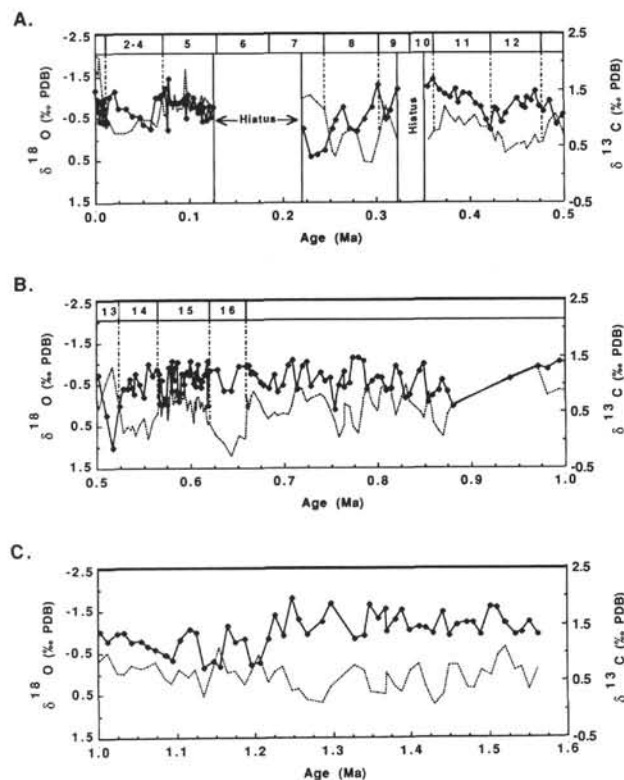


Figure 13. Comparison of $\delta^{18}\text{O}$ (dashed line) and $\delta^{13}\text{C}$ (solid line with solid dots) for *Globigerinoides sacculifer* in Hole 818B. **A.** 0 to 0.5 Ma. **B.** 0.5 to 1.0 Ma. **C.** 1.0 to 1.6 Ma. Isotope stages are numbered through stage 16.

the transition from interglacial to glacial stages and/or early during glacial stages (Fig. 13A).

Figure 14A is a plot of $\delta^{13}\text{C}$ measured for the benthic foraminifer *Cibicides* spp. and $\delta^{13}\text{C}$ values for *G. sacculifer* in Hole 818B. *Cibicides* spp. $\delta^{13}\text{C}$ values are usually slightly heavier than *G. sacculifer* $\delta^{13}\text{C}$ values, rarely by more than 0.5‰, and both records generally covary. Calculation of $\Delta\delta^{13}\text{C}$ (shallow - intermediate) ($\delta^{13}\text{C}$ of *G. sacculifer* minus $\delta^{13}\text{C}$ of *Cibicides* spp.) shows that significant exceptions to the above relationship include early stage 13, when the benthic $\delta^{13}\text{C}$ was 1.2‰ heavier than planktonic $\delta^{13}\text{C}$, and stage 7, when benthic $\delta^{13}\text{C}$ was 0.75‰ heavier than planktonic $\delta^{13}\text{C}$ (Fig. 14B). The only times when *Cibicides* spp. $\delta^{13}\text{C}$ is significantly lighter than *G. sacculifer* were during stage 12 and early during stage 5.

DISCUSSION

Aragonite and Mg Calcite Input

The metastable carbonate content in Holes 818B and 817A is primarily the result of variations through time of primary influx of aragonite and Mg calcite, seafloor dissolution, and burial diagenesis. To reconstruct the Quaternary fluctuations of the CaCO_3 saturation state of intermediate water, which directly influences seafloor carbonate dissolution or preservation, it is necessary to estimate the individual weight of each variable. The foraminiferal $\delta^{18}\text{O}$ record was used as a proxy for sea level and to indirectly indicate the flooding or exposure of the bank tops. Input of fine aragonite and Mg calcite into the Townsville Trough is assumed to be greater during sea-level highstands (light $\delta^{18}\text{O}$), when bank tops were flooded, than during sea-level lowstands (heavy $\delta^{18}\text{O}$), when bank tops were exposed. This relationship between $\delta^{18}\text{O}$ and metastable carbonate input is justified

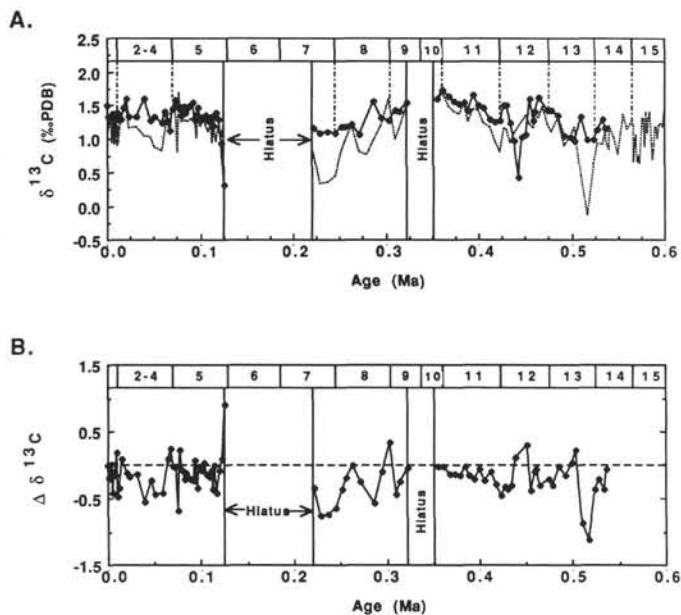


Figure 14. A. Comparison of $\delta^{13}\text{C}$ for *Globigerinoides sacculifer* (dashed line) and *Cibicidoides* spp. (solid line with solid dots) for the past 0.54 m.y. B. $\Delta\delta^{13}\text{C}$ for Hole 818B during the past 0.54 m.y. $\Delta\delta^{13}\text{C}$ is the difference between $\delta^{13}\text{C}$ of the planktonic foraminifer *Globigerinoides sacculifer* and the benthic $\delta^{13}\text{C}$ for *Cibicidoides* spp.

by recent research on Quaternary periplatform sediments from the Bahamas, the Nicaragua Rise, and the Maldives, which indicates that at water depths significantly above the aragonite lysocline, high fine aragonite content correlates to light $\delta^{18}\text{O}$ values and low fine aragonite content correlates to heavy $\delta^{18}\text{O}$ values in planktonic foraminifers (Droxler et al., 1983, 1988, 1990). Once shed into deep water, the fate of fine aragonite and Mg calcite is a function of the amount of dissolution that occurs on the seafloor and within the sediments during shallow burial diagenesis.

Seafloor Dissolution

General Trends During the Quaternary

It would be unwise to interpret any one of our dissolution indices alone as representing the single dissolution record for Holes 818B or 817A. However, by comparing the variations of the three indices (percent of fine aragonite content, percent of fine Mg calcite content, and percent of whole pteropods (>355 μm) for each hole and by comparing the variations that occurred simultaneously in both holes, possible periods of dissolution or preservation can be identified.

Looking at the Quaternary record as a whole, the dissolution indices for Hole 818B (745 mbsl) show a general increase in apparent preservation through time. The preservation increase is briefly interrupted at 0.87 Ma when percent of fine aragonite content dropped from 50% to 40%. This aragonite low coincides with a local minimum in the percent of Mg calcite and in the percent of whole pteropods. Low aragonite at 0.87 Ma is followed by a sharp increase in percent of fine aragonite content at 0.86 Ma that coincides with a spike in the percent of whole pteropods. The percent of fine Mg calcite record shows no comparable increase at this time. The aragonite increase is interpreted to have resulted from an increase of aragonite input from the surrounding banks, coupled with improved preservation. Between 0.41 and 0.86 Ma, preservation in Hole 818B was variable but generally good. Strong dissolution occurred from 0.36 to 0.41 Ma (stage 11) with no Mg calcite, no whole pteropods, and unexpectedly low aragonite content for an interglacial stage. From 0.65 Ma to present, carbonate preservation was better during interglacial stages

than during glacial stages with the exception of the interval from 0.35 to 0.5 Ma (mid-Brunhes Chron) when the opposite was true.

Aragonite first appeared in Hole 817A (1015 mbsl) at the Pliocene/Pleistocene boundary (1.6 Ma). No aragonite was detected in Pliocene or older sediments in this hole. Aragonite cycles between 0.9 and 1.35 Ma (Figs. 7B and 7C) have an approximate periodicity of 41 k.y. and, therefore, are probably tied to Milankovitch obliquity cycles present in oxygen isotope records during this interval (e.g., Shackleton and Opdyke, 1976; Prell, 1982; Ruddiman, 1989). Because an oxygen isotope record is currently not available for the interval from 0.9 to 1.6 Ma, the origin of these cycles cannot be tied definitively to flooding and exposure of the neighboring bank tops (sea level change) or to changes in CaCO₃ preservation. After a local aragonite low between 0.875 and 0.9 Ma, there was a dramatic increase of aragonite content at 0.875 Ma that coincided with the first appearance of whole pteropods in Hole 817A. As in Hole 818B, the interval from 0.875 to 0.9 Ma is interpreted to correspond to a period of dissolution centered at 0.89 Ma (0.87 Ma in Hole 818B) followed by a major increase in aragonite input coupled with preservation at 0.875 Ma (0.86 Ma in Hole 818B). During the late Pleistocene, after a hiatus from 0.32 to 0.748 Ma, preservation generally increased to the present in Hole 817A and was more pronounced during interglacial stages than during glacial stages.

Comparison to Other Carbonate Records

The percent of whole pteropods and the percent of fine aragonite content records for Holes 818B and 817A were compared to the carbonate preservation record of the central equatorial Pacific Ocean (Farrell and Prell, 1991) to determine if the dissolution records of the Northeast Australia margin have more than a regional significance (Figs. 15 and 16). The Farrell and Prell (1991) record is based on the CaCO₃ content measured in a large number of piston cores and DSDP holes from the eastern equatorial Pacific Ocean. Assuming that variations of CaCO₃ content in these cores are related more to changes in the CaCO₃ saturation state of deep and bottom waters than to changes in productivity, Farrell and Prell (1991) demonstrated that CaCO₃ preservation has generally increased since the Pliocene/Pleistocene boundary. Intervals of poor preservation were centered on interglacial to glacial boundaries or during late interglacial stages whereas intervals of good preservation occurred at glacial to interglacial boundaries or during late glacial stages. In addition, Farrell and Prell observed two intervals of pronounced CaCO₃ dissolution, from 0.87 to 0.89 Ma and from 0.2 to 0.4 Ma.

Early Quaternary CaCO₃ Preservation

The Quaternary record of percent whole pteropods for both holes 818B and 817A is compared to the Farrell and Prell (1991) record of the 20%–40% CaCO₃ isopleth in Figures 15A and 15B. In Hole 818B (Fig. 15A), whole pteropods first appeared at 1.15 Ma, however, values remain zero or near zero until about 0.86 Ma when percent of whole pteropods briefly increased to 38%. In Hole 817A, the first appearance of whole pteropods was dated at 0.875 Ma. The sharp increase of whole pteropods in Hole 818B and the first appearance of whole pteropods in Hole 817A between 0.86 and 0.88 Ma may be the result of improved aragonite preservation. This preservation pulse is also observed in the deep central equatorial Pacific Ocean as a 300 m deepening of the 20%–40% CaCO₃ isopleth in Farrell and Prell's record.

The record for the percentage of fine aragonite content from Holes 818B and 817A was also compared to the CaCO₃ preservation record of Farrell and Prell (Figs. 16A and 16B). The gradual increase of fine aragonite content during the early Pleistocene (from 1.6 to 0.9 Ma) in Holes 818B and 817A corresponds to the general improvement of preservation observed in Farrell and Prell's carbonate record for the same period of time. Between 0.85 and 0.9 Ma, in both Holes 818B and 817A, low fine aragonite values (dissolution) were followed by an

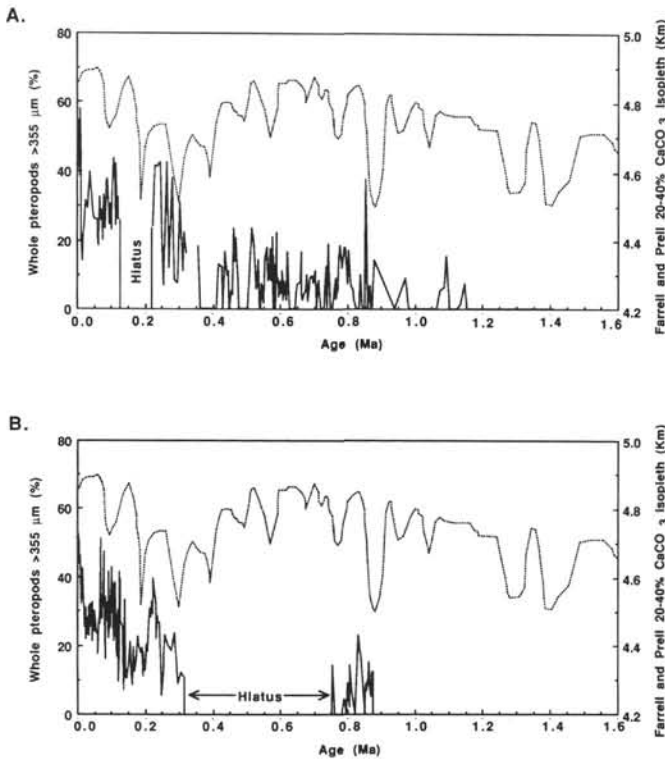


Figure 15. Late Pleistocene comparison of percentage of whole pteropods (>355 μm) (solid line) and the 20%–40% CaCO_3 isopleth from Farrell and Prell (1991) (dashed line) for (A) Hole 818B and (B) Hole 817A. The 20%–40% isopleth tracks the movement, but not the position, of the lysocline defined by the 10% CaCO_3 isopleth.

abrupt and permanent increase of fine aragonite content (preservation). The inferred changes in aragonite preservation for this interval are comparable to the changes of CaCO_3 preservation in Farrell and Prell's record that indicates that there was a major shallowing of the top of the calcite lysocline in the deep central equatorial Pacific Ocean near 0.9 Ma, followed by a rapid and major deepening of the calcite lysocline between 0.85 and 0.9 Ma. However, although the Farrell and Prell (1991) record displays an improvement of carbonate preservation from 0.85 to 0.9 Ma, this interval does not mark a permanent increase in percent CaCO_3 content, whereas improved CaCO_3 preservation in Holes 818B and 817A is part of a major and permanent shift to higher percent of fine aragonite content. It is possible that as aragonite input to the northern Townsville Trough increased, the aragonite lysocline deepened due to the buffering effect of metastable carbonate sediment settling through the water column. A possible analogy is the deep modern aragonite lysocline near the Bahama Banks that may also be related to the input of aragonite and Mg calcite from the surrounding carbonate banks (Droxler et al., 1988).

The swing in the CaCO_3 preservation pattern near 0.9 Ma has also been observed in other intermediate and deep-water records. An aragonite low was observed at ~0.9 Ma in Hole 716B (554 mbsl) from the Maldives (Droxler et al., 1990) and in Hole 633A (1681 mbsl) from the Bahamas (Droxler et al., 1988). The intermediate water-depth aragonite low may correlate to the M3 CaCO_3 low of Hays et al. (1969) and Vincent (1985). In the Bahamas, the aragonite low at ~0.9 Ma in Hole 633A is followed at 0.85 Ma by the highest fine aragonite content of the entire Quaternary (Droxler et al., 1988, 1990). Similarities between the CaCO_3 preservation patterns observed in the Pacific, Indian, and Atlantic oceans and between deep and intermediate water depths suggests that there may have been an oceanwide CaCO_3 dissolution increase near 0.9 Ma, followed by a rebound

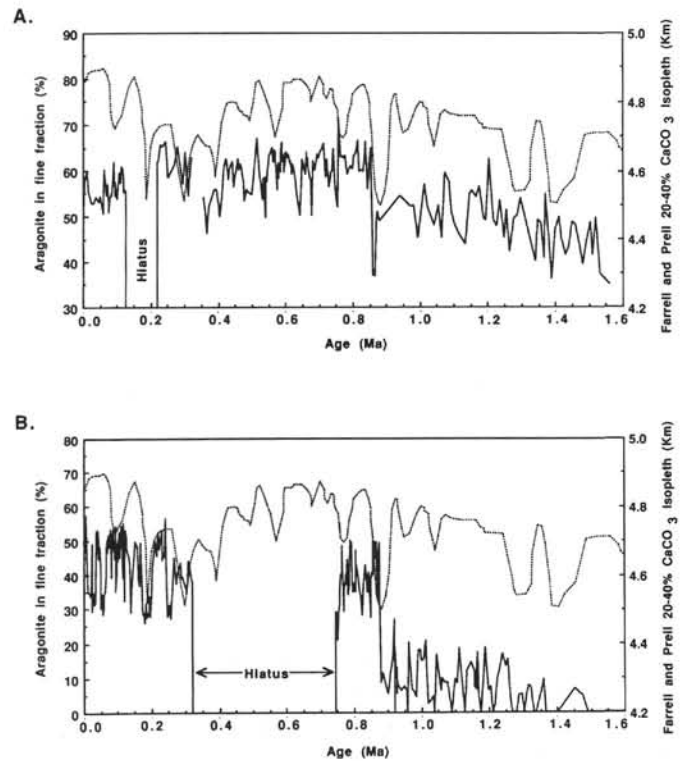


Figure 16. Late Pleistocene comparison of percentage of aragonite in the fine fraction (<63 μm) (solid line) and the 20%–40% CaCO_3 isopleth from Farrell and Prell (1991) (dashed line) for (A) Hole 818B and (B) Hole 817A. The 20%–40% isopleth tracks the movement, but not the position, of the lysocline as defined by the 10% CaCO_3 isopleth.

towards good preservation between 0.85 and 0.9 Ma, which involved the entire water column of the world's low-latitude oceans.

Alternative Explanations for the Aragonite Increase Near 0.87 Ma

The abrupt and permanent increase in percentage of fine aragonite content that occurred between 0.86 and 0.875 Ma in Holes 817A and 818B may have resulted from (1) an abrupt and permanent deepening of the aragonite lysocline resulting in a permanent increase in aragonite preservation (as discussed above); (2) a change in local environmental conditions such as temperature, salinity, and nutrients, which could have promoted a dramatic increase of shallow water carbonate production and sediment export; or (3) an increase in banktop production and off-bank transport possibly related to the change in the frequency and amplitude of sea level fluctuations that occurred between 0.73 and 0.9 Ma.

Environmental change apparently did occur during the middle Pleistocene in the Great Barrier Reef and Coral Sea region. Isern et al. (this volume) determined from $\delta^{18}\text{O}$ temperature calculations that surface-water temperature increased during the middle Pleistocene and may have first reached optimum levels for reef growth (20° to 25°C) at that time. Feary et al. (1991) also documented a temperature increase during the Pleistocene. Isern et al. suggest that the warming trend during the Pleistocene may be responsible for the initiation of the Great Barrier Reef. Kroon et al. (this volume) report a change in the planktonic/benthic foraminifer ratio (PF/BF) after stage 19 (0.73 Ma) in Hole 819, adjacent to the Great Barrier Reef. PF/BF ratios have been related to water depth; an increase in PF/BF suggests an increase in relative sea level (Wright, 1977). However, the highest PF/BF ratios occur during glacial intervals (low sea level), which Kroon et al. (this volume) attribute to high glacial productivity. It is

possible that high PF/BF ratios after stage 19 are due to greater productivity related to an increase in late Pleistocene upwelling. High productivity implies high nutrients in surface waters near the Great Barrier Reef. An increase in surface-water nutrient concentrations during the mid- to late Pleistocene seems to be inconsistent with the initiation of reef growth on the northeast Australia shelf and with the inferred increase of carbonate production on the Queensland Plateau between 0.85 and 0.9 Ma. It must be kept in mind, however, that nutrients control the type of carbonate secreting organisms (corals vs. sponges and algae) (Hallock and Schlager, 1986; Hallock et al., 1988) but may not control the overall carbonate production and export. For example, platforms of the Nicaragua Rise export large volumes of fine carbonate mud (Glaser and Droxler, 1991) even though nutrient levels are high, the bank tops are at a water depth of 40 m, and corals are rare or absent. This is because calcareous algae can prosper in water much deeper and more nutrient rich than is required for frame-building corals (Hallock et al., 1988). Therefore, an increase in nutrient levels along the northeastern Australia margin during the middle Pleistocene is not necessarily incompatible with an increase in carbonate production of the Queensland Plateau/Great Barrier Reef carbonate system. It is possible, therefore, that the large increase of aragonite content that occurred in Holes 818B and 817A between 0.85 and 0.9 Ma was the result of some local change in nutrients or temperature, that may also have led to the initiation of the Great Barrier Reef.

Seismic profiles in the Great Barrier Reef area show a middle Quaternary change from progradation to aggradation dated at approximately 0.9 Ma (Davies, McKenzie, Palmer-Julson, et al., 1991); close to the time of aragonite increase in Holes 818B and 817A. There are several possible interpretations that may explain this seismic stratal geometry, (1) an increase in subsidence, (2) a long-term eustatic rise, (3) a combination of subsidence and eustasy, (4) a change in the amplitude and frequency of sea level change, and finally (5) a change in the type of sediment deposited on the shelf (i.e., clastic to carbonate; uncemented carbonate grains to cemented skeletal boundstones). Subsidence may have increased during the middle Pleistocene based on the PF/BF ratios determined for Hole 819; however, as discussed above, there are other explanations for the change in the PF/BF ratio at 0.73 Ma that may be more reasonable. A long-term eustatic rise starting near 0.9 Ma is not indicated in the Haq et al. (1988) sea-level curve, nor in the revised Pliocene–Pleistocene sea-level curve of Wornardt and Vail (1991), nor is a late Pleistocene general sea-level rise inferred from $\delta^{18}\text{O}$ records (Fig. 17). On the other hand, several oxygen isotope records clearly show a change from high frequency and low-amplitude Milankovitch cycles (41 k.y.) during the early Pleistocene, prior to 0.9 Ma, to low frequency and high amplitude cycles (100 k.y.) during the late Pleistocene, after 0.73 Ma (e.g., Shackleton and Opdyke, 1976; Pisias and Moore, 1981; Prell, 1982; Ruddiman et al., 1989; Raymo et al., 1990). Assuming that changes in the Quaternary $\delta^{18}\text{O}$ isotopic composition of foraminifers were primarily due to changes of global ice volume, the frequency and amplitude of sea-level fluctuations must also have changed between 0.73 and 0.9 Ma. This change in amplitude and frequency of sea-level cycles should have had a major effect on sedimentation on and near continental shelves (Prell, 1982) and carbonate platforms. Finally, the change from siliciclastic to mixed carbonate/siliciclastic sedimentation that occurred on the northeast Australia shelf during the middle Pleistocene (Davies, McKenzie, Palmer-Julson, et al., 1991) may be responsible for the progradational to aggradational geometry. The growth of the Great Barrier Reef itself may have served as a sediment dam that trapped sediment on the shelf during sea-level highstands, thus promoting aggradation, whereas the pre-existing fluvial-deltaic system was characterized by highstand progradation of the shelf and shelf edge. Although a switch from predominantly siliciclastic to mixed carbonate/siliciclastic sedimentation may explain the change in the stratal geometry of the shelf, we

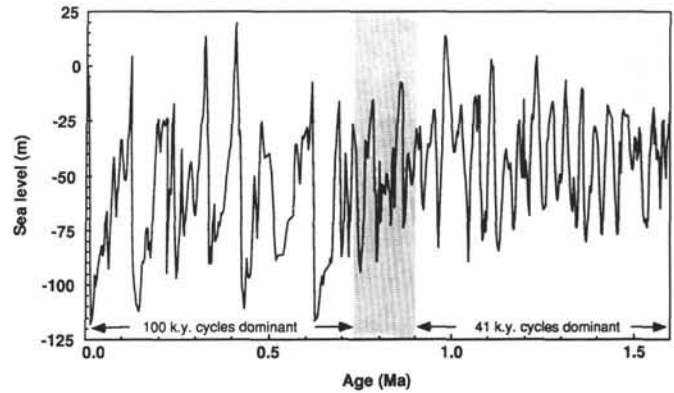


Figure 17. Quaternary glacio-eustatic fluctuations in sea level calculated from the benthic foraminiferal $\delta^{18}\text{O}$ record from Site 607 (North Atlantic Ocean). Isotope data are from Raymo et al. (1990). Sea level was calculated by assuming that the global ice volume component of the last glacial to interglacial $\delta^{18}\text{O}$ change was $\sim 1.25\text{‰}$ (1.2‰ reported by Shackleton and Duplessy, 1986) and that the remainder of the amplitude in the benthic record results from temperature and salinity effects. The salinity and temperature components then were removed from the remainder of the record by multiplying the original $\delta^{18}\text{O}$ values by 0.67; the ratio in Hole 607 between the ice volume component of 1.25‰ and the LGM to Holocene $\delta^{18}\text{O}$ change of 1.87‰ . The temperature/salinity corrected isotope record was then converted to sea level by assuming that the last sea-level rise of 118 m (Fairbanks, 1989; Bard et al., 1990) corresponds to the 1.25‰ isotopic change, or 10 m of sea level change equals -0.11‰ . This value for the relationship between sea level and $\delta^{18}\text{O}$ was first determined by Fairbanks and Mathews (1977) from analyses of uplifted coral terraces in Barbados.

are still left without an explanation for the change in sediment type and the initiation of the Great Barrier Reef.

The near simultaneous increase of the fine aragonite content in sediments deposited in the Townsville Trough (Holes 818B and 817A) adjacent to the Queensland Plateau, the change in seismic stratal geometry from progradation to aggradation along the northeast Australia shelf, and the change in mode of global sea level fluctuations, inferred from $\delta^{18}\text{O}$ records, suggest that eustatic sea-level change may have played an important role in the increase of carbonate production and off-bank transport on the Queensland Plateau and in the initiation of the modern Great Barrier Reef. Further support for this hypothesis comes from the Bahamas in the western North Atlantic Ocean and from Mururoa Atoll in the central South Pacific Ocean. Age vs. depth curves for one platform interior and one platform margin core from Great Bahama Bank indicate that rapid accumulation of platform carbonates started near 0.8 Ma (McNeill et al., 1988; McNeill, 1989) with a coincident increase in the sediment accumulation rate in Hole 632A from Exuma Sound, Bahamas (Austin and Schlager, et al., 1988). Reijmer et al. (1992) reported a major increase in shedding of ooids and skeletal material (platform interior sediments) in turbidites deposited in Exuma Sound near 0.73 Ma. Aïssaoui et al. (1990) reported a large accumulation increase on Mururoa Atoll between 0.73 and 0.91 Ma based on magnetostratigraphic dating and they showed that the accumulation rate histories for Mururoa Atoll and San Salvador, Bahamas are similar for the past 3.4 m.y. Both Mururoa Atoll and San Salvador Island experienced a major increase of shallow water carbonate accumulation starting between 0.73 and 0.91 Ma with high accumulation continuing to the present (Aïssaoui et al., 1990). These authors attributed the increase in carbonate production during the middle Pleistocene to a rise in eustatic sea level that flooded the Bahama Banks and Mururoa Atoll near 0.73 Ma following an overall lowstand from 0.73 to 2.9 Ma. We suggest that the near simultaneous increase in the production and offbank transport of shallow water carbonates in the Bahamas, French Polynesia, and in the Great Barrier Reef/Queensland Plateau system

may not simply be the response to a single long-term rise of sea level, but to a change in the frequency and amplitude of global sea level fluctuations that occurred between 0.73 and 0.9 Ma. After 0.73 Ma, sea level fluctuations of up to 120 m (Fairbanks et al., 1989; Bard et al., 1990) repeatedly flooded and exposed carbonate platforms and shelves at 100 k.y. intervals. Prior to 0.9 Ma, early Pleistocene fluctuations in sea level of 30 to 80 m, which occurred at 41 k.y. intervals, may not have been of sufficient amplitude to flood the platforms, or sea level may not have flooded the platforms for a long enough duration of time to produce significant carbonate sediment. The period between 0.73 and 0.9 Ma marks a transition during which 41 k.y. cycles were replaced by 100 k.y. cycles. It is likely that the change in frequency and amplitude of sea level fluctuations was accompanied by environmental changes on a global scale that may also have contributed to the increase of shallow-water carbonate production during the middle Pleistocene.

CaCO₃ Preservation During the Brunhes Chron

Primarily in an attempt to determine the significance of what appears to be a CaCO₃ dissolution maximum in Hole 818B during the mid-Brunhes Chron, we compared our preservation records to the deep-sea CaCO₃ preservation record of Peterson and Prell (1985b). Peterson and Prell (1985a) used a combination of six commonly used carbonate dissolution indices determined for 45 Holocene core-top samples to develop a composite dissolution index (CDI) for sediments from the Ninetyeast Ridge in the Indian Ocean. Utilizing the CDI on sediments from a depth transect of piston cores from the Ninetyeast Ridge, Peterson and Prell (1985b) were able to estimate the changes in calcite preservation both above and below the calcite lysocline during the past 0.7 m.y. The Peterson and Prell record is displayed as water-depth contours of equal CDI values (isopleths) which range from -12 to 4. Positive values indicate better preservation, whereas negative values indicate poorer preservation. The CDI=0 isopleth approximates the modern calcite saturation horizon of 3800 m based on the critical carbonate ion concept of Broecker and Takahashi (1978) (Peterson and Prell, 1985b). The Peterson and Prell record shows good preservation at glacial to interglacial transitions and/or late during glacial stages and poor preservation at interglacial to glacial transitions and/or late during interglacial stages. This record also shows a broad interval of relatively high dissolution during the middle Brunhes Chron from 0.3 to 0.6 Ma. The Farrell and Prell (1989) record from the central equatorial Pacific Ocean displays a similar CaCO₃ preservation history to the Peterson and Prell (1985b) record with a mid-Brunhes dissolution interval between 0.2 and 0.4 Ma.

The percentage of whole pteropods for Hole 818B and the CDI=0 isopleth of Peterson and Prell (1985b) are similar in their general trends but different in detail during the past 0.7 m.y. (Fig. 18A). Dissolution intervals are evident in both records from 0.475 to 0.5 Ma and from 0.36 to 0.41 Ma during the mid-Brunhes Chron. The percent fine aragonite and percent fine Mg calcite records also suggest that strong dissolution occurred during the mid-Brunhes Chron in Hole 818B. The mid-Brunhes Chron interval is missing from Hole 817A due to a hiatus corresponding to the interval from 0.32 to 0.748 Ma (Fig. 18B). After 0.36 Ma, pteropod preservation improved overall up to the present in both Holes 818B and 817A which is in good agreement with the deepening of Peterson and Prell's CDI = 0 isopleth and Farrell and Prell's 20%–40% CaCO₃ isopleth during this time interval. Based primarily on the percentage of whole pteropods record, the interval from the mid-Brunhes Chron to the present is characterized by good CaCO₃ preservation during interglacial stages and poor preservation during glacial stages.

The mid-Brunhes Chron dissolution interval (mid-Brunhes cycle of Adelseck, 1977) apparently occurred oceanwide affecting CaCO₃ sediments within intermediate waters of the Bahamas (Droxler et al., 1988) (Fig. 19A) and the Maldives (Fig. 19B) (Droxler et al., 1990;

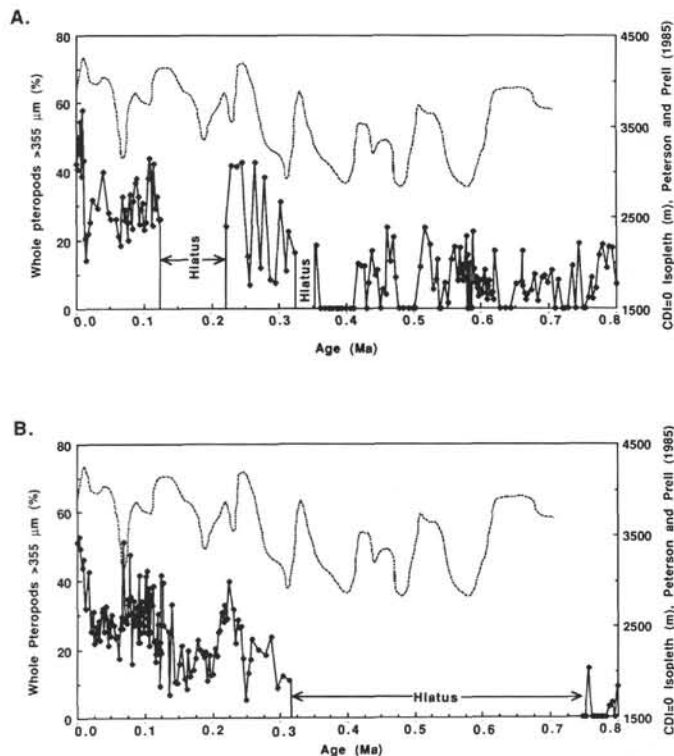


Figure 18. The Brunhes Chron record of percentage of whole pteropods (>355 μm) (solid line with solid dots) compared to the CDI=0 isopleth from Peterson and Prell (1985) (dashed line) for (A) Hole 818B and (B) Hole 817A. High percentages of whole pteropod values correspond to good aragonite preservation. The CDI (Composite Dissolution Index) was calculated by determining the variation of six commonly used CaCO₃ dissolution indices and combining them through factor analysis. CDI values were calculated in several piston cores from a broad depth range and small geographic extent along the Ninetyeast Ridge. The CDI=0 isopleth tracks the movement of the calcite lysocline, but not necessarily its depth. The shallower the CDI=0 water depth, the greater the CaCO₃ dissolution.

Bassinot et al., 1992), as well as within deep and bottom waters of the middle and low latitude oceans (Adelseck, 1977; Johnson et al., 1977; Moore et al., 1982; Crowley, 1985; Peterson and Prell, 1985b; Farrell and Prell, 1989). This dissolution interval appears to correlate to a deterioration in continental climate that may be linked to a perturbation in the Earth's 0.4-m.y. eccentricity cycle (Jansen et al., 1986). The possible link between the mid-Brunhes dissolution interval, global climate change, and the anomalously high production rate of NADW during oxygen isotope stages 7, 9, and 11 (Oppo and Fairbanks, 1990; Hodell, in press) is not currently known. The "Atlantic-type" CaCO₃ preservation pattern expressed in Holes 818B and 817A after the mid-Brunhes Chron, in which good preservation occurred during interglacial stages and poor preservation occurred during glacial stages, has not previously been observed in cores from the Pacific Ocean. The results from this study suggest that the glacial/interglacial CaCO₃ preservation pattern for sediments deposited at intermediate water depths shallower than ~1000 m in the South Pacific Ocean (within AAIW) is nearly out of phase with the deep Pacific Ocean CaCO₃ preservation cycles that display good preservation during glacial stages and poor preservation during interglacial stages (Oba, 1969; Hays et al., 1969; Berger, 1973; Thompson and Saito, 1974; Pisiás et al., 1975; Adelseck, 1977; Volat et al., 1980; Crowley, 1985; Farrell and Prell, 1989; Berger, 1992). Many more cores from shallow intermediate water depths are needed to confirm this preservation pattern.

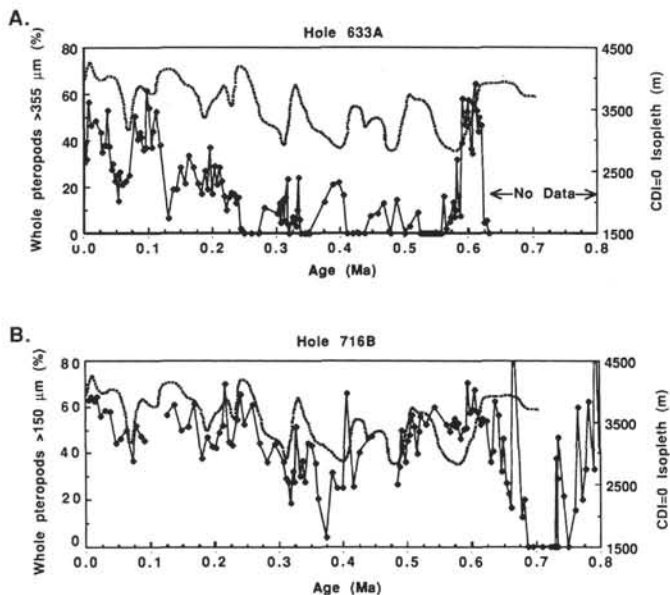


Figure 19. The Brunhes Chron record of percentage of whole pteropods (>355 μm) (solid line with solid dots) and the CDI = 0 isopleth from Peterson and Prell (1985) (dashed line) for (A) Hole 633A from a water depth of 1681 m in Exuma Sound (Bahamas, western North Atlantic Ocean) and (B) Hole 716B from a water depth of 540 m in the Inner Sea of the Maldives (Indian Ocean).

Shallow Burial Diagenesis vs. Input and Seafloor Dissolution

To assess the effect of burial diagenesis on altering the primary metastable carbonate signal, the results of shipboard pore water chemistry analyses (Davies, McKenzie, Palmer-Julson, et al., 1991) were compared to the fine aragonite records for Holes 818B and 817A. In Hole 818B, pore water $[\text{Sr}^{2+}]$ values increase from seawater values of 97 μM at the core top, to 662 μM at 41 mbsf, and then increase only slightly below this depth to reach a maximum of 746 μM at 89 mbsf (Fig. 20A). Baker et al. (1982) showed that aragonite dissolution during shallow burial of aragonitic sediments releases Sr^{2+} to the pore fluids. The primary conclusions from the shipboard pore water study were that aragonite and Mg calcite dissolved with core depth and that significant recrystallization to low Mg calcite had occurred (Davies, McKenzie, Palmer-Julson, et al., 1991). However, although the downcore increase of Sr^{2+} in the pore waters of Hole 818B must be the result of burial dissolution of aragonite, the percent of fine aragonite values actually increase on average down to 46 mbsf. At this level, an abrupt change in the fine aragonite content occurs where the aragonite content drops from 60% to 37%. Aragonite slightly increases on average below 46 mbsf to a local maximum of 62% at 67 mbsf, below which aragonite decreases to 40% at 80 mbsf. If variations in the aragonite content were simply the result of downcore dissolution, the pore water $[\text{Sr}^{2+}]$ would be expected to increase as aragonite content decreases. The lack of correspondence between the percentage of fine aragonite in the sediments and the associated pore water $[\text{Sr}^{2+}]$ concentration indicates that, although original aragonite values may have decreased downcore through dissolution, the primary aragonite signal (i.e., input plus seafloor preservation/dissolution) has been preserved.

Figure 20B compares the pore water $[\text{Sr}^{2+}]$ record to the percent of fine aragonite content down to 70 mbsf in Hole 817A. Pore water $[\text{Sr}^{2+}]$ values increase downcore to a maximum of 530 μM at 42 mbsf and then gradually decrease below this depth. Between 0 and 42 mbsf, the percent of fine aragonite record displays high amplitude fluctuations ranging between values of 25% and 60%. The average fine aragonite content decreases downcore through this interval. An abrupt

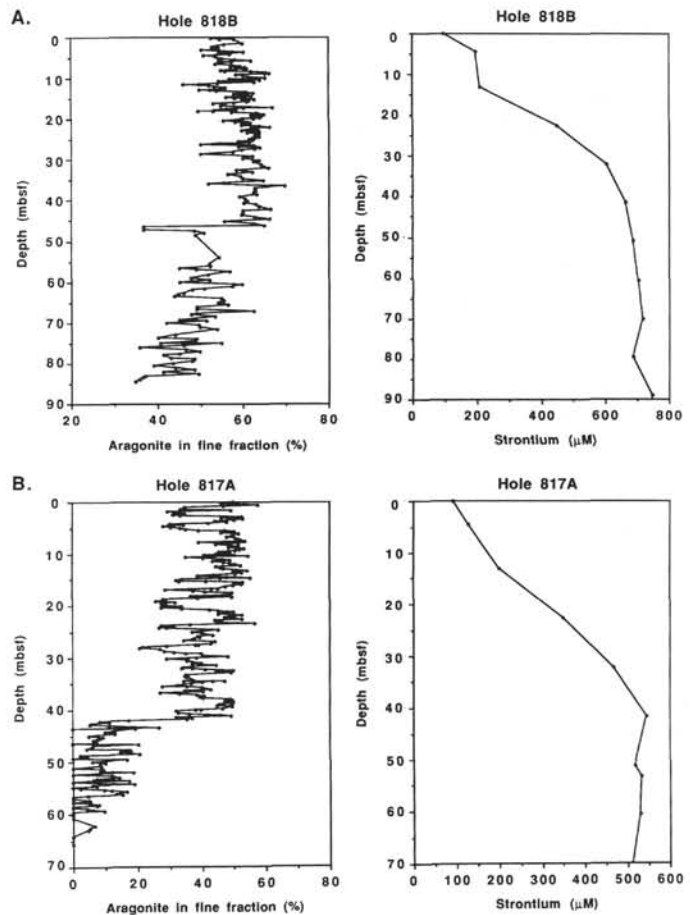


Figure 20. Percentage of aragonite in the fine fraction and $[\text{Sr}^{2+}]$ measured in the pore waters for (A) Hole 818B and (B) Hole 817A. Pore water measurements are from Davies, McKenzie, Palmer-Julson, et al. (1991).

decrease in the percent of fine aragonite content at 42 mbsf from a value of 50% to values ranging between 0% and 25% corresponds to the maximum $[\text{Sr}^{2+}]$ in the pore water. Below 42 mbsf, the percent of fine aragonite values decrease on average down to the first occurrence of aragonite at 64 mbsf. This interval corresponds to an interval of constant pore water $[\text{Sr}^{2+}]$. The general downward decrease of aragonite and the increase of pore water $[\text{Sr}^{2+}]$ is consistent with a diagenetic explanation for the aragonite content. However, because $[\text{Sr}^{2+}]$ steadily increases from the core top to 42 mbsf while the percent of fine aragonite content displays significant fluctuations and only slightly decreases, it is difficult to explain the fine aragonite fluctuations by shallow burial diagenesis alone. Therefore, we interpret the percent of fine aragonite content in Hole 817A to reflect the primary aragonite signal that has been reduced, but not removed, by shallow burial dissolution of aragonite.

$\delta^{13}\text{C}$ Record in Hole 818B

Background

The utility of $\delta^{13}\text{C}$ as a tracer of seawater paleoenvironments and paleocirculation is due to the processes that control its distribution in the sea. Typically, surface waters are relatively enriched in ^{13}C because of the preferential sequestering of ^{12}C in organic matter with a fractionation factor of -20 to -25 (Craig, 1953; Wong and Sackett, 1978). Surface waters, therefore, tend to have heavy $\delta^{13}\text{C}$ of ΣCO_2 values in high productivity regions. However, upwelling of nutrient-rich and light $\delta^{13}\text{C}$ water can have the affect of actually lowering surface water $\delta^{13}\text{C}$ even though productivity is stimulated by the

nutrient increase (Tilbrook, 1982; Oppo and Fairbanks, 1989; Charles and Fairbanks, 1990). The extent and temperature of equilibration between surface water and atmospheric CO_2 also controls the carbon isotopic ratio of surface water ΣCO_2 ; the greater the equilibration and the colder the air temperature, the heavier the $\delta^{13}\text{C}$ of ΣCO_2 of the equilibrated water (Mook et al., 1974; Kroopnick, 1974). Equilibration is greatest if surface waters are in contact with the atmosphere for long periods of time, such as North Atlantic surface waters, and in areas of high air/sea gaseous exchange, which is primarily a function of wind-induced sea-surface roughness (Liss and Merlivet, 1986). $\delta^{13}\text{C}$ is a much better constrained tracer of deep water-mass circulation than it is for surface water conditions because the only important variables that determine the $\delta^{13}\text{C}$ of deep water ΣCO_2 are (1) the $\delta^{13}\text{C}$ of the source water (preformed value), (2) the water mass age, and (3) the amount of mixing with adjacent water masses. Oxidation of organic matter (remneralization) in the water column and on the seafloor releases light carbon in the form of CO_2 and decreases the $\delta^{13}\text{C}$ of seawater ΣCO_2 . Through remneralization of organic matter, deep and bottom waters become ^{13}C -depleted (lighter $\delta^{13}\text{C}$), CO_2 and nutrient enriched, and more corrosive relative to CaCO_3 with increasing age (Broecker, 1981).

$\delta^{13}\text{C}$ of Antarctic Intermediate Water and Coral Sea Surface Water

The foraminiferal $\delta^{13}\text{C}$ record for Hole 818B is characterized by (1) benthic foraminiferal $\delta^{13}\text{C}$ values that have generally been heavier than planktonic foraminiferal $\delta^{13}\text{C}$ values (i.e., $\Delta\delta^{13}\text{C}_{\text{surface-intermediate}} < 0$), at least during the last 0.54 m.y. (this study) and possibly back to the late Miocene (Isern this volume); (2) covariant benthic and planktonic foraminiferal $\delta^{13}\text{C}$ values; (3) the tendency during the last 0.54 m.y. for benthic and planktonic foraminiferal $\delta^{13}\text{C}$ values to be heavy at interglacial to glacial transitions and/or early during glacial stages, and for benthic and planktonic foraminiferal $\delta^{13}\text{C}$ to be light during glacial to interglacial transitions and/or early during interglacial stages; and (4) a pattern during the period from 0.75 to 1.6 Ma in which heavy planktonic foraminiferal $\delta^{13}\text{C}$ values covaried with heavy planktonic foraminiferal $\delta^{18}\text{O}$ values and light planktonic foraminiferal $\delta^{13}\text{C}$ covaried with light planktonic foraminiferal $\delta^{18}\text{O}$ values.

To determine why intermediate water $\delta^{13}\text{C}$ has been heavier than surface water $\delta^{13}\text{C}$ in Hole 818B, we studied the $\delta^{13}\text{C}$ profiles from Kroopnick (1984) along the closest GEOSECS transect in the South Pacific Ocean. Profiles of $\delta^{13}\text{C}$ show that for GEOSECS Stations 269 and 278, $\delta^{13}\text{C}$ remains constant or becomes slightly heavier with water depth down to 700 to 1000 m (Fig. 21). This $\delta^{13}\text{C}$ gradient is reversed from the typical low and middle latitude oceanic gradient in which $\delta^{13}\text{C}$ is heavy at the surface and becomes very light within the oxygen minimum zone, commonly between 500 and 1000 m. The reversed surface-to-intermediate water $\delta^{13}\text{C}$ gradient may indicate the presence at depth of AAIW, which has heavy $\delta^{13}\text{C}$ of ΣCO_2 primarily because it forms from surface waters of the APFZ that have partially equilibrated with cold air, whereas the $\delta^{13}\text{C}$ of ΣCO_2 of Coral Sea surface water is relatively light because it equilibrates with a warm atmosphere. Therefore, one possible explanation for similar or slightly heavier benthic foraminiferal $\delta^{13}\text{C}$ values as compared to planktonic foraminiferal $\delta^{13}\text{C}$ values in Hole 818B may be related to the continuous presence of heavy $\delta^{13}\text{C}$ AAIW in the Townsville Trough throughout the last 0.54 m.y.

AAIW can be identified and traced it to its origin by determining the phosphate-normalized $\delta^{13}\text{C}$ of ΣCO_2 ($\delta^{13}\text{C}_{\text{P-N}}$) for a transect of water-depth profiles (cf. Oppo and Fairbanks, 1989). $\delta^{13}\text{C}_{\text{P-N}}$ is the $\delta^{13}\text{C}$ a watermass would have were phosphate completely removed by primary producers and calculated according to the equation:

$$\delta^{13}\text{C}_{\text{P-N}} = \delta^{13}\text{C}_{\text{seawater}} - (-0.93) \times \text{PO}_4^{3-}$$

(Oppo and Fairbanks, 1989).

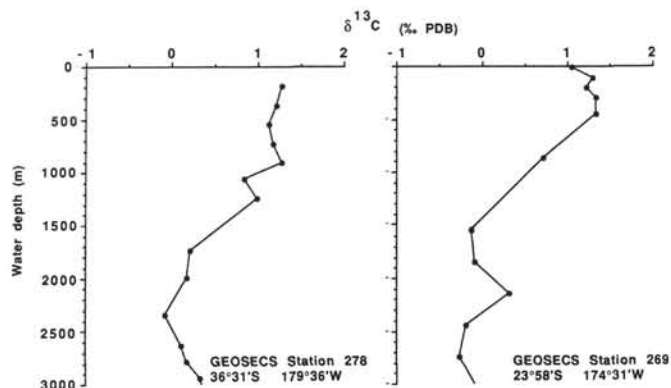


Figure 21. Water-column $\delta^{13}\text{C}$ of ΣCO_2 from GEOSECS Stations 278 and 269 from the western South Pacific (Kroopnick, 1985).

For our South Pacific Ocean calculations we used $\delta^{13}\text{C}$ of ΣCO_2 values from Kroopnick (1984) and PO_4^{3-} values from Broecker et al. (1982).

Nutrient-rich surface waters flow northward from the Antarctic Divergence Zone, acquiring an increasingly heavy $\delta^{13}\text{C}$ ratio of ΣCO_2 through the combined effects of high productivity and high equilibration with a cold atmosphere, and sink in the region of the APF to form AAIW. In spite of the extremely high productivity of circum-Antarctic surface waters, nutrients are underutilized in this region and sinking AAIW retains high nutrient concentrations. AAIW is distinctly different from other major intermediate and deep watermasses because of its high nutrient content and relatively heavy $\delta^{13}\text{C}$ ratio of ΣCO_2 . NADW, for example, has a low nutrient content and a heavy $\delta^{13}\text{C}$ ratio of ΣCO_2 and AABW has a high nutrient content and a light $\delta^{13}\text{C}$ ratio of ΣCO_2 . Because of the unique combination of high nutrient content and heavy $\delta^{13}\text{C}$ of ΣCO_2 , AAIW is easily recognized by its heavy $\delta^{13}\text{C}_{\text{P-N}}$.

Water depth profiles of $\delta^{13}\text{C}_{\text{P-N}}$ from GEOSECS Station 290 at 58°S latitude, northward to Station 251 at 4°S latitude are shown in Figure 22. Heavy surface water $\delta^{13}\text{C}$ at 58°S is the combined result of high gas exchange between surface water and the atmosphere at cold temperatures, and the high surface-water productivity. If all nutrients were consumed, the surface-water $\delta^{13}\text{C}$ ratio at GEOSECS Station 290 would be the calculated $\delta^{13}\text{C}_{\text{P-N}}$ value of 3.6‰ instead of the measured value of 2.2‰. The preformed $\delta^{13}\text{C}_{\text{P-N}}$ value of AAIW is probably similar to the surface-water $\delta^{13}\text{C}_{\text{P-N}}$ value at GEOSECS Station 290. The $\delta^{13}\text{C}_{\text{P-N}}$ profile for GEOSECS Station 278 at 36°S reveals the presence of AAIW water on its northward course with $\delta^{13}\text{C}_{\text{P-N}}$ values of 2.5‰ to 3.0‰ at water depths between 500 and 1500 m. Continuing northward, the GEOSECS Station 269 profile displays anomalously heavy $\delta^{13}\text{C}_{\text{P-N}}$ of up to 2.6‰ between 500 and 1000 m. Heavy $\delta^{13}\text{C}_{\text{P-N}}$ values of 2.5‰ to 3.0‰ also were observed between 500 and 1500 m at GEOSECS Station 251.

Through mixing between intermediate water and tropical surface water, not necessarily tied to upwelling, it is possible for the $\delta^{13}\text{C}$ of ΣCO_2 of surface water to change in concert with changes in the preformed $\delta^{13}\text{C}$ of ΣCO_2 and nutrient concentration of intermediate water (Oppo and Fairbanks, 1989). Surface water that is mixed with a high $\delta^{13}\text{C}_{\text{P-N}}$ intermediate water mass will have a heavier $\delta^{13}\text{C}$ of ΣCO_2 than surface water that mixes with a low $\delta^{13}\text{C}_{\text{P-N}}$ intermediate water mass. Heavy fossil planktonic foraminiferal $\delta^{13}\text{C}$ values in Hole 818B may reflect the influence of heavy $\delta^{13}\text{C}$ and nutrient rich AAIW whereas light planktonic $\delta^{13}\text{C}$ ratios may reflect the influence of an AAIW that was relatively light in $\delta^{13}\text{C}$ and nutrient depleted. This link between surface and intermediate water $\delta^{13}\text{C}$ might explain the covariance of planktonic and benthic carbon isotopic ratios during the last 0.54 m.y. and also suggests that values of $\Delta\delta^{13}\text{C}_{\text{(surface-intermediate)}}$ may be largely unrelated to local carbon fluxes in the Townsville Trough.

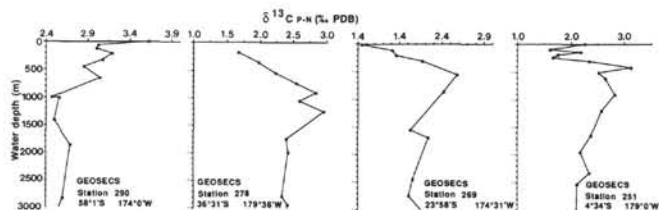


Figure 22. Phosphate-normalized $\delta^{13}\text{C}$ plotted on a transect from 58° to 4°S in the western South Pacific Ocean (GEOSECS Stations 290, 278, 269, and 251). $\delta^{13}\text{C}$ values are from Kroopnick (1985) and phosphate values are from Broecker et al. (1982). The combination of heavy preformed $\delta^{13}\text{C}$ and excess nutrients make the $\delta^{13}\text{C}_{\text{P-N}}$ values of AAIW anomalously heavy. AAIW is easily traced from its origin in Antarctic surface waters (Station 290), where it descends to a depth of 500 to 1500 m (Station 278) and then slightly ascends northward to a depth of 500 to 1000 m (Station 269) before it begins to lose its identity near the equator.

Furthermore, both the benthic and foraminiferal $\delta^{13}\text{C}$ ratios in Hole 818B and other cores from the Townsville Trough may monitor changes in the preformed $\delta^{13}\text{C}$ of ΣCO_2 of AAIW.

If fluctuations of intermediate and surface-water $\delta^{13}\text{C}$ in Hole 818B reflect changes in the $\delta^{13}\text{C}$ of AAIW, an interpretation of the foraminiferal $\delta^{13}\text{C}$ variations for the Quaternary is possible. The light $\delta^{13}\text{C}$ values for *Cibicidoides* spp. during glacial to interglacial transitions, and/or early during interglacial stages, may reflect the influence of relatively light $\delta^{13}\text{C}$ AAIW. AAIW would have been lighter in $\delta^{13}\text{C}$ if (1) upwelling rates of Circumpolar Deep Water (CPDW) increased, (2) primary producers were less able to utilize nutrients than today (i.e., lower productivity), (3) there was less isotopic equilibration with the atmosphere because of reduced wind speeds and/or warmer temperatures near the APF, or (4) the $\delta^{13}\text{C}$ of ΣCO_2 of upwelled CPDW decreased. The latter would occur if the relative contribution of NADW to CPDW were to decrease (Charles and Fairbanks, 1990). Heavy AAIW $\delta^{13}\text{C}$ during past interglacial to glacial transitions, and early during past glacial intervals, would occur if some combination of the opposite of the conditions listed above was realized.

The number and complexity of variables that control the preformed $\delta^{13}\text{C}$ of AAIW make it very difficult to determine which variable has been the most important in producing changes in the carbon isotopic composition of this intermediate water mass. Planktonic foraminiferal $\delta^{13}\text{C}$ data suggest that nutrients were higher in Antarctic surface waters during the LGM (Labeyrie and Duplessy, 1985). Charles and Fairbanks (1990) determined that the $\delta^{13}\text{C}$ of ΣCO_2 of surface water at the APF was lighter during the LGM and they made a strong case against models that invoke higher productivity near Antarctica during the LGM than during the Holocene to explain the lower glacial atmospheric CO_2 concentrations measured in Antarctic ice cores (e.g., polar nutrient models of Knox and McElroy, 1985; Siegenthaler and Wenk, 1984; Sarmiento and Toggweiler, 1985; Keir, 1988; Lyle and Pisias, 1990; Martin, 1990). Instead, the light planktonic foraminiferal $\delta^{13}\text{C}$ values seem to indicate that glacial productivity in the region of the APF was lower than today (Charles and Fairbanks, 1990). However, the link between changes in $\delta^{13}\text{C}$ of ΣCO_2 and nutrient concentrations in AAIW remains somewhat of an open question primarily because Cd data from the Southern Ocean indicate that virtually no glacial to interglacial change occurred in PO_4^{3-} (nutrient concentration) (Boyle, 1990). It is possible that the air/sea isotopic exchange at the APF can completely decouple nutrients from the $\delta^{13}\text{C}$ of ΣCO_2 (Charles and Fairbanks, 1990). If this is true, $\delta^{13}\text{C}$ of AAIW may also decouple from pCO_2 and $[\text{CO}_3^{2-}]$, which implies that foraminiferal $\delta^{13}\text{C}$ may be a poor proxy for studying changes in the AAIW CaCO_3 saturation. The decoupling of CO_2 and the pre-formed $\delta^{13}\text{C}$ of AAIW also may explain the lack of correlation between the percent of whole pteropods

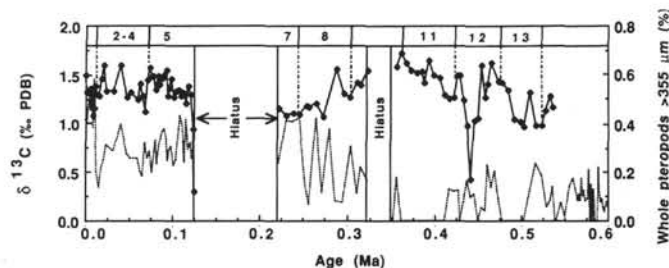


Figure 23. Comparison of the record of $\delta^{13}\text{C}$ for *Cibicidoides* spp. (solid line with solid dots) and the percentage of whole pteropods ($>355\ \mu\text{m}$) (dashed line) in Hole 818B for the past 0.54 m.y. Light benthic $\delta^{13}\text{C}$ values in deep-sea sediments usually correspond to corrosive waters. However, in Hole 818B, no relationship exists between light $\delta^{13}\text{C}$ and low percentages of whole pteropods (aragonite dissolution). Instead, the maximum dissolution interval from 0.36 to 0.41 Ma correlates with some of the heaviest benthic $\delta^{13}\text{C}$ values during the past 0.54 m.y.

(aragonite preservation) and the $\delta^{13}\text{C}$ record for *Cibicidoides* spp. measured in Hole 818B (Fig. 23).

CONCLUSIONS

1. Based on the occurrence and variations of fine aragonite content, Mg calcite content, and percent whole pteropods, CaCO_3 preservation clearly improved between 0.9 and 1.6 Ma in both Holes 818B and 817A. Aragonite first appeared in Hole 817A (1016 mbsl) at the Pliocene-Pleistocene boundary, whereas, aragonite was present in the shallower Hole 818B (745 mbsl) back to 2.9 Ma (Droxler et al., this volume). An increase of carbonate preservation during the early Pleistocene was also discovered by Farrell and Prell (1991) in cores from the deep central equatorial Pacific Ocean.

2. A dissolution pulse occurred in both Holes near 0.9 Ma that was followed by an abrupt and permanent preservation increase. CaCO_3 dissolution near 0.9 Ma has also been noted in deep-sea records (Hays et al., 1969; Saito et al., 1975; Moore et al., 1982; Vincent, 1985; Farrell and Prell, 1991) and within intermediate waters (Droxler et al., 1988, 1990).

3. The sharp increase of fine aragonite content and percent whole pteropods between 0.86 and 0.875 Ma was the result of greater sediment input from carbonate banks of the Queensland Plateau, possibly accompanied by an improvement of CaCO_3 preservation. The timing of the aragonite increase in Holes 818B and 817A is very close to the age of the initiation of the Great Barrier Reef determined by the Leg 133 Scientific Party (Davies, McKenzie, Palmer-Julson, et al., 1991). The dramatic and permanent increase in bank production on the Queensland Plateau near 0.86 to 0.875 Ma is also similar in age to carbonate production increases discovered at Mururoa atoll in French Polynesia (Aïssaoui et al., 1990) and in the Bahamas (McNeill et al., 1989; Aïssaoui et al., 1990). Generally high aragonite content in periplatform sediments since 0.8 Ma may indicate greater high-stand shedding from bank tops in response to the global change in sea level fluctuations from low amplitude, high frequency variations before 0.9 Ma to high amplitude and low frequency variations after 0.73 Ma (as inferred from the oxygen isotope record).

4. A decrease in fine aragonite, fine Mg calcite, and the percent of whole pteropods occurred between 0.36 and 0.41 Ma that corresponds with the strongest dissolution episode of the well-established mid-Brunhes CaCO_3 dissolution interval observed in sediment cores from deep-sea (Hays et al., 1969; Adelseck, 1977; Moore et al., 1982; Vincent, 1985; Peterson and Prell, 1985b; Crowley, 1985; Farrell and Prell, 1989) and intermediate-water depths (Droxler et al., 1988, 1990; Haddad, 1990) around the world.

5. Heavy $\delta^{13}\text{C}$ of *Cibicidoides* spp. relative to *G. sacculifer* during the past 0.54 m.y. may be due to the continuous presence of AAIW, characterized by heavy $\delta^{13}\text{C}$ of ΣCO_2 , in the Townsville Trough.

During the past 0.525 m.y., benthic and planktonic $\delta^{13}\text{C}$ are often heavy during interglacial to glacial transitions, and light during glacial to interglacial transitions. From 0.75 to 1.6 Ma, planktonic $\delta^{13}\text{C}$ is generally heavy when $\delta^{18}\text{O}$ is heavy and light when $\delta^{18}\text{O}$ is light. We suggest that this pattern represents changes in the $\delta^{13}\text{C}$ of the source water for AAIW and might reflect changes in nutrient utilization by primary producers, upwelling rates, the $\delta^{13}\text{C}$ of water upwelled into Antarctic surface waters (possibly a function of the NADW flux) (Charles and Fairbanks, 1990), or changes in the extent and/or temperature of gas exchange between surface water and the atmosphere near the APF.

6. Poor correlation between percent of whole pteropods (aragonite preservation) and $\delta^{13}\text{C}$ of *Cibicides* spp. during the past 0.54 m.y. may be the result of a decoupling of $\delta^{13}\text{C}$ from $p\text{CO}_2$ due to the numerous and complex variables that combine to produce the preformed $\delta^{13}\text{C}$ of AAIW.

ACKNOWLEDGMENTS

This study was funded primarily through a JOI/USSAC Graduate Fellowship with partial support from a NASA Graduate Fellowship in Global Change Research and from the Donors of the Petroleum Research Fund administered by the American Chemical Society. We are grateful to L. Peterson and A. Gardulski for their prompt and thoughtful reviews, which helped to improve the manuscript greatly. We also thank J. Mahr and V. Meyers for their invaluable assistance with sample processing and XRD analyses.

REFERENCES*

- Acker, J.G., 1988. Factors influencing the dissolution of aragonite in the oceanic water column [Ph.D. dissert.]. Univ. South Florida, Tampa, FL.
- Adelseck, C.G., Jr., 1977. Recent and late Pleistocene sediments from the eastern equatorial Pacific Ocean: sedimentation and dissolution [Ph.D. dissert.]. Univ. of California, San Diego.
- Aïssaoui, D.M., McNeill, D.F., and Kirschvink, J.L., 1990. Magnetostratigraphy dating of shallow-water carbonates from Mururoa atoll, French Polynesia: implications for global eustasy. *Earth Planet. Sci. Lett.*, 97:102–112.
- Amolgi-Labin, A., Luz, B., and Duplessy, J.-C., 1986. Pteropod preservation and stable-isotope record of the Red Sea. *Palaeogeogr., Palaeoclimatol., Palaeoecol.*, 57:195–211.
- Archer, D.E., 1990. The dissolution of calcite in deep sea sediments: an in situ microelectrode study [Ph.D. dissert.]. Univ. Washington, Seattle.
- , 1991. Equatorial Pacific calcite preservation cycles: production or dissolution? *Paleoceanography*, 6:561–571.
- Arrhenius, G., 1952. Sediment cores from the east Pacific. *Rep. Swed. Deep-Sea Exped. 1947–1948*, 5.
- , 1988. Rate of production, dissolution and accumulation of biogenic solids in the ocean. *Palaeogeogr., Palaeoclimatol., Palaeoecol.*, 67:119–146.
- Austin, J.A., Jr., Schlager, W., Palmer, A.A., et al., 1986. *Proc. ODP, Init. Repts.*, 101: College Station, TX (Ocean Drilling Program).
- Baker, P.A., Gieskes, J.M., and Elderfield, H., 1982. Diagenesis of carbonates in deep-sea sediments: evidence from $\text{Sr}^{2+}/\text{Ca}^{2+}$ ratios and interstitial dissolved Sr^{2+} data. *J. Sediment. Petrol.*, 52:71–82.
- Balsam, W.B., 1983. Carbonate dissolution on the Muir Seamount (western North Atlantic): interglacial/glacial changes. *J. Sediment. Petrol.*, 53:719–731.
- Bard, E., Hamelin, B., and Fairbanks, R.G., 1990. U-Th ages obtained by mass spectrometry in corals from Barbados: sea level during the past 130,000 years. *Nature*, 346:456–458.
- Barnola, J.M., Raynaud, D., Korotkevich, Y.S., and Lorius, C., 1987. Vostok ice core provides 160,000-year record of atmospheric CO_2 . *Nature*, 329:408–414.
- Bassinot, F.C., Beaufort, L., Lancelot, Y., and Vincent, E., 1992. Sonostratigraphy of equatorial Indian Ocean piston cores: toward a rapid and high-resolution tool for tracking dissolution cycles in Pleistocene carbonate sediments. *Fourth Int. Conf. Paleoceanogr.*, Kiel, Germany, 55. (Abstract)
- Bassinot, F.C., Labeyrie, L., Vincent, E., Beaufort, L., Lancelot, Y., Meynadier, L., and Valet, J.P., 1992. Influence of monsoon on pelagic carbonate sedimentation in the equatorial Indian Ocean: high-resolution record from a 54 m piston core. *Fourth Int. Conf. Paleoceanogr.*, Kiel, Germany, 54. (Abstract)
- Bé, A.W.H., and Gilmer, R.W., 1977. A zoogeographic and taxonomic review of Euthecosomatous pteropoda. In Ramsay, A.T.S. (Ed.), *Oceanic Micropaleontology* (Vol. 1): New York (Academic Press), 733–808.
- Bé, A.W.H., Morse, J.W., and Harrison, S.M., 1975. Progressive dissolution and ultrastructural breakdown of planktonic foraminifera. In Sliter, W.V., Bé, A.W.H., and Berger, W.H. (Eds.), *Dissolution of Deep-Sea Carbonates*. Spec. Publ. Cushman Found. Foraminifer Res., 13:7–55.
- Berger, W.H., 1968. Planktonic foraminifera: selective solution and paleoclimatic interpretation. *Deep-Sea Res. Part A*, 15:31–43.
- , 1973. Deep-sea carbonates: Pleistocene dissolution cycles. *J. Foraminifer Res.*, 3:187–195.
- , 1977. Deep-sea carbonate and the deglaciation preservation spike in pteropods and foraminifera. *Nature*, 269:301–304.
- , 1978. Deep-sea carbonate: pteropod distribution and the aragonite compensation depth. *Deep-Sea Res. Part A*, 25:447–452.
- , 1985. CO_2 increase and climate prediction: clues from deep-sea carbonates. *Episodes*, 8:163–168.
- , 1992. Pacific carbonate cycles revisited: arguments for and against productivity control. In Ishizaki, K., and Saito, T. (Eds.), *Centenary of Japanese Micropaleontology*: Tokyo (Terra Sci.), 15–25.
- Berner, R.A., 1977. Sedimentation and dissolution of pteropods in the ocean. In Andersen, N.R., and Malahoff, A. (Eds.), *The Fate of Fossil Fuel CO_2 in the Oceans*: New York (Plenum), 243–260.
- Berner, R.A., Berner, E.K., and Keir, R.S., 1976. Aragonite dissolution on the Bermuda Pedestal: its depth and geochemical significances. *Earth Planet. Sci. Lett.*, 30:169–178.
- Berner, R.A., and Honjo, S., 1981. Pelagic sedimentation of aragonite: its geochemical significance. *Science*, 211:940–942.
- Betzer, P.R., Byrne, R.H., Acker, J.G., Lewis, C.S., Jolley, R.R., 1984. The oceanic carbonate system: a reassessment of biogenic controls. *Science*, 226:1074–1076.
- Boardman, M.R., 1978. Holocene deposition in northwest Providence Channel, Bahamas: a geochemical approach [Ph.D. dissert.]. Univ. of North Carolina, Chapel Hill.
- Boardman, M.R., and Neumann, A.C., 1984. Sources of periplatform carbonates: Northwest Providence Channel, Bahamas. *J. Sediment. Petrol.*, 54:1110–1112.
- Boyle, E.A., 1986a. Deep ocean circulation, preformed nutrients, and atmospheric carbon dioxide: theories and evidence from oceanic sediments. In Hsü, K. (Ed.), *Mesozoic and Cenozoic Oceans*. Am. Geophys. Union, Geodyn. Ser., 15:49–60.
- , 1986b. Paired carbon isotope and cadmium data from benthic foraminifera: implications for changes in oceanic phosphorus, oceanic circulation, and atmospheric carbon dioxide. *Geochim. Cosmochim. Acta*, 50:265–276.
- , 1988a. Cadmium: chemical tracer of deepwater paleoceanography. *Paleoceanography*, 3:471–490.
- , 1988b. The role of vertical chemical fractionation in controlling late Quaternary atmospheric carbon dioxide. *J. Geophys. Res.*, 93:15701–15714.
- , 1990. Effect of depleted planktonic $^{13}\text{C}/^{12}\text{C}$ on bottom water during periods of enhanced relative Antarctic productivity. *Eos*, 71:1357–1358.
- Boyle, E.A., and Keigwin, L., 1987. North Atlantic thermohaline circulation during the past 20,000 years linked to high-latitude surface temperature. *Nature*, 330:35–40.
- Broecker, W.S., 1981. Glacial to interglacial changes in ocean and atmosphere chemistry. In Berger, A. (Ed.), *Climatic Variations and Variability: Facts and Theories*: Hingham, MA (D. Reidel), 109–120.
- , 1982. Ocean chemistry during glacial time. *Geochim. Cosmochim. Acta*, 46:1689–1705.
- Broecker, W.S., Andree, M., Wolfi, W., Oeschger, H., Bonani, G., Kennett, J., and Peteet, D., 1988. The chronology of the last deglaciation: implications to the cause of the Younger Dryas event. *Paleoceanography*, 3:1–19.
- Broecker, W.S., Peng, T.H., and Engh, R., 1980. Modeling the carbon system. *Radiocarbon*, 22:565–598.
- Broecker, W.S., Spencer, W., and Craig, H., 1982. *GEOSecs Pacific Expedition, Hydrographic Data, 3*, Washington (U.S. Govt. Printing Office).

* Abbreviations for names of organizations and publication titles in ODP reference lists follow the style given in *Chemical Abstracts Service Source Index* (published by American Chemical Society).

- Broecker, W.S., and Takahashi, T., 1978. The relationship between lysocline depth and *in-situ* carbonate ion concentration. *Deep-Sea Res. Part A*, 27:591–613.
- Byrne, R.H., Acker, J.G., Betzer, P.R., Feely, R.A., and Cates, M., 1984. Water column dissolution of aragonite in the Pacific Ocean. *Nature*, 12:321–326.
- Charles, C.D., and Fairbanks, R.G., 1990. Glacial to interglacial changes in the isotopic gradients of Southern Ocean surface water. In Bleil, U., and Thiede, J. (Eds.), *Geological History of Polar Oceans: Arctic Versus Antarctic*: Netherlands (Kluwer Academic), 519–538.
- Chen, C., 1964. Pteropod ooze from Bermuda Pedestal. *Science*, 144:60–62.
- , 1968. Pleistocene pteropods in pelagic sediments. *Nature*, 219:1145–1149.
- Cofer-Shabica, N.B., 1987. The late Pleistocene deep water history of the Venezuela Basin in the Eastern Caribbean Sea [M.S. thesis]. Univ. of Miami, Coral Gables, FL.
- Craig, H., 1953. Carbon-13 in plants and the relationship between carbon-13 and carbon-14 variations in nature. *Geology*, 62:115–149.
- Craig, H., Broecker, W.S., and Spencer, D., 1981. *GEOSECS Pacific Expedition, Sections and Profiles, 4*. Washington (U.S. Govt. Printing Office).
- Crowley, T.J., 1983. Calcium carbonate preservation patterns in the central North Atlantic during the last 150,000 years. *Mar. Geol.*, 51:1–41.
- , 1985. Late Quaternary carbonate changes in the North Atlantic, and Atlantic-Pacific comparisons. In Sundquist, E.T., and Broecker, W.S. (Eds.), *The Carbon Cycle and Atmospheric CO₂: Natural Variations, Archean to Present*. Am. Geophys. Union Monogr. Ser., 32:271–284.
- Cullen, J.L., and Droxler, A.W., 1990. Late Quaternary variations in planktonic foraminifers faunas and pteropod preservation in the equatorial Indian Ocean. In Duncan, R.A., Backman, J., Peterson, L.C., et al., *Proc. ODP, Sci. Results*, 115: College Station, TX (Ocean Drilling Program), 579–588.
- Curry, W.B., and Crowley, T.J., 1987. The $\delta^{13}\text{C}$ of equatorial Atlantic surface waters: implications for ice-age pCO₂ levels. *Paleoceanography*, 2:489–517.
- Curry, W.B., Duplessy, J.C., Labeyrie, L.D., and Shackleton, N.J., 1988. Changes in the distribution of $\delta^{13}\text{C}$ of deep water ΣCO_2 between the last glacial and the Holocene. *Paleoceanography*, 3:317–341.
- Damuth, J.E., 1975. Quaternary climate change as revealed by calcium carbonate fluctuations in western equatorial Atlantic sediments. *Deep-Sea Res. Part A*, 22:725–743.
- Davies, P.J., McKenzie, J.A., Palmer-Julson, A., et al., 1991. *Proc. ODP, Init. Repts.*, 133: College Station, TX (Ocean Drilling Program).
- Diester-Haas, L., 1985. Late Quaternary sedimentation on the eastern Walvis Ridge, southeast Atlantic (HPC 532 and four piston cores). *Mar. Geol.*, 65:145–189.
- Dietrich, G., Kalle, K., Krauss, W., and Siedler, G., 1980. *General Oceanography: an Introduction*. New York (Wiley).
- Droxler, A.W., 1984. Late Quaternary glacial cycles in the Bahamian Deep Basins and in the adjacent ocean [Ph.D. dissert.]. Univ. Miami, Coral Gables, FL.
- Droxler, A.W., Bruce, C.H., Sager, W.W., and Watkins, D.H., 1988. Pliocene-Pleistocene variations in aragonite content and planktonic oxygen-isotope record in Bahamian periplatform ooze, Hole 633A. In Austin, J.A., Jr., Schlager, W., et al., *Proc. ODP, Sci. Results*, 101: College Station, TX (Ocean Drilling Program), 221–244.
- Droxler, A.W., Haddad, G.A., Mucciarone, D.A., and Cullen, J.L., 1990. Pliocene-Pleistocene aragonite cyclic variations in Holes 714A and 716B (The Maldives) compared with Hole 633A (The Bahamas): records of climate-induced CaCO₃ preservation at intermediate water depths. In Duncan, R.A., Backman, J., Peterson, L.C., et al., *Proc. ODP, Sci. Results*, 115: College Station, TX (Ocean Drilling Program), 539–577.
- Droxler, A.W., Morse, J.W., Glaser, K.S., Haddad, G.A., and Baker, P.A., 1991. Surface sediment carbonate mineralogy and water column chemistry: Nicaragua Rise versus the Bahamas. *Mar. Geol.*, 100:277–289.
- Droxler, A.W., Morse, J.W., and Kornicker, W.A., 1988. Controls on carbonate mineral accumulation in Bahamian basins and adjacent Atlantic Ocean sediments. *J. Sediment. Petrol.*, 58:120–130.
- Droxler, A.W., Schlager, W., and Whallon, C.C., 1983. Quaternary aragonite cycles and oxygen-isotope record in Bahamian carbonate ooze. *Geology*, 11:235–239.
- Duplessy J.-C., Shackleton, N.J., Fairbanks, R.G., Labeyrie, L., Oppo, D., and Kalle, N., 1988. Deep-water source variations during the last climatic cycle and their impact on global deepwater circulation. *Paleoceanography*, 3:343–360.
- Emerson, S., and Bender, M., 1981. Carbon fluxes at the sediment-water interface of the deep-sea: calcium carbonate preservation. *J. Mar. Res.*, 39:139–162.
- Emerson, S., Fischer, K., Reimers, C., and Heggie, D., 1985. Organic carbon dynamics and preservation in deep-sea sediments. *Deep-Sea Res. Part A*, 32:1–21.
- Fairbanks, R.G., 1989. A 17,000-year glacio-eustatic sea level record: influence of glacial melting rates on the Younger Dryas event and deep-ocean circulation. *Nature*, 342:637–642.
- Fairbanks, R.G., and Matthews, R.K., 1978. The marine oxygen isotope record in Pleistocene coral, Barbados, West Indies. *Quat. Res.*, 10:181–196.
- Farrell, J.W., and Prell, W.L., 1989. Climatic change and CaCO₃ preservation: an 800,000 year bathymetric reconstruction from the central equatorial Pacific Ocean. *Paleoceanography*, 4:447–466.
- , 1991. Pacific CaCO₃ preservation and $\delta^{18}\text{O}$ since 4 Ma: paleoceanic and paleoclimatic implications. *Paleoceanography*, 6:485–498.
- Feary, D.A., Davies, P.J., Pigram, C.J., and Symonds, P.A., 1991. Climatic evolution and control on carbonate deposition in Northeast Australia. *Palaeogeogr., Palaeoclimatol., Palaeoecol.*, 89:341–361.
- Gardner, J.V., 1975. Late Pleistocene carbonate dissolution cycles in the eastern equatorial Atlantic. In Sliter, W.V., Bé, A.W.H., and Berger, W.H. (Eds.), *Dissolution of Deep-Sea Carbonates*. Spec. Publ. Cushman Found. Foraminiferal Res., 13:129–141.
- Gardulski, A.F., Mullins, H.T., Oldfield, B., Applegate, J., and Wise, S.W., Jr., 1986. Carbonate mineral cycles in ramp slope sediment: Eastern Gulf of Mexico. *Paleoceanography*, 1:555–565.
- Glasby, G.P., 1990. *Antarctic Sector of the Pacific*: Amsterdam (Elsevier).
- Glaser, K.S., and Droxler, A.W., 1991. High production and highstand shedding from deeply submerged carbonate banks, northern Nicaragua Rise. *J. Sediment. Petrol.*, 61:128–142.
- Haddad, G.A., 1986. A study of carbonate dissolution, stable isotope chemistry and minor element composition of pteropods and foraminifers deposited in the Northwest Providence Channel, Bahamas during the past 500,000 years [M.S. thesis]. Duke Univ., Durham, NC.
- Haddad, G.A., Droxler, A.W., and Mucciarone, D.A., 1990. The last 500 k.y. carbonate preservation record at intermediate depths based upon pteropod fragmentation and fine bank-derived aragonite content in periplatform environments of the Maldives and the Bahamas. *Geol. Soc. Am. Abstr. Programs*, 195–196. (Abstract)
- Hallock, P., Hine, A.C., Vargo, G.A., Elrod, J.A., and Joap, W.C., 1988. Platforms of the Nicaraguan Rise: examples of the sensitivity of carbonate sedimentation to excess trophic resources. *Geology*, 16:1104–1107.
- Hallock, P., and Schlager, W., 1986. Nutrient excess and the demise of coral reefs and carbonate platforms. *Palaios*, 1:389–398.
- Haq, B.U., Hardenbol, J., and Vail, P.R., 1988. Mesozoic and Cenozoic chronostratigraphy and cycles of sea-level change. In Wilgus, C.K., Hastings, B.S., Kendall, C.G.St.C., Posamentier, H.W., Ross, C.A., and Van Wagoner, J.C. (Eds.), *Sea-Level Changes—An Integrated Approach*. Spec. Publ.—Soc. Econ. Paleontol. Mineral., 42:72–108.
- Hawley, J., and Pytkowicz, R.M., 1969. Solubility of calcium carbonate in seawater at high pressure and 2 degrees C. *Geochim. Cosmochim. Acta*, 33:1557–1561.
- Hays, J.D., Saito, T., Opdyke, N.D., and Burckle, L.R., 1969. Pliocene-Pleistocene sediments of the equatorial Pacific: their paleomagnetic, biostratigraphic, and climatic record. *Geol. Soc. Am. Bull.*, 80:1481–1513.
- Hodell, D.A., in press. Late Pleistocene paleoceanography of the South Atlantic sector of the Southern Ocean: linkage to NADW production. *Paleoceanography*.
- Imbrie, J., Hays, J.D., Martinson, D.G., McIntyre, A., Mix, A.C., Morley, J.J., Pisias, N.G., Prell, W.L., and Shackleton, N.J., 1984. The orbital theory of Pleistocene climate: support from a revised chronology of the marine $\delta^{18}\text{O}$ record. In Berger, A., Imbrie, J., Hays, J., Kukla, G., and Saltzman, B. (Eds.), *Milankovitch and Climate* (Pt. 1): Dordrecht (D. Reidel), 269–305.
- Jansen, J.H.F., Kuijpers, A., and Troelstra, S.R., 1986. A mid-Brunhes climatic event: long-term changes in global atmospheric and ocean circulation. *Science*, 232:619–622.
- Johnson, D.A., Ledbetter, M., and Burckle, L.H., 1977. Vema Channel paleoceanography: Pleistocene dissolution cycles and episodic bottom water flow. *Mar. Geol.*, 23:1–33.
- Kier, R.S., 1988. On the late Pleistocene ocean geochemistry and circulation. *Paleoceanography*, 3:413–445.
- Kier, R.S., and Pilkey, O.H., 1971. The influence of sea-level changes on sediment carbonate mineralogy, Tongue of the Ocean, Bahamas. *Mar. Geol.*, 11:189–200.
- Knox, F., and McElroy, M.B., 1984. Changes in atmospheric CO₂: influence of the marine biota at high latitude. *J. Geophys. Res.*, 89:4629–4637.

- Kroopnick, P., 1974. Correlation between $\delta^{13}\text{C}$ and ΣCO_2 in surface waters and atmospheric CO_2 . *Earth Planet. Sci. Lett.*, 22:397–403.
- , 1985. The distribution of ^{13}C of ΣCO_2 in the world oceans. *Deep-Sea Res. Part A*, 32:57–84.
- Labeyle, L.D., and Duplessy, J.-C., 1985. Changes in the oceanic $^{13}\text{C}/^{12}\text{C}$ ratio during the last 140,000 years: high latitude surface water records. *Palaeogeogr., Palaeoclimatol., Palaeoecol.*, 50:217–240.
- Le, J., and Shackleton, N.J., 1992. Carbonate dissolution fluctuations in the western equatorial Pacific during the late Quaternary. *Paleoceanography*, 7:21–42.
- Liss, P.S., and Merlivat, L., 1986. Air-sea exchange rates: introduction and synthesis. In Baut-Menard, P. (Ed.), *The Role of Air-Sea Exchange in Geochemical Cycling*: Hingham, MA (D. Reidel), 113–127.
- Luz, B., and Shackleton, N.J., 1975. CaCO_3 solution in the tropical east Pacific during the past 130,000 years. *Spec. Publ. Cushman Found. Foraminiferal Res.*, 13:142–150.
- Lyle, M., and Pisias, N.G., 1990. Ocean circulation and atmospheric CO_2 changes: coupled use of models and paleoceanographic data. *Paleoceanography*, 5:15–41.
- Martin, J.H., 1990. Glacial-interglacial CO_2 change: the iron hypothesis. *Paleoceanography*, 5:15–41.
- McNeill, D.F., 1989. Magnetostratigraphic dating and magnetization of Cenozoic platform carbonates from the Bahamas [Ph.D. dissert.]. Univ. of Miami, Coral Gables, FL.
- McNeill, D.F., Ginsburg, R.N., Chang, S.-B.R., and Kirschvink, J.L., 1988. Magnetostratigraphic dating of shallow-water carbonates from San Salvador, Bahamas. *Geology*, 16:8–12.
- Milliman, J.D., 1974. *Marine Carbonates* (2nd ed.): Berlin (Springer-Verlag).
- Mix, A.C., Pisias, N.G., Zahn, R., Rugh, W., Lopez, C., and Nelson, K., 1991. Carbon 13 in Pacific deep and intermediate waters, 0–370 Ka: implications for ocean circulation and Pleistocene CO_2 . *Paleoceanography*, 6:205–226.
- Mook, W.G., Bommerson, J.C., and Staverman, W.H., 1974. Carbon isotope fractionation between dissolved bicarbonate and gaseous carbon dioxide. *Earth Planet. Sci. Lett.*, 22:169–176.
- Moore, T.C., Pisias, N.G., and Dunn, D.A., 1982. Carbonate time series of the Quaternary and late Miocene sediments in the Pacific Ocean: a spectral comparison. *Mar. Geol.*, 46:217–233.
- Müller, G., and Gastner, M., 1971. The "Karbonat-bombe": a simple device for determination of the carbonate content in sediments, soils and other materials. *Neues Jahrb. Mineral. Monatsh.*, 10:466–469.
- Neumann, A.C., and Land, L.S., 1975. Lime mud deposition and calcareous algae in the Bight of Abaco, Bahamas: a budget. *J. Sediment. Petrol.*, 45:763–786.
- Oba, T., 1969. Biostratigraphy and isotopic paleotemperatures of some deep-sea cores from the Indian Ocean. *Sci. Rep. Tohoku Univ., Ser. 2*, 41:129–195.
- Oppo, D.W., and Fairbanks, R.G., 1987. Variability in the deep and intermediate water circulation of the Atlantic Ocean during the past 25,000 years: Northern Hemisphere modulation of the Southern Ocean. *Earth Planet. Sci. Lett.*, 86:1–15.
- , 1989. Carbon isotope composition of tropical surface water during the past 22,000 years. *Paleoceanography*, 4:333–351.
- , 1990. Atlantic Ocean thermohaline circulation of the last 150,000 years: relationship of climate and atmospheric CO_2 . *Paleoceanography*, 5:277–288.
- Peterson, L.C., and Prell, W.L., 1985a. Carbonate dissolution in Recent sediments of the eastern equatorial Indian Ocean: preservation patterns and carbonate loss above the lysocline. *Mar. Geol.*, 64:259–290.
- , 1985b. Carbonate preservation and rates of climatic change: an 800 kyr record from the Indian Ocean. In Sundquist, E.T., and Broecker, W.S. (Eds.), *The Carbon Cycle and Atmospheric CO_2 : Natural Variations Archean to Present*: Am. Geophys. Union Monogr., 32:251–270.
- Pickard, G.L., Donguy, J.R., Henin, C., and Rougerie, F., 1977. *A Review of the Physical Oceanography of the Great Barrier Reef and western Coral Sea*. Aust. Inst. Mar. Sci. Monogr. Ser., 2:61–135.
- Piaskal, C.H., Neumann, A.C., and Bane, J., 1989. Periplatform carbonate flux in the northern Bahamas. *Deep-Sea Res. Part A*, 36:1391–1406.
- Pisias, N.G., Heath, R.G., and Moore, T.C., 1975. Lag times for oceanic temperature responses to climatic change. *Nature*, 256:716–717.
- Pisias, N.G., and Moore, T.C., Jr., 1981. The evolution of Pleistocene climate: a time series approach. *Earth Planet. Sci. Lett.*, 52:450–458.
- Pisias, N.G., and Rea, D.K., 1988. Late Pleistocene paleoclimatology of the central equatorial Pacific: sea-surface temperature response to the south-east Trade Winds. *Paleoceanography*, 3:21–37.
- Prell, W.L., 1982. Oxygen and carbon isotope stratigraphy for the Quaternary of Hole 502B: evidence for two modes of isotopic variability. In Prell, W.L., Gardner, J.V., et al., *Init. Repts. DSDP*, 68: Washington (U.S. Govt. Printing Office), 455–464.
- Raymo, M.E., Ruddiman, W.F., Shackleton, N.J., and Oppo, D.W., 1990. Evolution of global ice volume and Atlantic-Pacific $\delta^{13}\text{C}$ gradients over the last 2.5 m.y. *Earth Planet. Sci. Lett.*, 97:353–368.
- Reijmer, J.J.G., Schlager, W., Bosscher, H., Beets, C.J., and McNeill, D.F., 1992. Pliocene/Pleistocene platform facies transition recorded in calciturbidites (Exuma Sound, Bahamas). *Sediment. Geol.*, 78:171–179.
- Ruddiman, W.F., Raymo, M.E., Martinson, D.G., Clement, B.M., and Backman, J., 1989. Pleistocene evolution: Northern Hemisphere ice sheets and North Atlantic Ocean. *Paleoceanography*, 4:353–412.
- Saito, T., Burckle, L.H., and Hays, J.D., 1975. Late Miocene to Pleistocene biostratigraphy of equatorial Pacific sediments. In Saito, T., and Burckle, L.H. (Eds.), *Late Neogene Epoch Boundaries*. Spec. Publ. Micropaleontol., 1:226–244.
- Sarmiento, J.L., and Toggweiler, J.R., 1985. A new model for the role of the oceans in determining atmospheric carbon dioxide pCO_2 levels. *Nature*, 308:621–624.
- Schlager, W., and James, N.P., 1978. Low-magnesian calcite limestones forming at the deep-sea floor, Tongue of the Ocean, Bahamas. *Sedimentology*, 25:675–702.
- Schlanger, S.O., and Douglas, R.G., 1974. The pelagic ooze-chalk-limestone transition and its implication for marine stratigraphy. In Hsü, K.J., and Jenkyns, H.C. (Eds.), *Pelagic Sediments: On Land and Under the Sea*. Spec. Publ. Int. Assoc. Sedimentol., 1:117–148.
- Shackleton, N.J., 1977. Carbon-13 in *Uvigerina*: tropical rainforest history and the equatorial Pacific carbonate dissolution cycles. In Andersen, N.R., and Malahoff, A. (Eds.), *The Fate of Fossil Fuel CO_2 in the Oceans*: New York (Plenum), 401–427.
- Shackleton, N.J., and Duplessy, J.-C., 1986. Temperature changes in ocean deep waters during the late Pleistocene. *Second Int. Conf. on Paleoclimatol.*, Woods Hole, MA, 63. (Abstract)
- Shackleton, N.J., and Opdyke, N.D., 1976. Oxygen-isotope and paleomagnetic stratigraphy of Pacific Core V28-239: late Pliocene to latest Pleistocene. In Cline, R.M., and Hays, J.D. (Eds.), *Investigations of Late Quaternary Paleoclimatology and Paleoclimatology*. Mem.—Geol. Soc. Am., 145:449–464.
- Shinn, E.A., Steiner, R.P., Lidz, B.H., and Swart, R.K., 1989. Whittings, a sedimentologic dilemma. *J. Sediment. Petrol.*, 59:147–161.
- Siegenthaler, U., and Wenk, T.H., 1984. Rapid atmospheric CO_2 variations and ocean circulation. *Nature*, 308:624–626.
- Slowey, N.C., 1985. Fine-scale acoustic stratigraphy of Northwest Providence Channel, Bahamas [M.S. thesis]. Univ. North Carolina, Chapel Hill, NC.
- Sundquist, E.T., 1985. Geological perspectives on carbon dioxide and the carbon cycle. In Sundquist, E.T., and Broecker, W.S. (Eds.), *The Carbon Cycle and Atmospheric CO_2 : Natural Variations, Archean to Present*. Am. Geophys. Union Monogr. Ser., 32:5–59.
- Supko, P.R., 1963. A quantitative X-ray diffraction method for the mineralogical analysis of carbonate sediments from Tongue of the Ocean [M.S. thesis]. Univ. of Miami, Coral Gables, FL.
- Thompson, D.R., Bé, A.W.H., Duplessy, J.C., and Shackleton, N.J., 1979. Disappearance of pink-pigmented *Globigerinoides ruber* at 120,000 yr B.P. in the Indian and Pacific Oceans. *Nature*, 280:554–558.
- Thompson, P.R., and Saito, T., 1974. Pacific Pleistocene sediments: planktonic foraminifera dissolution cycles and geochemistry. *Geology*, 2:333–335.
- Thunell, R.C., 1976. Optimum indices of calcium carbonate dissolution in deep-sea sediments. *Geology*, 4:525–528.
- Tillbrook, B.D., 1982. Variations in the stable carbon isotopic composition of tropical Pacific surface waters [M.S. thesis]. Univ. Hawaii, Honolulu.
- Toggweiler, J.R., and Sarmiento, J.L., 1985. Glacial to interglacial changes in atmospheric carbon dioxide: the critical role of ocean surface water in high latitudes. In Sundquist, E.T., and Broecker, W.S. (Eds.), *The Carbon Cycle and Atmospheric CO_2 : Natural Variations, Archean to Present*. Am. Geophys. Union Monogr. Ser., 32:163–184.
- Vincent, E., 1985. Distribution stratigraphique de la teneur en carbonate dans les sédiments néogènes et quaternaires de l'océan Pacifique. *Bull. Soc. Geol. Fr.*, 8:915–924.
- Volat, J.-L., Pastouret, L., and Vergnaud-Grazzini, C., 1980. Dissolution and carbonate fluctuations in Pleistocene deep-sea cores: a review. *Mar. Geol.*, 34:1–28.
- Walter, L.M., and Morse, J.W., 1984. Magnesian calcite stabilities: a reevaluation. *Geochim. Cosmochim. Acta*, 48:1059–1069.

- Williams, D.F., Gribble, D., Healy-Williams, N., and Leschak, P., 1985. Dissolution and water-mass patterns in the southeast Indian Ocean, Part II: the Pleistocene record from Brunhes to Matuyama age sediments. *Geol. Soc. Am. Bull.*, 96:190–202.
- Wong, W.W., and Sackett, W.M., 1978. Fractionation of stable carbon isotopes by marine phytoplankton. *Geochim. Cosmochim. Acta.*, 42:1802–1815.
- Wornardt, W.W., and Vail, P.R., 1991. Revision of the Plio-Pleistocene cycles and their application to sequence stratigraphy and shelf and slope sediments in the Gulf of Mexico. *Trans. Gulf Coast Assoc. Geol. Soc.*, 41:719–744.
- Worthington, L.V., 1970. The Norwegian Sea as a Mediterranean basin. *Deep-Sea Res. Part A*, 17:77–84.
- Wright, R.G., 1977. Planktonic-benthonic ratio in Foraminifera as paleobathymetric tool: quantitative evaluation. *Annu. AAPG and Soc. Econ. Paleontol. Mineral. Conv.*, Washington, D.C., 65. (Abstract)
- Wyrski, K., 1960. The surface circulation of the Coral and Tasman Seas. *Aust. CSIRO Div. of Fisheries and Oceanogr. Tech. Pap.*, 8.
- Zahn, R., Sarnthein, M., and Erlenkeuser, H., 1987. Benthic isotope evidence for changes of the Mediterranean outflow during the late Quaternary. *Paleoceanography*, 2:543–559.

Date of initial receipt: 1 May 1992
Date of acceptance: 22 January 1993
Ms 133SR-229

APPENDIX A
Carbonate Mineralogy, Percentage of Whole Pteropods, and Oxygen and Carbon Isotope Data for Sediment Samples from Hole 818B

Depth (mbsf)	Age (Ma)	Carbonate mineralogy					Whole pteropods (>355 µm) (%)	$\delta^{18}\text{O}_{\text{PDB}}$ <i>G. sacculifer</i> (‰)	$\delta^{18}\text{O}_{\text{PDB}}$ <i>Cibicides</i> spp. (‰)	$\delta^{13}\text{O}_{\text{PDB}}$ <i>G. sacculifer</i> (‰)	$\delta^{13}\text{O}_{\text{PDB}}$ <i>Cibicides</i> spp. (‰)
		Fine fraction (%)	Fine carbonate (%)	Fine aragonite (%)	Fine calcite (%)	Fine Mg calcite (%)					
0.05	0.000	84					42	-1.692	1.922	1.494	1.496
0.25	0.002	86	96	53	15	28	41	-1.579	1.836	1.131	1.325
0.45	0.004	85	96	55	13	28	50	-1.539	1.824	1.319	1.303
0.65	0.006	85	96	58	15	23	45	-1.951	1.832	0.937	1.364
0.85	0.008	92					55	-1.285	2.038	1.256	1.359
1.05	0.010	92					39	-1.066	1.937	0.921	1.079
1.25	0.012	93					58	-0.679	2.315	1.336	1.162
1.45	0.014	79					43	-0.311	2.447	0.905	1.380
1.55	0.015	55	95	60	17	18	20	-0.280	2.700	0.955	1.300
1.75	0.017	40	96	56	22	18	14	-0.422	3.291	1.372	1.284
1.95	0.020	51					22		3.272		1.462
2.15	0.022	56					25	-0.133	3.047	1.474	1.602
2.35	0.024	61	96	53	24	19	32	-0.135	2.996	1.165	1.336
2.55	0.032	68	97	53	26	18	29	-0.155	2.765	1.180	1.329
2.75	0.040	61	96	54	24	18	40	-0.219	2.898	1.040	1.601
2.95	0.047	68	97	53	27	16	28	-0.500	2.705	1.025	1.268
3.05	0.051	63	97	54	27	16	26	-0.445	2.691	0.878	1.327
3.25	0.059	69	97	50	29	18	26	-0.456	2.608	0.818	1.244
3.45	0.062	64	97	55	24	18	21		2.969		1.406
3.65	0.065	78	97	60	16	20	18	-0.308	2.870	1.358	1.282
3.85	0.068	89	97	57	21	20	32	-0.500	2.669	1.360	1.118
4.05	0.071	90	97	54	22	21	26	-0.983	2.816	1.412	1.441
4.25	0.074	82	96	57	24	15	29	-0.552	2.421	1.530	1.567
4.45	0.076	84	97	54	22	21	20	-0.588	2.545	0.797	1.485
4.55	0.077	84	97	51	29	17	25	-0.726	2.578	1.697	1.479
4.75	0.080	84	96	54	27	16	33	-1.046	2.386	1.264	1.350
4.95	0.082	89					23	-0.713	2.372	1.272	1.485
5.15	0.085	88	97	55	24	18	31	-1.049	2.368	1.274	1.390
5.35	0.087	90	96	54	22	20	36	-0.658	2.281	1.262	1.455
5.55	0.090	84	96	58	19	19	38	-0.738	2.325	1.289	1.502
5.75	0.092	76	98	62	17	19	33	-0.693	2.452	1.301	1.544
5.92	0.094	84	94	54	24	15	25	-0.811	2.437	1.355	1.288
6.05	0.096	81	95	58	16	21	29	-1.663	2.658	1.005	1.361
6.25	0.099	78	97	54	19	23	31	-0.803	2.220	1.427	1.458
6.45	0.101	84					23	-0.652	2.338	1.188	1.275
6.65	0.104	83	95	54	25	17	25	-0.808	2.445	1.354	1.328
6.85	0.106	88	96	57	22	17	38	-0.935	2.425	1.192	1.342
7.05	0.109	89	97	60	20	18	44	-0.755	2.397	1.099	1.280
7.25	0.111	89	97	57	25	14	40	-0.864	2.328	1.241	1.323
7.45	0.114	82	97	60	19	17	24	-1.028	2.559	0.935	1.304
7.55	0.115	92	97	61	19	17	42	-0.864	2.327	1.199	1.204
7.75	0.117	77	97	60	19	18	29	-0.972	2.457	0.962	1.378
7.95	0.120	85	96	58	19	19	32	-0.885	2.662	1.207	1.301
8.15	0.122	91	97	55	23	19	26	-0.821	1.614	1.026	0.939
8.36	0.125	85	98	56	25	17	26	-0.773	1.901	1.199	0.304
8.45	0.222	86	98	62	28	7	24	-0.960	1.581	0.806	1.163
8.65	0.229	86	96	66	22	9	42	-1.037	1.842	0.322	1.087
8.85	0.237	89	97	65	20	12	41	-0.847	1.454	0.354	1.108
9.05	0.245	88	95	66	16	12	43	-0.689	2.304	0.436	1.090
9.25	0.253	50	97	58	24	15	15	0.287	2.903	0.814	1.183
9.34	0.256	53					7	0.404	2.974	0.968	1.172
9.54	0.264	81	97	60	32	5	42	-0.085	1.797	1.198	1.208
9.74	0.272	88	97	61	34	2	12	-0.223	2.289	0.810	1.073
9.94	0.280	88	96	65	24	7	38	-0.118		0.773	
10.14	0.287	54	97	62	29	7	8	0.544	3.221	0.977	1.555
10.34	0.295	67	97	57	35	6	7	0.570	2.749	1.199	1.308
10.54	0.303	77	98	64	30	4	31	-0.082	2.481	1.590	1.265
10.74	0.311	70	97	54	39	4	11	-0.771	2.497	0.982	1.427
10.84	0.315	81	97	58	36	3	22	-0.502	2.315	1.136	1.397
11.04	0.323	80	97	63	32	2	16	0.024	2.534	1.504	1.542
11.10	0.352										
11.24	0.356	80	98	54	44	0	18	0.030	2.131	1.550	1.585
11.44	0.362	78	98	50	48	0	0	-0.169	2.090	1.687	1.722
11.64	0.368	74	98	46	52	0	0	-0.190	1.806	1.489	1.625
11.84	0.374	80	98	52	46	0	0	-0.756	1.941	1.410	1.553
12.04	0.380	80	99	53	45	0	0	-0.520	1.913	1.370	1.526
12.24	0.385	85					0	-0.367	1.902	1.516	1.536
12.34	0.388	85	99	56	43	0	0	-0.511	1.772	1.263	1.427
12.54	0.394	82	99	56	43	0	0	-0.298	1.925	1.444	1.654
12.74	0.400	80	98	52	45	0	0	-0.422	2.040	1.424	1.496
12.94	0.406	76	98	50	48	0	0	-0.550	1.732	1.241	1.469
13.14	0.412	85	98	54	44	0	0	-0.260	2.252	1.183	1.292
13.34	0.418	91	97	61	36	0	13	-0.266	2.317	0.965	1.254
13.52	0.423	88	97	62	33	2	12	-0.225	2.204	0.798	1.266
13.74	0.428	83	98	61	37	0	12	0.071	2.300	1.165	1.493
13.84	0.430	83	97	58	40	0	0	-0.150	1.656	1.137	1.500
14.04	0.434	86	96	60	36	0	7	0.017	2.673	0.933	1.243
14.24	0.438	75	97	61	34	2	17	0.343	1.751	1.078	0.976
14.44	0.442	83	98	62	34	2	10		1.678		0.422
14.64	0.447	83	98	56	42	0	11		2.484		1.037
14.84	0.451	80	98	58	40	0	0	0.131	2.066	1.342	1.057

Appendix A (continued).

Depth (mbsf)	Age (Ma)	Fine fraction (%)	Fine carbonate (%)	Carbonate mineralogy			Whole pteropods (>355 μ m) (%)	$\delta^{18}\text{O}_{\text{PDB}}$ <i>G. sacculifer</i> (‰)	$\delta^{18}\text{O}_{\text{PDB}}$ <i>Cibicoides</i> spp. (‰)	$\delta^{13}\text{O}_{\text{PDB}}$ <i>G. sacculifer</i> (‰)	$\delta^{13}\text{O}_{\text{PDB}}$ <i>Cibicoides</i> spp. (‰)
				Fine aragonite (%)	Fine calcite (%)	Fine Mg calcite (%)					
15.04	0.455	81	99	61	38	0	6	0.144	2.570	1.217	1.601
15.22	0.459	84	97	63	35	0	4	0.084	2.592	1.163	1.273
15.34	0.461	74	97	60	36	1	24	0.263	2.354	1.355	1.412
15.54	0.465	79	97	62	35	1	14	0.117	2.547	1.310	1.617
15.74	0.470	79	97	61	34	2	21	-0.078		1.483	
15.94	0.474	79	98	58	39	1	9	0.118	2.277	1.213	1.429
16.14	0.478	80	98	53	45	0	0	0.090	2.422	1.112	1.423
16.34	0.485	85	98	56	42	0	0	-0.389	2.445	1.307	1.343
16.54	0.492	84	98	55	43	0	0	-0.579	1.925	0.887	1.049
16.74	0.499	85	99	55	40	0	0	-0.184	2.300	1.055	1.021
16.84	0.503	88					0	0.078	2.296	1.178	0.964
17.04	0.510	90					12	-0.520	2.496	0.441	1.322
17.24	0.517	89	95	67	24	4	24	-0.935	2.671	-0.137	0.982
17.44	0.524	68	95	60	27	8	19	0.008	3.161	0.625	0.987
17.64	0.529	57	96	56	34	5	6	0.672	3.072	0.925	1.134
17.84	0.534	61	96	54	40	3	8	0.520	3.041	0.916	1.286
17.95	0.536	65	97	58	35	3	14	0.596	2.791	1.104	1.164
18.04	0.538	71	97	53	41	3	0	0.494		0.936	
18.14	0.541	76	97	50	44	3	0	0.595		0.834	
18.15	0.541	68	97	58	36	2	0	0.731		1.194	
18.35	0.546	78	97	58	36	4	7	0.455		1.004	
18.55	0.551	79	97	63	32	2	2	0.308		0.763	
18.75	0.555	72	96	64	30	3	14	0.809		1.360	
18.95	0.560	76	97	65	28	4	18	0.388		1.144	
19.15	0.565	73	97	62	31	4	8	0.188		1.267	
19.34	0.567	77	98	62	32	4	11	-0.185		1.194	
19.45	0.568	76	97	64	29	4	8	-0.251		0.652	
19.65	0.569	74	97	64	30	4	18	0.260		1.070	
19.85	0.571	81	97	62	31	3	10	-0.121		0.652	
20.05	0.573	82	98	60	34	4	13	-0.034		0.745	
20.25	0.574	85	97	59	38	0	8	-0.085		0.641	
20.45	0.576	80	98	56	42	0	9	0.355		1.307	
20.65	0.578	81	98	61	37	0	21	-0.195		1.300	
20.84	0.579	84	99	58	41	0	0	-0.303		0.885	
20.95	0.580	85	99	62	37	0	15	-0.747		1.415	
21.15	0.582	84	98	60	39	0	0	-0.027		1.076	
21.35	0.584	87	98	60	37	0	13	-0.100		1.311	
21.55	0.585	84	98	60	38	0	0	-0.390		1.399	
21.75	0.587	84	98	64	34	0	0	-0.078		0.692	
21.95	0.589	90	98	66	31	1	22	-0.245		0.839	
22.15	0.590	87	97	62	33	2	11	-0.156		1.183	
22.34	0.592	77	96	63	28	4	7	-0.175		1.176	
22.45	0.593	70	97	63	29	4	9	-0.148		1.005	
22.65	0.595	72	96	61	28	6	6	-0.395		1.196	
22.85	0.596		96	60	31	5	3	0.130		1.230	
23.05	0.598	73	96	64	28	4	8	-0.009		1.170	
23.25	0.600	75	96	61	31	5	5	-0.126		1.416	
23.65	0.603	76	96	64	30	3	4	0.443		1.026	
23.85	0.605	80	96	63	31	2	9	-0.094		1.211	
23.95	0.606	80	96	63	30	2	11	0.129		0.966	
24.15	0.607	81	96	63	32	2	7	-0.170		1.362	
24.35	0.609	80	95	64	29	2	2	-0.206		1.103	
24.55	0.611	80	95	63	30	2	7	0.093		0.952	
24.75	0.612	84	96	62	32	2	8	-0.061		1.062	
24.95	0.614	84	95	61	32	2	4	0.150		1.166	
25.15	0.616	84	96	62	32	1	4	-0.001		1.162	
25.34	0.617	82	97	60	36	0	4	0.317		1.419	
25.45	0.618	77	97	59	38	0	2	0.459		0.627	
25.65	0.620	75	98	61	35	2	17	0.420		1.247	
25.85	0.628	76	97	59	38	0	0	0.740		1.268	
26.05	0.636	77	97	55	42	0	0	0.917		0.880	
26.25	0.643	74	95	50	45	0	0	1.222		0.894	
26.45	0.651	68	96	62	31	2	7	0.730		1.316	
26.65	0.659	71	96	59	35	1	8	0.815		1.328	
26.85	0.661	70	97	63	32	2	17	-0.175		1.340	
26.95	0.662	74	96	64	30	2	6	0.112		1.323	
27.15	0.664	77	97	63	30	3	4	-0.119		1.195	
27.28	0.665	77	95	63	27	5	2	-0.215		1.220	
27.55	0.668	74	96	60	33	3	4	-0.333		1.185	
28.15	0.674	68	96	58	37	2	5	-0.100		1.037	
28.55	0.678	76	95	50	43	2	10	0.152		0.975	
29.05	0.683	69	97	62	32	2	2	0.335		0.922	
29.65	0.689	71	97	60	35	2	9	0.187		1.178	
30.05	0.693	82	97	64	30	3	10	0.265		0.875	
30.55	0.698	71	97	62	31	4	7	0.200		0.989	
31.15	0.704	84	98	64	32	2	11	0.223		1.336	

Appendix A (continued).

Depth (mbsf)	Age (Ma)	Fine fraction (%)	Fine carbonate (%)	Carbonate mineralogy			Whole pteropods (>355 µm) (%)	$\delta^{18}\text{O}_{\text{PDB}}$ <i>G. sacculifer</i> (‰)	$\delta^{18}\text{O}_{\text{PDB}}$ <i>Cibicidoides</i> spp. (‰)	$\delta^{13}\text{C}_{\text{PDB}}$ <i>G. sacculifer</i> (‰)	$\delta^{13}\text{C}_{\text{PDB}}$ <i>Cibicidoides</i> spp. (‰)
				Fine aragonite (%)	Fine calcite (%)	Fine Mg calcite (%)					
31.55	0.708	75	98	64	32	1	0	0.024		1.441	
32.05	0.713	85	98	66	31	1	8	-0.442		0.898	
32.65	0.720	80	98	58	40	0	0	-0.380		1.318	
33.05	0.724	85	98	62	36	0	0	-0.070		1.391	
33.55	0.729	82	99	56	42	0	0	-0.155		0.954	
34.15	0.735	83	98	60	38	0	12				
34.55	0.739	87	97	60	37	0	0	-0.254		1.208	
35.05	0.744	82	95	65	28	3	19	-0.162		1.059	
35.65	0.750	74	95	55	38	2	0			1.114	
36.05	0.754	75	96	52	42	2	0	0.397		0.545	
36.55	0.759	72	96	70	22	4	3	0.800		0.980	
37.05	0.764	69	97	63	29	5	9	0.491		1.225	
37.15	0.765	74	97	63	28	5	3	-0.020		0.941	
37.65	0.770	77	97	63	28	6	6	0.052		1.024	
38.05	0.774	80	97	62	30	4	16	0.520		1.484	
38.55	0.779	82	98	63	32	2	19	0.690		1.471	
39.15	0.785	79	98	59	36	2	12	-0.144		1.427	
39.55	0.789	83	98	60	36	2	18	-0.471		0.904	
40.05	0.794	82	98	61	37	0	18	-0.027		1.057	
40.65	0.800	84	98	60	36	2	7	0.146		1.124	
41.05	0.804	82	98	63	33	2	17	-0.387		1.113	
41.55	0.809	84	98	64	33	1	7	-0.449		0.887	
42.15	0.815	85	98	66	32	0	6	-0.324		0.916	
42.55	0.819	77	98	60	38	0	2	0.265		1.319	
43.05	0.824	81	98	60	38	0	0	-0.039		1.188	
43.65	0.831	83	98	60	38	0	0	-0.476		0.745	
44.05	0.835	83	98	63	35	0	0	-0.071		0.813	
44.55	0.840	86	97	66	31	0	10				
45.15	0.846	82	98	56	42	0	0	0.175		1.225	
45.55	0.850	84	97	62	35	0	0	0.338		1.357	
46.05	0.855	88	95	65	26	4	38	-0.291		0.670	
46.54	0.860	74	96	37	59	0	0	0.441		0.789	
47.15	0.866	77	96	37	54	3	7	0.647		0.891	
47.55	0.870	76	96	49	47	0	0	0.762		1.077	
48.04	0.875	69	96	51	46	0	0	0.241		0.862	
48.65	0.881	76	97	49	45	2	14	0.010		0.599	
54.05	0.941	81	97	54	43	0	0	-0.604		1.096	
55.55	0.972	70	97	52	45	0	9	-0.877		1.303	
56.05	0.982	81	98	52	46	0	0	-0.218		1.257	
56.65	0.994	79	98	45	52	0	0	-0.342		1.404	
57.05	1.002	79	98	49	48	0	0	-0.335		1.386	
57.55	1.012	90	96	57	39	0	0	-0.506		1.214	
58.15	1.025	77	97	52	45	0	0	-0.015		1.345	
58.55	1.033	79					0	0.007		1.367	
59.05	1.043	76	97	48	49	0	0	-0.208		1.198	
59.65	1.055	84	97	52	45	0	0	-0.125		1.207	
60.05	1.063	80	97	45	52	0	0	-0.177		1.113	
60.55	1.073	90	96	60	37	0	5	-0.267		1.064	
61.15	1.086	80	97	57	37	2	6	0.104		0.964	
61.55	1.094	77	96	51	46	0	15	0.225		0.872	
62.05	1.104	81	97	48	49	0	0	-0.083		1.234	
62.65	1.116	76	97	46	51	0	0	0.091		1.426	
63.05	1.124	68	97	45	52	0	0	-0.103		1.355	
63.55	1.135	84	95	44	50	1	1	0.535		0.737	
64.15	1.147	81	97	55	42	0	7	-0.091		0.844	
64.55	1.155	85	98	56	43	0	0	-0.633		0.749	
65.05	1.165	88	98	54	44	0	0	-0.028		1.468	
65.55	1.175	86	98	56	41	0	0	-0.074		1.181	
66.15	1.187	74	98	49	49	0	0	0.255		1.243	
66.55	1.196	69	98	49	49	0	0	-0.052		0.798	
67.05	1.206	85	98	62	36	0	0	-0.451		0.838	
67.65	1.218	82	98	49	49	0	0	0.213		1.250	
68.05	1.226	77	99	48	51	0	0	-0.033		1.666	
68.55	1.236	81	99	54	45	0	0	-0.160		1.313	
69.15	1.249	78	98	45	53	0	0	0.408		1.964	
69.55	1.257	85	98	51	46	0	0	0.362		1.594	
70.05	1.267	82	95	42	53	0	0	0.618		1.327	
70.65	1.279	80	95	50	46	0	0				
71.05	1.287	81	97	50	47	0	0	0.691		1.556	
71.55	1.297	87	98	54	44	0	0	0.303		1.864	
73.05	1.328	85	97	44	53	0	0	-0.203		1.254	
73.65	1.340	84	97	40	57	0	0	-0.070		1.310	
74.05	1.348	91	98	49	49	0	0	0.435		1.853	
74.55	1.359	87	98	48	50	0	0	0.471		1.615	
75.05	1.369	88	97	41	57	0	0	0.477		1.777	
75.11	1.370	91	98	55	43	0	0	-0.031		1.388	

Appendix A (continued).

Depth (mbsf)	Age (Ma)	Carbonate mineralogy					Whole pteropods (>355 μm) (%)	$\delta^{18}\text{O}_{\text{PDB}}$ <i>G. sacculifer</i> (‰)	$\delta^{18}\text{O}_{\text{PDB}}$ <i>Cibicidoides</i> spp. (‰)	$\delta^{13}\text{O}_{\text{PDB}}$ <i>G. sacculifer</i> (‰)	$\delta^{13}\text{O}_{\text{PDB}}$ <i>Cibicidoides</i> spp. (‰)
		Fine fraction (%)	Fine carbonate (%)	Fine aragonite (%)	Fine calcite (%)	Fine Mg calcite (%)					
75.65	1.381	83	97	46	50	0	0	0.318		1.591	
76.05	1.389	75	96	36	60	0	0	0.442		1.758	
76.55	1.399	87	98	47	51	0	0	-0.064		1.390	
77.15	1.412	84	98	50	48	0	0	-0.224		1.461	
77.55	1.420	80	98	45	53	0	0	0.284		1.429	
78.05	1.430	78	98	41	57	0	0	0.728		1.345	
78.65	1.442	81	98	43	54	1	0	0.485		1.713	
9.05	1.450	88	97	48	49	0	0	-0.184		1.298	
79.55	1.460	86	98	48	50	0	0	-0.197		1.501	
80.15	1.473	85	97	44	53	0	0	0.328		1.537	
80.55	1.481	84	96	39	57	0	0	0.368		1.528	
81.05	1.491	88	97	44	53	0	0	-0.070		1.318	
81.65	1.503	92	97	49	48	0	0	0.068		1.811	
82.05	1.511	93	97	41	56	0	0	-0.431		1.804	
82.55	1.522	94	97	50	48	0	0	-0.616		1.531	
83.15	1.534	87	97	37	60	0	0	-0.080		1.316	
83.55	1.542	76	97	37	60	0	0	-0.147		1.369	
84.05	1.552	71	97	36	62	0	0	0.380		1.553	
84.55	1.562	78	97	35	62	0	0	-0.097		1.325	

APPENDIX B
**Carbonate Mineralogy, Percentage of Whole Pteropods, and Oxygen Isotope Data for Sedi-
 ment Samples from Hole 817A**

Depth (mbsf)	Age (Ma)	Carbonate mineralogy					Whole pteropods (>355 µm) (%)	$\delta^{18}\text{O}_{\text{PDB}}$ <i>G. sacculifer</i> (‰)
		Fine fraction (%)	Fine carbonate (%)	Fine carbonate (%)	Fine aragonite (%)	Fine calcite (%)		
0.06	0.001	84	95	50	29	16	51	-1.464
0.26	0.003	87	95	46	34	15	53	-1.328
0.45	0.005	88	94	48	32	15	49	-1.303
0.65	0.007	90	94	58	23	14	44	-1.149
0.85	0.010	90	94	47	29	18	46	-1.311
1.04	0.012	85	94	35	43	16	32	-0.768
1.25	0.017	87	95	35	46	15	42	-0.248
1.45	0.021	86	95	34	49	12	25-0.268	
1.56	0.024	88	94	49	36	9	31	-0.493
1.75	0.026	86	95	29	58	8	22	-0.871
1.95	0.028	85	95	32	56	6	27	-0.828
2.15	0.030	85	95	35	53	7	23	-0.556
2.35	0.032	86	95	31	57	7	28	-0.951
2.54	0.034	86	95	32	59	4	23	-0.758
2.75	0.036	85	94	34	56	5	31	-0.452
2.95	0.038	91	96	53	30	14	32	-1.183
3.06	0.039	82	96	46	37	13	25	-0.959
3.25	0.041	93	95	53	26	17	29	-0.728
3.45	0.044	92	96	50	32	14	33	-1.242
3.64	0.045	84	97	44	42	10	21	-0.981
3.83	0.047	86	97	48	34	15	28	-1.464
4.04	0.050	76	96	42	40	14	24	-1.295
4.25	0.052	86	94	30	57	6	30	-1.404
4.55	0.055	86	94	34	55	4	27	-0.597
4.75	0.057	89	94	28	59	7	23	-1.274
4.95	0.059	85	95	30	58	6	24	-0.371
5.15	0.061	84	95	34	55	7	17	-0.376
5.35	0.064	87	95	35	53	7	26	-0.407
5.53	0.066	90	95	39	47	9	29	-0.408
5.60	0.067	91	96	47	35	14	26	-0.406
5.75	0.069	92	96	50	31	14	51	-0.469
5.95	0.071	90	96	46	37	13	28	-0.804
6.15	0.072	92	95	52	29	15	29	-0.912
6.35	0.073	87	96	50	34	12	28	-1.110
6.55	0.074	92	96	49	32	15	30	-1.516
6.75	0.075	93	95	48	35	13	35	-1.427
6.95	0.077	92	96	51	33	13	33	-1.217
7.15	0.078	94	96	51	30	14	35	-1.608
7.25	0.078	93	96	52	28	16	47	-1.250
7.45	0.079		95	53	23	18	31	-1.086
7.65	0.080		96	53	27	16	35	-0.802
7.85	0.082	83	96	39	46	11	16	-0.132
8.05	0.083	90	97	51	34	12	28	-0.644
8.25	0.084	93	96	45	36	15	34	-0.676
8.45	0.085	90	96	48	35	13	27	
8.65	0.086	93	96	52	32	13	30	-0.956
8.75	0.086	92	96	48	35	14	28	-1.020
8.95	0.088	92	96	53	28	15	30	-1.099
9.15	0.089	93	97	52	27	18	33	-0.776
9.35	0.090	93	96	50	30	16	32	-0.920
9.55	0.091	88	97	46	38	14	22	-0.886
9.75	0.092	86	97	49	36	12	42	-1.171
9.95	0.093	87	97	44	43	9	22	-0.118
10.15	0.094	92	98	50	31	16	28	-1.028
10.25	0.095	86	98	41	50	7	25	-0.641
10.45	0.096	91	96	54	31	10	34	-1.118
10.65	0.097	90	98	35	62	0	32	-0.847
10.85	0.098	87	98	40	52	5	25	-0.129
11.05	0.099	90	97	46	44	7	27	-0.775
11.25	0.100	89	98	49	44	6	31	-1.395
11.45	0.101	89	95	44	45	7	41	-1.030
11.65	0.103	89	96	47	40	9	34	-1.165
11.75	0.103	90	96	49	37	10	43	-1.225
11.95	0.104	90	96	51	30	15	29	-0.996
12.15	0.105	92	96	52	33	11	24	-1.120
12.35	0.106	91	95	46	38	11	38	-0.932
12.55	0.108	88	95	45	44	6	21	-0.856
12.75	0.109	89	96	46	45	6	25	-0.971
12.95	0.110	88	97	47	43	7	36	-1.010
13.25	0.111	89	96	54	32	10	33	-1.003
13.45	0.113	90	96	50	34	11	38	-1.240
13.65	0.114	90	95	53	32	10	22	-1.031
13.85	0.115	88	95	50	36	8	23	-1.594
14.05	0.116	88	95	44	46	5	18	-1.328
14.25	0.117	87	95	39	49	8	16	-1.315
14.45	0.118	87	94	48	40	6	20	-1.333
14.65	0.119	90	90	55	27	9	27	-1.159
14.75	0.120	84	92	46	36	10	30	-0.966
14.95	0.121	86	92	34	51	7	19	-0.374
15.15	0.122	89	92	32	54	6	20	-0.296

Appendix B (continued).

Depth (mbsf)	Age (Ma)	Carbonate mineralogy					Whole pteropods (>355 μm) (%)	δ ¹⁸ O _{PDB} <i>G. sacculifer</i> (‰)
		Fine fraction (%)	Fine carbonate (%)	Fine carbonate (%)	Fine aragonite (%)	Fine calcite (%)		
15.25	0.122	86	90	33	52	5	22	-0.134
15.25	0.122		95	42	47	6	9	-0.544
15.45	0.124	68	96	53	38	5	19	-1.210
15.65	0.125	92	95	50	37	8	41	-1.327
15.85	0.126	92	95	53	34	8	40	
16.05	0.127	87	96	50	41	5	40	
16.25	0.128	87	96	48	44	4	27	
16.65	0.135	86	97	45	52	0	25	-0.359
16.75	0.137	89	97	43	54	0	7	0.014
16.95	0.141	85	97	29	68	0	33	0.178
17.15	0.144	87	96	37	59	0	10	-0.033
17.35	0.148	91	97	41	56	0	10	-0.799
17.55	0.152	93	97	50	44	3	16	-0.473
17.75	0.155	94	97	48	46	2	21	-0.311
17.95	0.159	83	96	48	42	6	11	-0.923
18.15	0.162	88	97	39	58	0	8	-0.350
18.25	0.164	76	96	37	53	6	20	-0.069
18.45	0.168	75	98	49	45	3	12	-0.363
18.65	0.172	87	97	39	54	4	14	
18.85	0.175	84	93	28	60	6	17	-0.236
19.05	0.179	85	99	29	66	5	22	-0.109
19.25	0.182	86	91	26	61	4	20	-0.123
19.45	0.186	83	89	32	58	0	19	-0.307
19.65	0.189	87	92	27	65	0	18	-0.646
19.75	0.190	86	94	29	65	0	19	-0.762
19.95	0.193	87	93	28	66	0	11	-1.266
20.15	0.196	85	94	34	56	4	18	-0.680
20.35	0.198	88	95	28	67	0	12	-0.658
20.55	0.201	89	94	34	60	0	13	-0.357
20.75	0.204	86	94	42	47	4	20	-0.885
20.95	0.207	89	94	45	45	4	18	-1.343
21.15	0.209	86	95	48	42	5	25	-1.465
21.25	0.211	85	95	50	40	5	26	-1.626
21.45	0.213	89	94	48	39	7	31	-1.566
21.65	0.216	88	96	45	45	5	28	-1.472
21.85	0.219	90	96	52	38	5	33	-1.547
22.05	0.222	85	96	50	40	5	29	-1.341
22.25	0.224	85	94	47	44	3	40	-1.292
22.75	0.231	89	95	53	37	5	32	-0.573
22.95	0.234	88	95	44	47	4	22	-0.981
23.15	0.237	89	96	46	47	3	29	-0.504
23.35	0.240	88	96	45	48	3	26	-1.276
23.55	0.242	92	94	56	30	8	27	-1.077
23.75	0.245	85	94	36	50	8	18	-0.176
23.95	0.250	87	93	28	63	3	5	-0.077
24.15	0.254	87	93	31	58	3	13	0.235
24.25	0.256	88	93	29	64	0	17	-0.551
24.33	0.258	89	93	27	66	0	23	0.150
24.75	0.268	90	96	45	44	6	20	0.054
25.03	0.274	92	97	37	60	0		
25.25	0.278	91	97	40	53	4	18	-0.255
25.45	0.282	94	96	41	55	0		
25.75	0.287	90	96	43	48	5	24	-0.276
25.95	0.291	93	97	39	58	0		
26.10	0.293	93	96	40	57	0		
26.25	0.296	92	97	38	59	0	9	-0.429
26.53	0.301	93	97	37	60	0		
26.75	0.305	94	98	35	64	0	12	-0.351
26.95	0.308	92	97	44	53	0		
27.25	0.314	92	97	43	55	0	11	-1.269
27.45	0.317	92	97	39	58	0		
27.60	0.320	93	97	38	59	0		
27.75	0.748	92	97	29	68	0	0	-0.551
28.03	0.750	94	94	22	72	0		
28.25	0.752	92	95	21	75	0	0	
28.45	0.754	94	94	27	66	0		-0.344
28.75	0.757	93	95	28	66	0	14	-0.216
28.95	0.758	94	97	32	65	0		
29.10	0.760	93	95	35	60	0		
29.25	0.761	94	95	40	55	0	0	
29.53	0.763	92	96	40	56	0		
29.78	0.766	67	97	48	48	0	0	-1.238
29.95	0.767	94	96	38	57	0		
30.25	0.770	92	97	29	68	0	0	-0.625
30.45	0.771	92	96	36	60	0		
30.60	0.773	93	96	36	61	0		
30.75	0.774	92	96	37	60	0	0	-1.214
31.03	0.777	92	96	40	56	0		
31.25	0.778	92	96	37	59	0	0	-1.201

Appendix B (continued).

Depth (mbsf)	Age (Ma)	Carbonate mineralogy					Whole pteropods (>355 μm) (%)	$\delta^{18}\text{O}_{\text{PDB}}$ <i>G. sacculifer</i> (‰)
		Fine fraction (%)	Fine carbonate (%)	Fine carbonate (%)	Fine aragonite (%)	Fine calcite (%)		
31.45	0.780	93	96	44	51	0		
31.75	0.783	93	96	34	62	0	0	-0.483
31.95	0.785	93	95	34	61	0		
32.10	0.786	94	95	37	58	0		
32.25	0.787	93	96	41	55	0	3	-0.242
32.53	0.790	93	94	50	44	0		
32.75	0.792	93	96	45	52	0	4	-0.352
32.95	0.793	93	95	49	46	0		
33.25	0.796	93	96	35	60	0	0	-0.092
33.45	0.798	94	96	35	61	0		
33.60	0.799	93	96	35	60	0		
33.75	0.800	90	96	36	61	0	9	-0.165
34.25	0.805	89	97	38	59	0		
34.45	0.806	91	95	35	61	0	2	0.131
34.53	0.807	90	96	47	48	0	14	-0.288
34.57	0.808	94	96	44	52	0		
34.75	0.811	94	98	40	58	0	6	-0.605
34.95	0.815	86	96	37	59	0		
35.25	0.821	92	92	32	60	0	0	-0.070
35.42	0.824	92	92	28	64	0		
35.60	0.828	92	94	35	59	0		
35.75	0.831	93	95	40	55	0	23	-0.639
36.03	0.836	94	97	43	54	0		
36.25	0.840	93	94	35	59	0	15	-0.006
36.45	0.844	93	95	40	54	0		
36.75	0.850	91	94	27	67	0	0	-0.225
36.92	0.851	93	94	33	61	0		
37.10	0.852	93	97	38	58	0		
37.25	0.853	92	96	41	56	0	9	-0.728
37.53	0.855	94	98	39	58	0		
37.75	0.856	92	97	40	57	0	6	
37.95	0.857	94	96	49	47	0		
38.25	0.859	94	96	50	47	0	9	
38.42	0.860	94	96	47	49	0		
38.60	0.861	94	96	50	47	0		
38.75	0.862	94	96	49	47	0	8	
39.03	0.864	92	94	45	48	0		
39.25	0.865	94	96	45	51	0	15	
39.45	0.866	94	96	50	46	0		
39.75	0.868	92	96	46	50	0	8	
39.92	0.869	93	94	38	55	0		
40.10	0.870	93	95	40	55	0		
40.25	0.871	91	93	32	61	0	5	-1.372
40.53	0.872	92	94	33	61	0		
40.75	0.873	91	95	36	59	0	12	-0.763
40.95	0.874	92	96	46	50	0		
41.25	0.875	94	95	49	46	0	6	
41.42	0.876	91	94	32	62	0	5	
41.60	0.877	93	95	37	58	0	12	
41.75	0.878	91	95	35	59	0	0	-0.703
42.03	0.879	88	97	18	79	0	0	
42.25	0.880	87	96	8	88	0	0	
42.45	0.887	92	96	11	84	0	0	
42.75	0.897	88	96	6	90	0	0	-0.861
42.92	0.903	93	93	5	88	0	0	
43.10	0.910	90	96	11	84	0	0	
43.25	0.915	92	96	15	81	0	0	-0.901
43.53	0.921	92	93	27	66	0	0	
43.62	0.921	93	94	0	94	0	0	-0.435
43.75	0.922	90	96	20	76	0	0	
44.03	0.923	91	97	13	84	0	0	
44.25	0.924	90	94	10	84	0	0	-0.159
44.45	0.925	93	94	12	82	0	0	
44.75	0.926	89	95	13	82	0	0	-1.037
44.92	0.927	91	95	8	88	0	0	
45.10	0.928	92	95	5	90	0	0	
45.25	0.929	85	96	9	86	0	0	-0.602
45.53	0.930	92	96	8	87	0	0	
45.75	0.930	89	96	8	88	0	0	-0.909
45.95	0.941	87	91	6	85	0	0	
46.25	0.950	87	91	7	84	0	0	-0.429
46.45	0.955	90	93	6	87	0	0	
46.60	0.959	83	97	0	97	0	0	
46.75	0.964	91	94	20	74	0	0	-0.618
47.03	0.972	93	93	6	87	0	0	
47.25	0.978	90	89	6	83	0	0	-0.744
47.45	0.984	91	94	4	90	0	0	
47.75	0.992	92	95	18	77	0	0	
47.95	0.998	94	96	18	78	0	0	

Appendix B (continued).

Depth (mbsf)	Age (Ma)	Carbonate mineralogy					Whole pteropods (>355 μ m) (%)	$\delta^{18}\text{O}_{\text{PDB}}$ <i>G. sacculifer</i> (‰)
		Fine fraction (%)	Fine carbonate (%)	Fine carbonate (%)	Fine aragonite (%)	Fine calcite (%)		
48.10	1.002	93	96	15	82	0	0	
48.25	1.006	92	96	15	81	0	0	
48.53	1.014	92	94	21	73	0	0	
48.75	1.020	92	91	2	89	0	0	
48.95	1.026	90	90	3	87	0	0	
49.25	1.035	93	94	5	89	0	0	
49.45	1.040	92	96	0	96	0	0	
49.60	1.044	92	96	17	79	0	0	
49.75	1.049	92						
50.03	1.057	90	96	6	90	0	0	
50.25	1.063	90	96	10	86	0	0	
50.45	1.069	90	94	8	86	0	0	
50.75	1.077	90	95	9	86	0	0	
51.25	1.091	91	95	0	95	0	0	
51.53	1.099	80	94	10	84	0	0	
51.75	1.106	90	94	8	86	0	0	
51.95	1.113	89	95	19	76	0	0	
52.25	1.123	89	95	7	88	0	0	
52.45	1.129	89	97	0	97	0	0	
52.60	1.134	90	97	12	85	0	0	
52.75	1.139							
53.03	1.149	93	96	14	82	0	0	
53.25	1.156	93	95	12	83	0	0	
53.45	1.162	91	95	6	88	0	0	
53.25	1.156		94	7	87	0	0	
53.62	1.168	93	97	17	80	0	0	
53.45	1.162	93	96	12	83	0	0	
53.65	1.169	92	94	5	90	0	0	
53.85	1.176	92	95	0	95	0	0	
54.05	1.182	89	95	8	86	0	0	
54.21	1.187	88	92	19	73	0	0	
54.55	1.199	85	96	6	89	0	0	
54.75	1.205	87	96	7	89	0	0	
54.95	1.212	87	96	0	96	0	0	
55.15	1.219	88	96	2	94	0	0	
55.35	1.225	88	95	10	86	0	0	
55.55	1.232	90	96	12	84	0	0	
55.80	1.240	90	96	17	80	0	0	
56.05	1.248	90	95	13	82	0	0	
56.25	1.255	92	95	16	80	0	0	
56.45	1.261	89	94	5	89	0	0	
56.65	1.268	90	94	0	94	0	0	
56.85	1.275	90						
57.05	1.281	89	94	0	94	0	0	
57.25	1.288	90	90	5	85	0	0	
57.55	1.298	90	92	5	87	0	0	
57.75	1.304	92	96	0	96	0	0	
57.95	1.311	90	96	5	91	0	0	
58.15	1.318	89	96	8	88	0	0	
58.35	1.324	92	95	7	87	0	0	
58.55	1.331	91	94	0	94	0	0	
58.82	1.340	92	94	0	94	0	0	
59.05	1.347	92	94	4	90	0	0	
59.25	1.354	89	96	6	90	0	0	
59.45	1.360	91	94	10	84	0	0	
59.65	1.367	90	94	0	94	0	0	
59.85	1.374	90	94	0	94	0	0	
60.05	1.380	88	94	0	94	0	0	
60.28	1.388	89	91	0	91	0	0	
60.55	1.397	92	95					
60.75	1.403	91	96	0	96	0	0	
60.95	1.410	90	96					
61.15	1.417	90	95					
61.35	1.423	89	95					
61.55	1.430	90	95					
61.79	1.438	92	96					
62.05	1.446	91	96					
62.25	1.453	90	94	7	87	0	0	
62.45	1.460		95					
62.65	1.466	90	96					
62.85	1.473	90	96					
62.75	1.469	89	95	5	90	0	0	
63.07	1.476	84	96	5	91	0	0	
62.95	1.480	89	95					
63.15	1.483	87	92					
63.35	1.490	92	94					